A

Dissertation Report

On

Rotor Dynamic Modeling of Geared Systems

Submitted in Fulfilment of

The Requirements for the award of Degree of

Master of Technology in Design Engineering

By

BAJAK RAHUL CHHAGANBHAI

(2014PDE5064)

Under the Guidance of

Dr. T.C. GUPTA

Associate Professor

Department of Mechanical Engineering

MNIT, Jaipur

DEPARTMENT OF MECHANICAL ENGINEERING

MALAVIYA NATIONAL INSTITUTE OF TECHNOLOGY

JAIPUR –302017 (RAJASTHAN) INDIA

June-2016

DEPARTMENT OF MECHANICAL ENGINEERING
MALAVIYA NATIONAL INSTITUTE OF TECHNOLOGY

CERTIFICATE

This is to certify that the thesis entitled, "**Rotor Dynamic Modeling of Geared Systems**" being submitted by **Bajak Rahul Chhaganbhai** for the award of the degree of Master of Technology (Design Engineering) of MNIT Jaipur, is a record of bonafide research work carried out by him under my supervision and guidance. He has worked for one year on the above problem at the Department of Mechanical Engineering, Malaviya National Institute of Technology, Jaipur and this has reached the standard fulfilling the requirements and the regulation relating to the degree.

The contents of this thesis, in full or part, have not been submitted to any other university or institution for the award of any degree or diploma.

Bajak Rahul Chhaganbhai
2014PDE5064

This Dissertation report is hereby approved for submission.

Date:

Place:

Dr. T.C. Gupta
Associate Professor
Department of Mechanical Engineering
MNIT, Jaipur

Acknowledgement

First, to my parents, for their support, comfort and providing strength throughout my life and for instilling in me at an early age the value and importance of education. My sisters, **Sonal**, **Hetal**, and **Kundan** for encouraging me in every possible way throughout my studies.

I am deeply grateful to my mentor **Dr. T.C. Gupta** for his constant encouragement and instruction, and insight throughout this endeavor. His moral support and valuable feedback have been a great source of inspiration for enhancing my work in this dissertation work.

I am extremely grateful to respected **Dr. Himanshu Chaudhary, Dr. Dinesh Kumar** and **Dr. Amit Singh** for always being supportive and helpful throughout my academic.

I would like to thank my friends and classmates specially **Maulik**, **Rahul**, **Kamlesh**, **Vishal**, **Nilesh**, **Jaimin, Amit and Jignesh** for inspiring me throughout my work.

Lastly, I would like to thank **Manoj Gupta**, **Harsh Dixit** and **Ajit Singh** (Ph.D. Research Scholar) for helping me throughout my dissertation work.

Bajak Rahul Chhaganbhai
Design Engineering
(2014PDE5064)

Abstract

This thesis presents a methodology for generating rotor dynamic model of the geared system based on first principles. Nonlinearity of gear is examined for one mesh cycle, and gear mesh stiffness is determined.Gear disk is a model as a rigid disk in geared system. The three-dimensional gear-mesh model developed for the helical and spur gear using one orientation angle to specify the system arrangement and three-dimensional gear-mesh model developed for the straight bevel gear using two orientation angle. A 12×12 mesh stiffness matrix derived for the helical gear and bevel gear allow us to consider the effect of the meshing stiffness of gear on the vibration of the geared systems. A finite element model of the geared system is developed for helical and bevel gears. Natural frequency of the uncoupled system and coupled system is determined and compared with previously obtained results and a mode shape of coupled and the uncoupled system is plotted using the Matlab programming. Through this methodology, a robust rotor dynamic model for the geared system using finite element technique is developed.

Table of Contents

List of Figures

List of Tables

Nomenclature

LOA	Line of Action
A	Cross sectional area
E	Young's modulus
G	Shear modulus
I	Area moment of inertia
J	Area polar moment of inertia
I_t	Transverse mass moment of inertia
I_p	Polar mass moment of inertia
m	Mass
m_g	Mass of gear
m_d	Mass of disk
l	Length of element
r_g	Radius of gyration
$[\,]_s$	Shaft matrix
$[\,]_d$	Disk matrix
[C]	General damping matrix
[K]	General stiffness matrix
[G]	General gyroscopic matrix
[M]	General mass matrix
[D]	Sum of damping and gyroscopic matrix
$[\,]^{(e)}$	Element matrix
$[\,]^{(G)}$	Global matrix
$[K]_{mesh}$	Gear mesh-stiffness matrix
$[K_{ii}]$	Sub matrix of Gear-mesh stiffness matrix
{q}	Displacement vector
{F}	Force vector
F_n	Normal force along LOA
D	Generalize force

h	Gear height
d_g	Gear diameter
d_i	Shaft inner diameter
d_o	Shaft outer diameter
r_{pb} , r_{gb}	Base circle radius of pinion and gear, respectively
r_{pp} , r_{gp}	Pitch radius of pinion and gear, respectively
θp , θg	Angular displacement of pinion and gear, respectively
b	Tooth width
C.R.	Contact Ratio
N	Number of teeth
P	Pitch point
D_m	Mean diameter of bevel gear
D_p	Pitch circle diameter of bevel gear
k_q, K_q	Translational and rotational elastic stiffness, respectively
K_m	Average gear mesh-stiffness
K_t	Torsional gear-mesh stiffness
c_{cc}, c_{yy}, c_{zz}	Bearing damping values in x, y, and z direction, respectively
k_{xx}, k_{yy}, k_{zz}	Bearing stiffness values in x, y, and z direction, respectively
T	Kinetic energy
L	Lagrangian function
X,Y and Z	Global coordinates
X',Y' and Z'	Prime coordinates
x, y, and z	Translational degrees of freedoms
$\theta_x, \theta_y, and\ \theta_z$	Rotational degrees of freedoms
$\phi_x, \phi_y, and\ \phi_z$	Direction cosine
β	Helical angle
γ_i	Pitch angle of i^{th} bevel gear
φ	Orientation angle in helical gear
Ω	Shaft rotational speed
υ	Poisson's ratio

κ	Shear factor
Φ	Transverse shear parameter
i, j	Node i and j
θ_1, θ_2	Two orientation angles for bevel gear pair

Subscript

i, j	i^{th} and j^{th} gear
h	Helical gear
b	Bevel gear
s	Shaft
b	Bearing
d	Disk

Superscript

T	Transpose

1 Introduction

This chapter provides introduction to the geared rotor bearing system equipped with helical and bevel gear.

1.1 Introduction

Gear is a power transmission component which is used in transmission of power from one shaft to another shaft having relatively short distance. It is an essential part of many power transmission system. It's widely used to transmit power in a system like a helicopter through various gear train, transmit power in an automobile from the engine to wheel through the gear box, transmission of power in turbine system from turbine rotor to generator, spacecraft, and many other industrial as well as daily appliances.

A failure of rotor system can cause critical damage to the machine and may also lead to loss of life. For reliability and maintenance perspective it's essential to predict resonance frequencies, stability and force response of any system. In rotor dynamics system presences of additional component like gear box cause difficulties in the prediction of resonant frequencies and forced responses.Due to frequent engagement and disengagement of gear tooth, gearbox dynamics is a complex field of research. Gearbox dynamics contain a large number of complex interaction and many assumptions which do not apply to most of the gear system.

Since the beginning of rotating machinery, gear is used yet many aspects of gearbox dynamics are still in need to deeper understanding. Gears can create and transmit vibration throughout the whole rotor bearing system.Use of Gears in the coupling of shaft significantly influences its natural frequencies and mode shapes. Further external excitation such as forces produced due to unbalance and geometrical misalignment contributes in changing bearing stiffness properties.

A systematic study of gear dynamics started in the 1920s and early 1930s. The primary objectives of gear dynamic analysis are vast, and it includes various models based on phenomena like bending and contact stress, transmission efficiency, loads on other machine components, scoring and pitting, system natural frequencies and stability, reliability, rotor whirl and gear life. The first model is of finding loads acting on gear teeth with the help of many analytical and experimental techniques. A dynamic model of gears as a spring-mass emerged in the 1950s and early 1960s which include tooth compliance. Finite element model developed in the 1970s is the

first one which includes tooth compliance. That was a significant departure from treating the gears as lumped inertia and teeth as a massless spring since the problem could be formulated much closer to a continuum.

In this work a finite element model having 12 degrees of freedom per element is applied to a rotor system with helical as well as bevel gear to find the natural frequencies and mode shape of the system vibration by taking gear meshing stiffness in the account with consideration of coupling between lateral and torsional vibration. A 12 × 12 mesh stiffness matrix derived for the helical and the bevel gear which depends on average mesh stiffness value of gear pair. An equation used to find the average value of mash stiffness is verified for the helical gear pair and developed for the bevel gear pair by determining its value at a different point during one mesh cycle with the help of software and analytical method.

1.2 Thesis Outline

1. Chapter 1 contain basic introduction about the gear dynamics.
2. Chaper 2 contain a comprehensive literature review on the gear dynamics and discuss scope and objective of the work.
3. Chapter 3 contain a method to find non-linearity of the gear-mesh stiffness during the one mesh cycle. By using FEA software average gear mesh stiffness for the spur and bevel gear can be found.
4. Chapter 4 provides a modeling of the gear as a rigid disk in rotor dynamics.
5. Chapter 5 provides a detailed discussion of development of 12 DOF gear mesh stiffness matrix and discussion includes its application of the 12 DOF model to a geared shaft system.
6. Chapter 6 provides a discussion of the development of 12 DOF bevel gear mesh stiffness matrix with help of two orientation angle to specify its orientation in three-dimension. This physic based model applied to bevel geared system and results are validated with published data in literature.
7. Chapter 7 provides conclusion, limitation and recommendation of gear-mesh model of helical and bevel gears.

2 Literature Review, Scope, and Objective

2.1 Literature Review

B. Kishor (1989) provide an estimation of dynamic gear tooth load due to coupled lateral-torsional vibration in the geared rotor hydrodynamic bearing system.He includes gear mesh compliance and damping at gear teeth in his study with the effect of the geometrical unbalance and manufacture error.

Steady state analysis investigating the non-linear behavior of a spur gear is suggested by Singh (1990). He develops finite element model to find non-linear frequency response of the gear with a backlash and rotor bearing system response. His study focused on the effect of lightly and heavily loaded gear system.

Kahraman (1992) developed finite element model of geared rotor system having a flexible bearing. This model includes rotary inertia of shaft, flexibility of the shaft, damping of bearing, gear mesh stiffness and axial loading of the shaft.The procedure used to determine critical speed and response of shaft at any point due to geometrical eccentricities of gears, mass unbalanced and transmission errors.

The new spectral stiffness and transmissibility matrices developed based on the linear theory by Blankenship (1995), and development of new model rating indices can be used to rank order the importance of gear pair modes excited by various type of transmission error and coupling between bending and lateral modes.

Lau (1996) developed a model synthesis method for the vibrational analysis of complex geared systems which takes into account cross coupling effects caused by the system geometry and its dynamics. First, few natural frequencies and mode shape of the global system can be obtained by synthesizing all substructure using boundary condition at nodes which are related to engagement between a pair of gears..In this method, each shaft is modeled as an individuals substructure. The global system matrix was then derived from the model synthesis technique. The lateral-torsional-axial coupled in the form of stiffness matrix. The non-zero element of the stiffness matrix is used to calculate the global characteristic of the system.

Another finite element formulation to determine the coupled vibration characteristic of a geared rotor system is proposed by Rao(1995).His work on sensitivity analysis of various parameter on

system natural frequencies and mode shape such as pressure angle, gear mesh stiffness, type of bearing system, etc.

Choi (1999) develop a model on dynamic gear loading in response to unexpected vibration in specifically in the axial direction of a helical geared set.In this approach, he modeled a gear pair as a set of the rigid disk with a linearly distributed spring over contact line. He can determine the source of the instability with the help of transmission error analysis and redesign the turbo set to eliminate the high vibration.

Jian Lin (2002) present a method to analyze instabilities systematically in the two mesh multi-gear system during its operating condition. The simple formulas which describe the effect of contact ratios and mesh phasing on the stabilities boundary conditions were derived.

Wang (2002) Introduced one more new approach in which Geared system modeled using the Delft finite element theory(Werff, 1977). The definition of the element consists of both the nodal coordinates and deformation coordinates in this formulation. The gear element includes time-varying mesh stiffness, transmission error, and lateral –torsional vibration coupling.

M. Li and H.Y. Hu(2002,2003) present paper on spiral bevel gear dynamics to couple axial-lateral-torsional vibration of the rotor-bearing system. They proposed 6 DOF model of the spiral bevel gear using Lagrange's equations under certain conditions to find out the natural frequency and mode shape of the rotor-bearing system. The dynamics of spiral bevel gear analyze theoretically, and system behavior investigated numerically. They examine the effect of various boundary conditions such as torsional and axial stiffness of bearing on the threshold speed and stability of the system.

Ebrahimi (2006) consider the elastic effect between gear and body for contact analysis of meshing gear teeth. His work is applicable for both spur and helical gear. The tooth and body both were assumed to be rigid with an elastic element between them. Rigid gear tooth contact analysis used to determine resulting gear force and moment.

David Blake Stringer (2008) presents methodologies for rotor dynamic modeling of rotary-wing transmission based on the first principle. He developed three-dimensional finite element model of gear mesh stiffness for spur and helical gears and carried out non-linear analysis of geared system.For the faster analysis of gear systems and potentially providing model reduction, he develops a model synthesis technique.

Li Yinong (2010) developed 8-DOF non-linear dynamic model of a spiral bevel gear pair. He involves time-varying mesh stiffness, transmission error, backlash and asymmetric mesh stiffness.A numerical method is used to examine the effect of mesh stiffness on the vibration of the spiral bevel gear transmission system.

J.A. Kaplan and Saeid Doust (2013) developed finite element formulation of the coupling between shaft by gears which couple the axial, lateral, and torsional degrees of freedom of shafts. This formulation can apply to a wide variety of both helical and spur geared system having a shaft at different orientation angle and was based on the mathematical model computing the average mesh tooth stiffness. The shaft is a model as a 1-D Timoshenko beam element having 12 degrees of freedom per element.

S.B. Wadkar (2005) examined the effect of various parameters on the variation of the gear mesh stiffness. He proposed a method to find mesh stiffness from the combined torsional mesh stiffness of the gear pair.He explains how is the mesh stiffness of the gear pair increases when the second pair of gear tooth are in contact. Two and three-dimensional finite element model is developed to calculate the torsional mesh stiffness by Timo Kiekbusch (2010). Longbao Wang (2013) present new equality conservation method for mesh stiffness calculation of straight bevel gear of small teeth number and size.

Chun Hung (2009) studied on the gear mesh cycle. A non-linear quasi-static finite element modeling used to examine mesh stiffness of the gear pair. He Compare mesh stiffness based on meshing quality, integration method, types of element.

2.2 Research Gap

Choi (1999) develop 10 DOF gear dynamic model to predict unexpected vibration in the gear system specifically in the axial direction but it is applied only for helical and spur gear. J.A. Kaplan and Saeid Doust (2013) developed 12 DOF finite element formulation of the coupling between shaft by gears which couple the axial, lateral, and torsional degrees of freedom of shafts but this model can only apply to the helical and spur gear. Li Yinong (2010) developed 8-DOF non-linear dynamic model of a spiral bevel gear pair. David Blake Stringer (2008) develop 12 DOF model of the helical gear for the rotary wing transmission system . M. Li and H.Y. Hu (2002,2003) presented paper on spiral bevel gear dynamics of the rotor-bearing system but this model consist of only 3 DOF per node. 12 DOF finite element model can be developed

for the helical and bevel gear system which would couple axial-lateral-torsional vibration of the system.

2.3 Research Objective

The primary research objective of this research work is to identify the effect of the gear mesh stiffness of helical and bevel gear pair on the vibration of the geared system. Which includes Development of the stiffness, mass, and gyroscopic matrix for the whole geared system. The effect of gear mesh stiffness is taken into consideration using 12×12 gear mesh stiffness matrix for the helical and bevel gear. Examine the coupling between the axial-lateral-torsional vibration of geared system.A Matlab codes are used to Calculate the natural frequencies and mode shape for the system and to plot mode shape.

3 Methodology for Calculating Gear Mesh Stiffness

This chapter contains a calculation of the gear mesh stiffness for the spur gear and bevel gear using the methodology provided and softwares such as ANSYS Workbench 15.0 and Creo Parametric 2.0. Gear mesh stiffness obtained is verified with the mesh stiffness obtained from the equation provided in the literature. The equation provided for mesh stiffness calculation are then modified for the bevel gear pair.

3.1 Gear Mesh Stiffness Calculation for Helical Gear and Spur Gear

3.1.1 Methodology

Haward and Wang (2001, 2005) describe the relation between the torsional stiffness of gear pair and linear tooth mesh stiffness of gear pair. The gear mesh stiffness can be easily understood by the torsional and transverse motion of the gear system. Figure 3.1 explains coupling between torsional and transverse motion of the system.

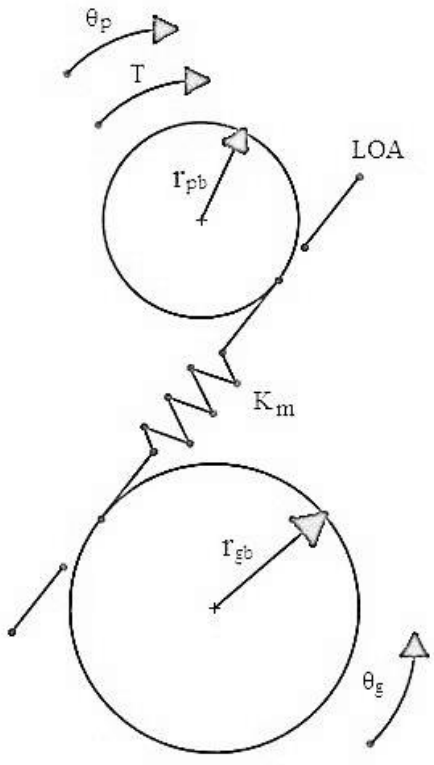

Figure 3.1: Coupling of the torsional and transverse motions of the spur gears (Chun, 2009)

Where ,

T = Input torque ,Nm

r_{pb} = Base circle radius of the pinion, m

θp= Angular displacement of the pinion, rad

r_{gb} = Base circle radius of gear, m

θ_g = Angular displacement of gear, rad

K_m = Linear tooth mesh stiffness, N/m

LOA = Line of action

During meshing of the gear pair, one of the most important factor is torsional mesh stiffness of the gear. In meshing gear's pitch circle rolls on one another without slipping(as shown in fig. 3.2).

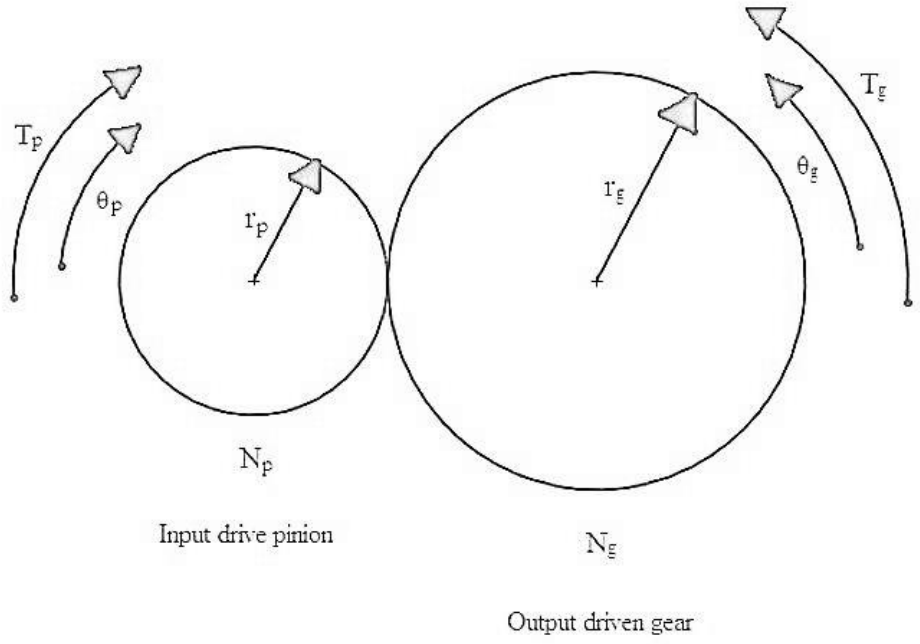

Figure 3.2: Schematic of spur gears in action (Chun, 2009)

Where,

T_p = Input pinion torque, Nm

θ_p = Angular displacement of the pinion, rad

r_p = Pitch radius of the pinion, m

N_p = Number of teeth of pinion

T_g = Output gear torque, Nm

θ_g = Angular displacement of gear, rad

r_g = Pitch radius of gear, m

N_g = Number of teeth of gear

The ratio of a number of teeth to it circumstance is always same for the meshing gears which yields the following relationship.

$$r_p\,\theta_p = r_g\,\theta_g \tag{3.1}$$

$$\frac{N_p}{N_g} = \frac{r_p}{r_g} = \frac{\theta_g}{\theta_p} \tag{3.2}$$

And with assumption of no energy dissipation in power transmission,

$$T_p\theta_p = T_g\theta_g \tag{3.3}$$

$$\frac{N_p}{N_g} = \frac{T_p}{T_g} = \frac{\theta_g}{\theta_p} \tag{3.4}$$

Linear tooth mesh stiffness can be calculated from the torsional stiffness of the gear. Torsional mesh stiffness is the ratio of the applied torque to angular deflection of the gear.

$$K_t = \frac{T}{\theta} = \frac{T_g}{\theta_g} = \frac{T_p}{\theta_p} \tag{3.5}$$

Where ,

T = Applied torque on the pinion, N/m

θ = Angular deflection , rad

K_T = Torsional mesh stiffness , Nm/rad

The linear mesh tooth stiffness can be defined as a ratio of force along Line of Action (F_n) to linear deflection of gear along a base circle (S) which yields following relationship.

$$K_m = \frac{F_n}{S} \tag{3.6}$$

K_m = linear tooth mesh stiffness, N/m

F_n = Normal force along line of action, N

S = Arc length (deflection) of base circle of pinion due to Force F_n,m

The torque in the gear is a force F_n multiply by the perpendicular distance, which in this case is base circle radius r_{pb} . thus $T = F_n\, r_{pb}$. Furthermore, with the assumption of small angle θ can be defined as $\theta = S / r_{pb}$. S is an arc length of the base circle of the pinion. Therefore, linear tooth mesh stiffness can be rewritten as,

$$K_m = \frac{F_n}{s} = \frac{\frac{T}{r_{pb}}}{r_{pb} * \theta} = \frac{T}{\theta * {r_{pb}}^2} = \frac{K_T}{{r_{pb}}^2} \tag{3.7}$$

So that linear tooth mesh stiffness can be written as the ratio of torsional mesh stiffness and square of base circle radius of the pinion.

$$K_m = \frac{K_T}{{r_{pb}}^2} \tag{3.8}$$

3.1.2 Modeling of Spur Gear Using Creo Parametric 2.0

For finite element analysis of any system creating a finite element model is a critical and time-consuming step. Finite element model must create with appropriate dimension, constraint, loads, mesh selection, element choice, etc. There two methods to construct finite element model. The first method includes the creation of CAD model using modeling software such as Creo Parametric, Solidworks, or CATIA, and export a model to ANSYS Workbench, Abaqus with appropriate file formats such as IGES, ACIS, or Parasolid for analysis. The second method used internal modeling capabilities of any analysis software to build the model. The primary disadvantage of the second method is user usually find difficulties to create a complex model.

In this work, Creo Parametric 2.0 used to create CAD model of the spur gear, and ANSYS Workbench 15.0 for the FEA of the gear system.

CAD model created using input parameter shown in Table 3.1

All dimensions are in mm

Pressure angle = PA = 20°

Table 3.1: Parameter used to construct Spur Gear in Creo Parametric 2.0

Parameter	Both gear of same size and material	Both gears are of different size and materials	
		1^{st} gear (pinion)	2^{nd} gear (gear)
Pitch Circle Diameter (D)	40	40	80
Base Circle Diameter(D_b = D * cos(PA))	37.5877	37.5877	75.1754
Number of teeth,(N)	21	21	42
Diametral Pitch ,(P)	0.5250	0.5250	0.5250
Addendum , (a =1/P)	1.9048	1.9048	1.9048
Outside Diameter , (D_o = D +2a)	43.8096	43.8096	83.8096
Circular Pitch , (p = 3.1416/P)	5.9840	5.984	5.9840
Whole Depth, (h_t = 2.157/P)	4.1086	4.1086	4.1086
Dedendum ,(b = h_t –a)	2.2038	2.2038	2.2038
Root Diameter ,(D_r = D -2b)	35.5924	35.5924	75.5924
Centre distance b/w both gear,(C)	40	40	60
Tooth width,(b)	6	6	6

CAD model of the gear system having same size of gears as shown in figure 3.3 and CAD model of gear system having different size of gears as shown in figure 3.4 created using CREO Parametric 2.0.

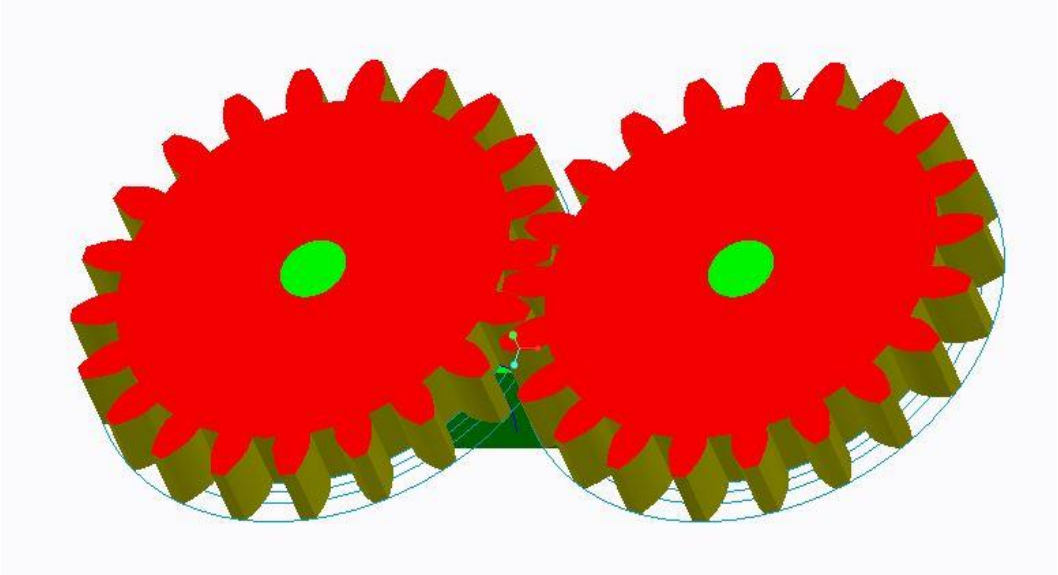

Figure 3.3: CAD model: Spur Gear (Both gears: Same size)

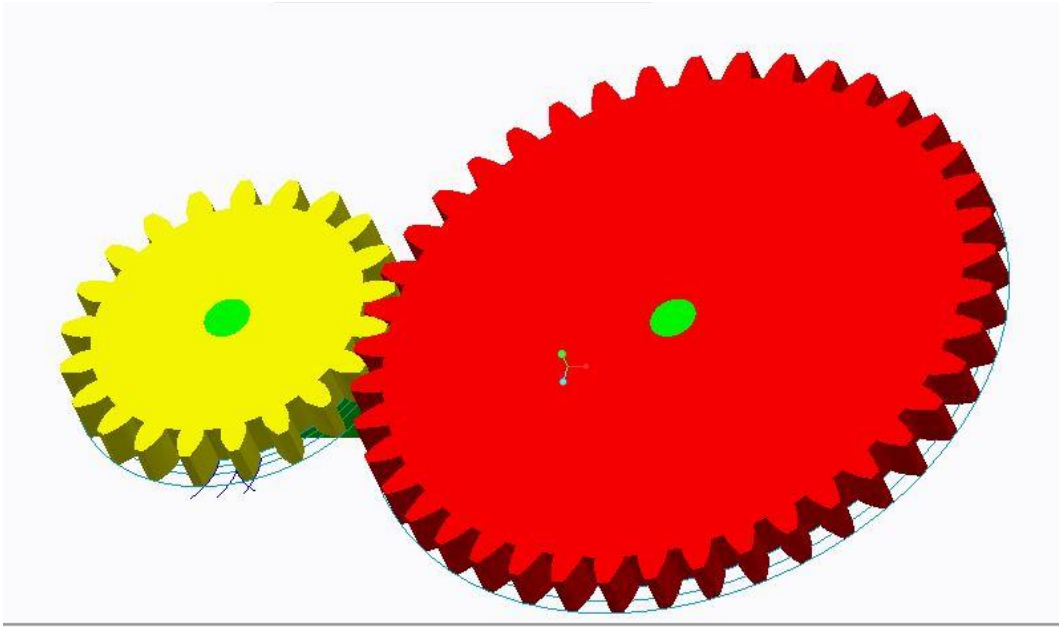

Figure 3.4: CAD model: Spur Gear (Both gears: Different size)

3.1.3 Boundary Conditions, Loads, and Displacement Field

Boundary conditions and loads in this work applied in such a way all degree of except one rotational degree of freedom are restricted in the pinion, and all degrees of freedom in gear are restricted. The only load applied on the system is input torque on the pinion as shown in figure 3.5. Figure 3.6 demonstrates the boundary conditions and applied load on the gear model.

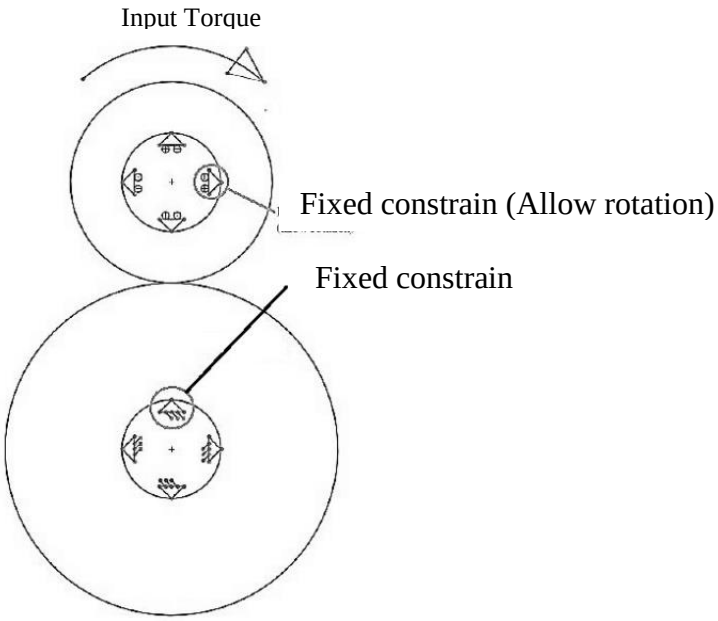

Figure 3.5: Boundary conditions and applied load for analysis (Chun, 2009)

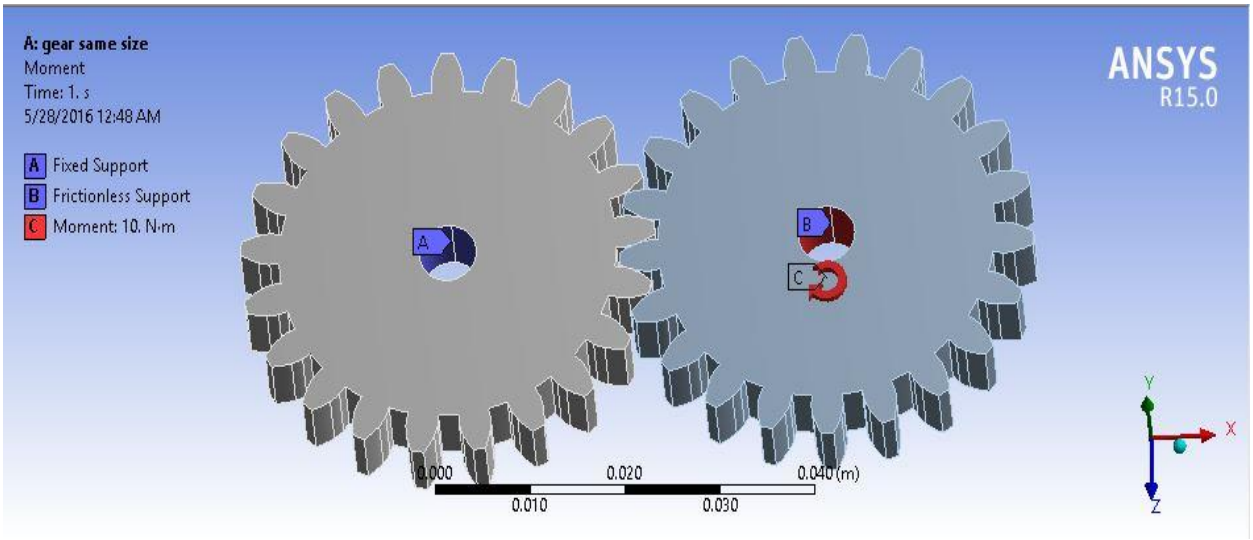

Figure 3.6: Boundary conditions in ANSYS Workbench 15.0 for spur gear (Both gears: Same size)

By applying above boundary conditions, ANSYS obtain the result in the form of displacement field as shown in figure 3.7. A displacement field in ANSYS is used to calculate mesh stiffness by the procedure explained earlier.

Displacement field for:

Moment = 10 Nm

Position = 0°

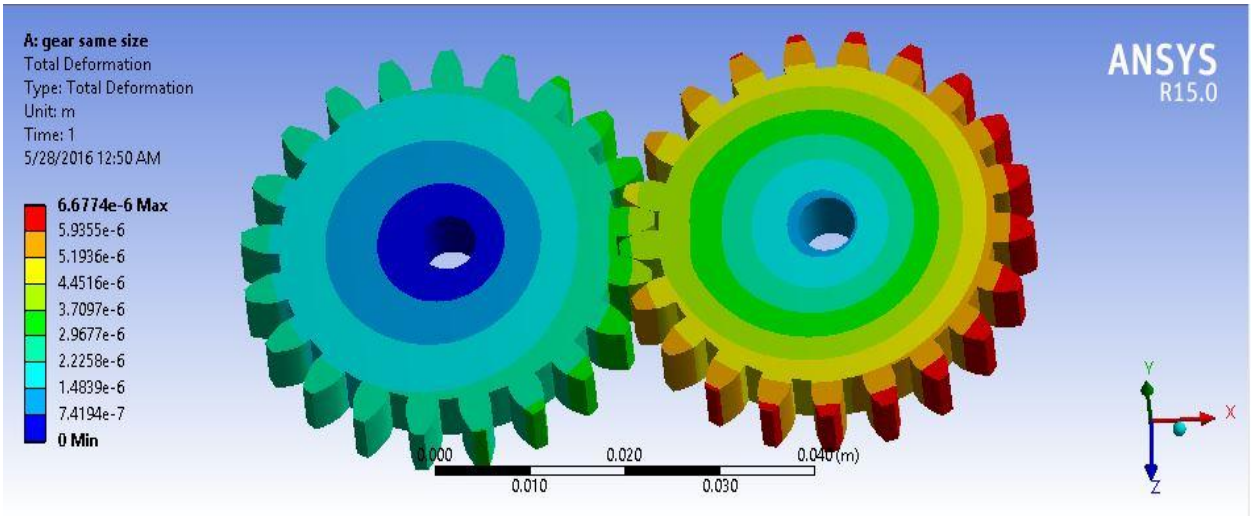

Figure 3.7: Displacement field in ANSYS Workbench 15.0 for spur gear (Both gears: Same size)

3.1.4 Results and Comparison

3.1.4.1 Both gears are of the same size and materials

Outside radius, r_a = 21.9048 mm

Base circle radius, r_{pb} = 18.79 mm

Moment/Torque T = 20 Nm

Mesh stiffness of gear pair at constant torque wrt position angle:

Table 3.2: Mesh stiffness of spur gear at constant torque pair wrt position angle

Angular position (Degree)	$S = r_a * \theta, 10^{-5}$ m	$\theta = \frac{S}{r_a}, 10^{-2}$ rad	$K_T = \frac{T}{\theta}$, Nm/rad	$K_m = \frac{K_t}{{r_{pb}}^2}$,10^6 N/m
-15.75	0.9845	0.044944030	44499.79	125.98
-15	1.0303	0.047035352	42521.20	120.38
-14.25	0.9733	0.044432270	45012.33	127.43
-13.5	0.9711	0.044331379	45114.77	127.72
-12.75	0.9747	0.044495726	44948.13	127.25
-12	0.9714	0.044345988	45099.90	127.68
-11.25	0.9733	0.044434096	45010.48	127.43
-10.5	0.9673	0.044159727	45290.13	128.22
-9.75	1.0037	0.045821007	43648.10	123.10

-9	1.3376	0.061064241	32752.39	92.72
-8.25	1.3173	0.060137504	33257.11	94.15
-7.5	1.2822	0.058535115	34167.52	96.73
-6.75	1.1916	0.054399035	36765.35	104.08
-6	1.1996	0.054764252	36502.17	103.39
-5.25	1.1759	0.053682297	37256.22	106.24
-4.5	1.1795	0.053846645	37142.51	105.15
-3.75	1.2009	0.054823600	36480.63	103.28
-3	1.2008	0.054819035	36483.67	103.29
-2.25	1.2109	0.055280121	36179.37	102.43
-1.5	1.1899	0.054321427	36817.88	104.23
-0.75	1.2826	0.058553376	34156.86	96.70
0	1.3355	0.060968372	32803.89	92.87
0.75	1.2988	0.059292940	33730.82	95.49
1.5	0.9847	0.044953617	44490.30	125.96
2.25	1.0328	0.047149483	42418.28	120.09
3	0.9739	0.044461031	44983.21	127.35
3.75	0.9737	0.044450074	44988.22	127.37
4.5	0.9730	0.044420401	45024.35	127.47
5.25	0.9706	0.044312205	45134.29	127.78
6	0.9734	0.044439118	45005.39	127.41
6.75	0.9661	0.044103575	45347.79	128.38
7.5	1.3286	0.060653372	32974.25	93.28
8.25	1.3396	0.611555450	32703.49	92.58
9	1.3190	0.060215112	33214.25	94.03
9.75	1.1960	0.054599905	36630.10	103.70
10.5	1.1921	0.054421861	36749.93	104.04
11.25	1.1993	0.054750556	36529.30	103.42
12	1.1764	0.053705123	37240.38	105.43
12.75	1.2009	0.054823600	36480.63	103.07
13.5	1.2022	0.054882948	36441.19	103.17
14.25	1.2008	0.054819035	36483.67	103.29
15	1.1971	0.054650122	36596.44	103.61
15.75	1.1907	0.054579480	36778.57	104.12

The mesh stiffness of the gear pair having both gears of the same size is varied during the rotation of the gears as shown in figure 3.8.

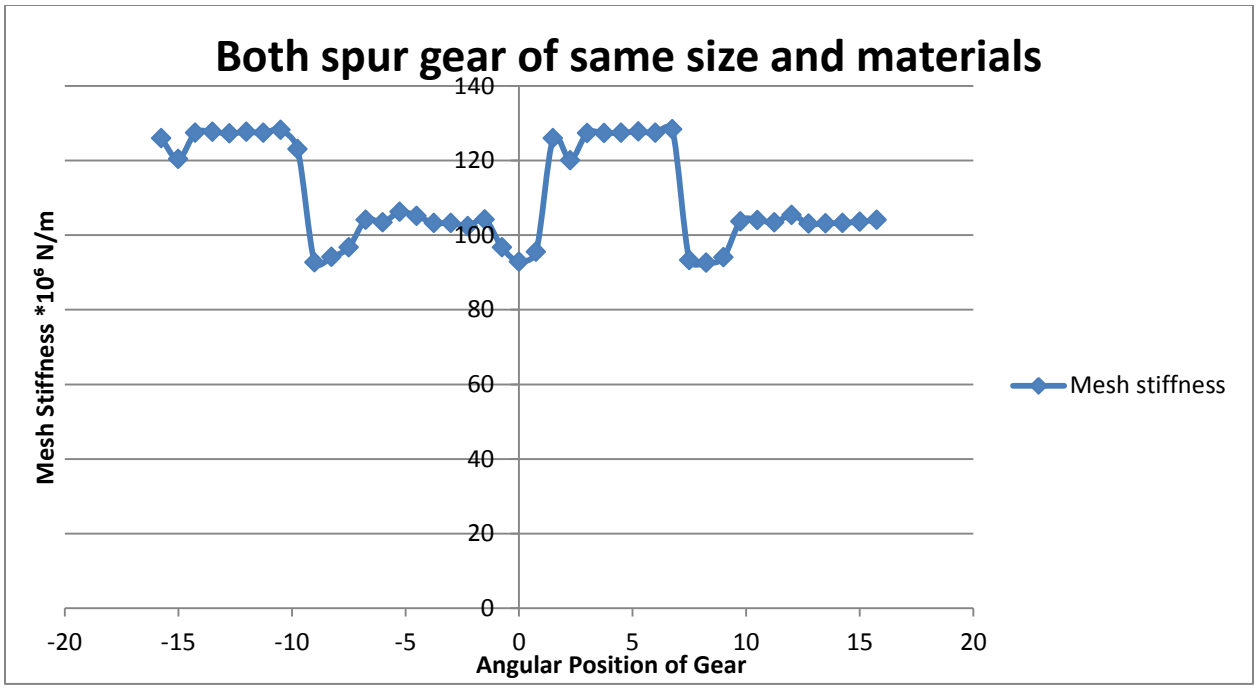

Figure 3.8: Mesh stiffness vs. angular position (Both gears: Same size)

3.1.4.2 Both gears are of different size but same materials

By applying same boundary condition as shown earlier to find gear mesh stiffness.

Outside radius of pinion, r_a = 21.9048 mm

Base circle radius of pinion, r_{pb} = 18.79 mm

Mesh stiffness of gear pair at constant torque wrt position angle:

Moment/Torque T = 20 N/m

Table 3.3: Mesh stiffness of spur gear pair at constant torque wrt position angle

Angular position (Degree)	$S = r_a * \theta, 10^{-5}$ m	$\theta = \frac{S}{r_a}, 10^{-2}$ rad	$K_T = \frac{T}{\theta}$, Nm/rad	$K_m = \frac{K_t}{{r_{pb}}^2}$,10^6 N/m
-7	1.7230	0.078658558	25426.34	71.98
-6.5	1.7403	0.079448340	25173.59	71.27
-6	1.7288	0.078923341	25341.04	71.74
-5.5	1.7141	0.078252255	25558.36	72.36
-5	1.4019	0.063999671	31250.16	88.47
-4.5	1.4184	0.064752930	30886.63	87.44

-4	1.404	0.064095540	31203.41	88.34
-3.5	1.9884	0.090774624	22032.58	62.37
-3	2.0601	0.094047879	21265.76	60.20
-2.5	1.9857	0.090651364	22062.54	62.46
-2	2.0259	0.092486578	21624.75	61.22
-1.5	2.0101	0.091765275	21794.73	61.70
-1	2.0415	0.093198750	21459.51	60.75
-0.5	2.0089	0.091710492	21807.75	61.74
0	1.4424	0.065848581	30372.71	85.99
0.5	1.4239	0.065004017	30767.32	87.10
1	1.4382	0.065656842	30461.41	86.24
1.5	1.7236	0.078685950	25417.49	71.96
2	1.7159	0.079530513	25147.58	71.19
2.5	1.7345	0.079183557	25257.76	71.50
3	1.7159	0.078334428	25531.55	72.28
3.5	1.4011	0.063963149	31268.00	88.52
4	1.4062	0.064195975	31154.60	88.20
4.5	1.3940	0.063639019	31427.26	88.97
5	1.9860	0.090665059	22059.21	62.45
5.5	2.0501	0.093591358	21369.49	60.50
6	2.0296	0.092655491	21585.33	61.11
6.5	2.0359	0.099430990	21518.54	60.92
7	2.0356	0.092929403	21521.71	60.93

The mesh stiffness of the gear pair having both gears of the different size is varied during the rotation of the gears as shown in figure 3.9.

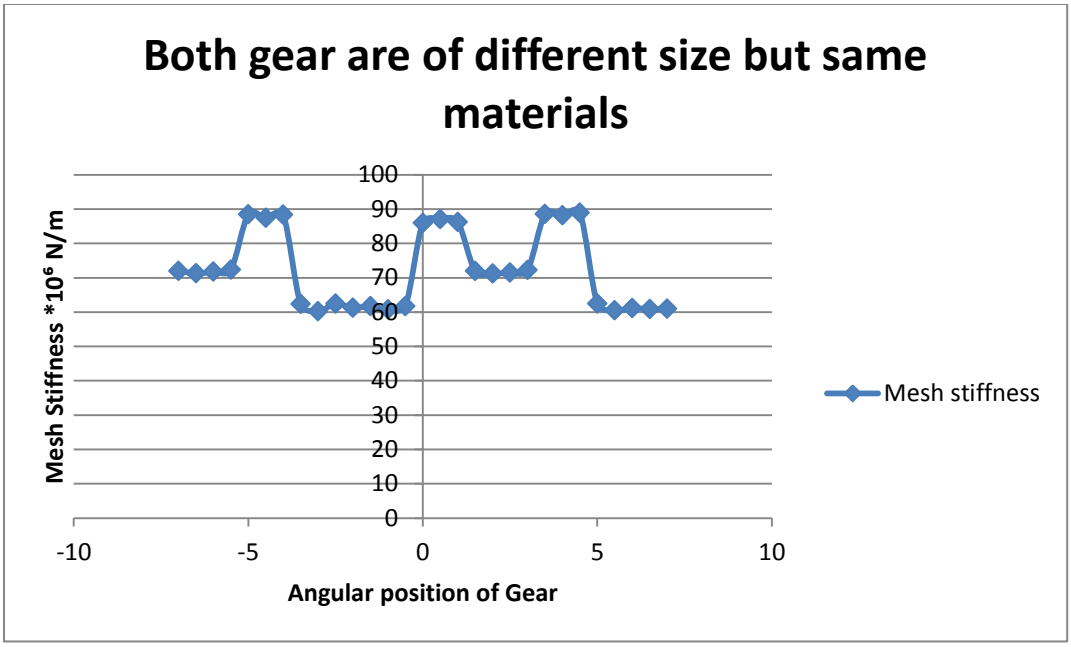

Figure 3.9: Mesh stiffness vs. Angular position (Both gears: Different size)

3.1.4.3 Comparison

Obtained result compares with the one that calculated from the equation provided in the literature. Spott's (1985) provided an equation for the gear to calculate average mesh stiffness of gear pair.

Average gear mesh stiffness obtained:

1. Both gears are of same size and material:

$$K_m = 110.30 \text{ MN/m}$$

2. Both gears are of different size but same materials:

$$K_m = 74 \text{ MN/m}$$

3. By using Scott's equation of average mesh stiffness:

$$K_m = \frac{b}{9} * \frac{E_1 * E_2}{E_1 + E_2} \quad (3.9)$$

$$= 66.66 \text{ MN/m}$$

Where,

E_1 = Elastic modulus of 1st gear = 200 GPa

E_2 = Elastic modulus of 2nd gear = 200 GPa

4. By using modified Spott's equation of average mesh stiffness:

$$K_m = \text{C.R.} * \frac{b}{9} * \frac{E_1 * E_2}{E_1 + E_2} \quad (3.10)$$

$$= 104 \text{ MN/m}$$

Where,

C.R. = Contact ratio = 1.56

From the above results, it is verified that Spott's equation of average mesh stiffness can be used in the calculation of mesh stiffness of the gear pair, and it gives an approximate value of the mesh stiffness.

3.2 Gear Mesh Stiffness Calculation for Bevel gear

3.2.1 Methodology

Gear mesh stiffness of bevel gear can also be correlated with torsional mesh stiffness by the same equation as used in case of the spur gear.

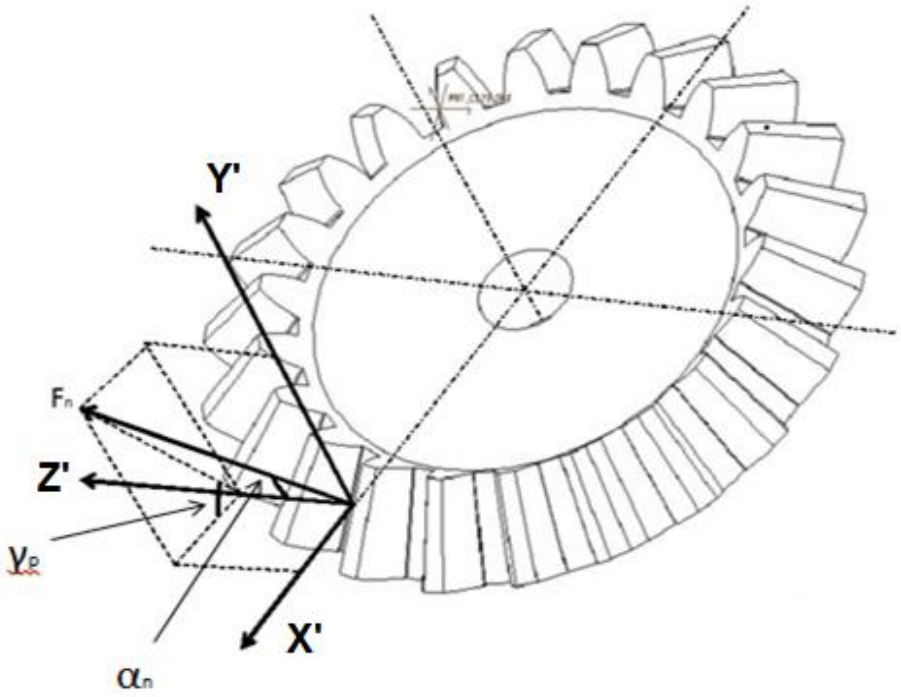

Figure 3.10: Bevel gear force component

K_m is mesh stiffness along the line of action or in the direction of F_n . Three component of the mesh stiffness can be resolved along X', Y' and Z' which gives axial, radial and tangential component K_m respectively.

The component of mesh stiffness in the direction of Z' is K_z, which gives tangential or torsional gear mesh stiffness of bevel gear which yields following equation (3.11).

$$K_z = K_m \cos(\alpha_n) \tag{3.11}$$

Where

α_n = Pressure angle

γ_p = Pinion pitch angle/semi cone angle of pinion gear

r_b = Base circle radius of pinion

K_z = Component of mesh stiffness in z direction, N/m

T = Torque/moment, Nm

θ = Angular deflection, rad

F_n = Normal force ,N

F_t = Tangential force on gear ,N

K_m = Mesh stiffness , N/m

K_t = Torsional stiffness , Nm/rad

By rewriting above equation.

$$K_m = \frac{K_z}{\cos(\alpha_n)}$$

$$K_m = \frac{F_t}{r_b * \theta * \cos(\alpha_n)} \tag{3.12}$$

Where,

r_b*θ = linear deflection in tangential direction, m

Normal force Fn can be related to tangential by equation (3.13).

$$F_n = \frac{F_t}{\cos(\alpha_n)} \tag{3.13}$$

By rewriting equation (3.12) the equation of K_m yields as below

$$K_m = \frac{F_n}{r_b * \theta} \tag{3.14}$$

$$K_m = \frac{F_n * rb}{{r_b}^2 * \theta}$$

$F_n * r_b = T$ = Applied torque, Nm

$$K_m = \frac{T}{{r_b}^2 * \theta} \quad (3.15)$$

So that linear tooth mesh stiffness can be written as the ratio of torsional mesh stiffness and square of base circle radius of the pinion.

$$K_m = \frac{K_T}{{r_{pb}}^2} \quad (3.16)$$

3.2.2 Modeling of Bevel Gear Using Creo Parametric 2.0

By using the first method for construction of finite element model, A CAD model of bevel gear is constructed in Creo Parametric 2.0 using parameter given in Table 3.4.

All dimension are in mm

PA = Pressure angle = 20°

Table 3.4: Parameter used to construct Bevel Gear in Creo Parametric 2.0

Parameter	Both gear of same size and material
Pitch Circle Diameter (D)	40
Base Circle Diameter(D_b = D * cos(PA))	37.5877
Number Of Teeth,(N)	22
Diametric Pitch ,(P)	0.55
Pitch angle of i^{th} gear, γi =tan ⁻¹(Np/Ng)	45
Addendum , (a =1/P)	1.818
Outside Diameter , (D_o = D +2a)	43.636
Circular Pitch , (p = 3.1416/P)	5.984
Whole Depth, (h_t = 2.188/P) + 0.002	3.980
Dedendum ,(b = h_t –a)	2.162
Root Diameter ,(D_r = D -2b)	35.676
Gear thickness	6

CAD model of the bevel gear system created using Creo Parametric 2.0 is shown in figure 3.11.

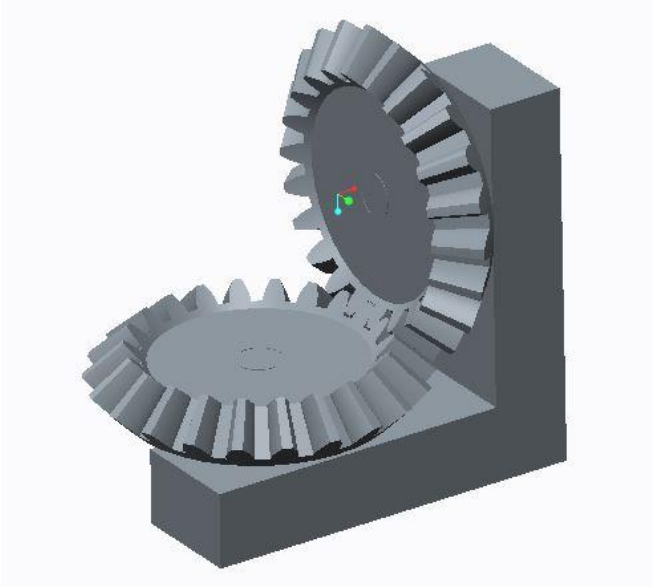

Figure 3.11: CAD model of bevel gear (Both gears: Same size)

3.2.3 Boundary Conditions, Loads, and Displacement Field

For this research, The boundary conditions and loads should be applied as such: Pinion – restrict all DOFs except the rotational degree of freedom. Gear – completely restrict all DOF. The only load that applies to the model is the input torque(as shown in fig. 3.12), and it is applied on the pinion.

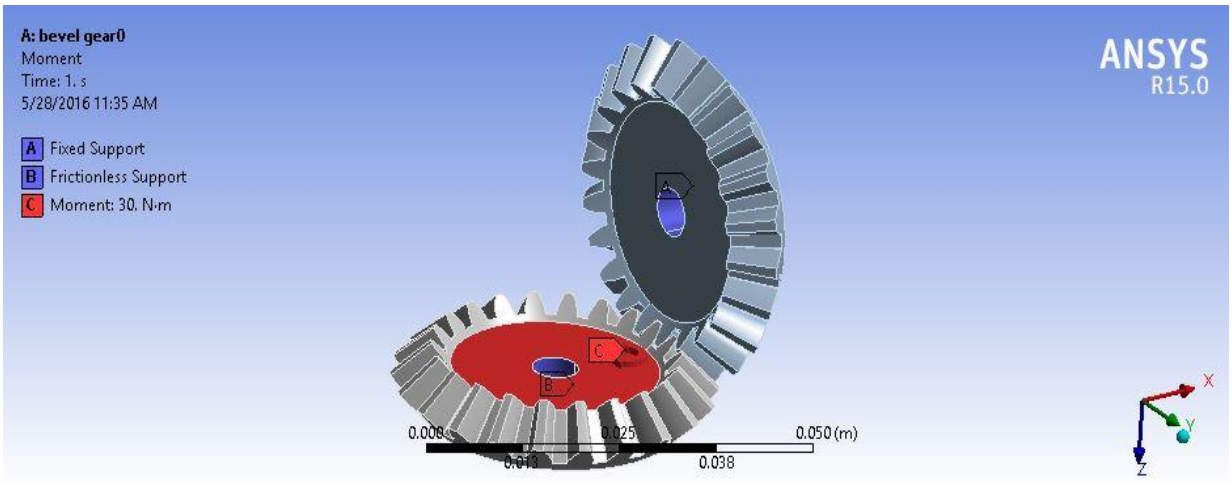

Figure 3.12: Boundary conditions in ANSYS Workbench 15.0 for bevel gear (Both gears: Same size)

By applying above boundary conditions, ANSYS obtain the result in the form of displacement field as shown in figure 3.13. A displacement field in ANSYS is used to calculate mesh stiffness by the procedure explained earlier.

Displacement field for:

Moment = 30 Nm

Position = 0 $^{\circ}$

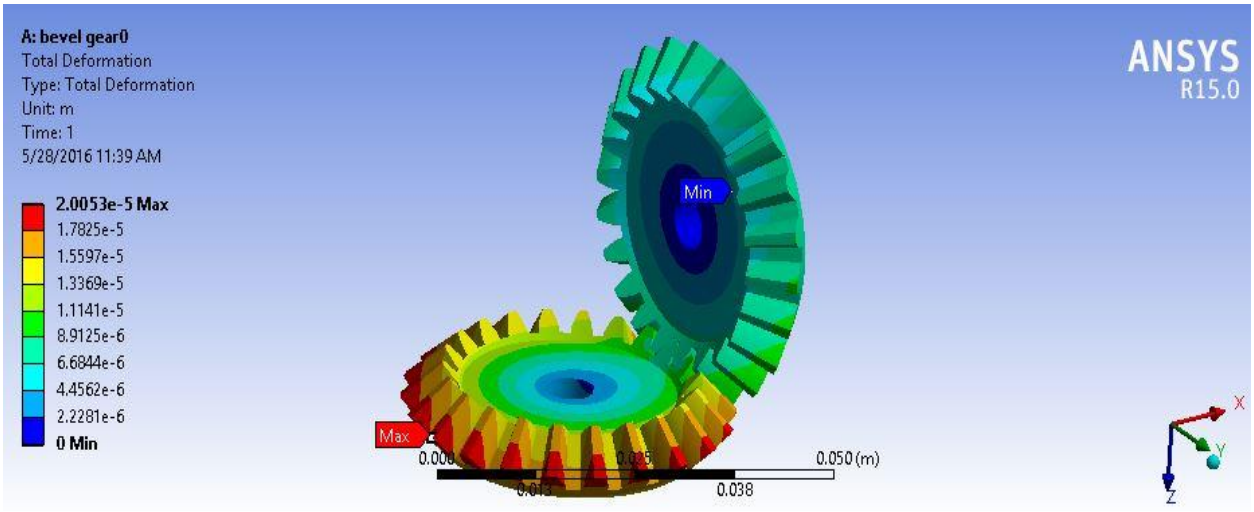

Figure 3.13: Displacement field in ANSYS Workbench 15.0 for bevel gear (Both gears: Same size)

3.2.4 Results and Comparison

3.2.4.1 Both gears are of the same size and materials

Outside radius, r_a = 21.2855 mm

Base circle radius, r_{pb} = 18.7938 mm

Moment T = 20 Nm

Mesh stiffness of bevel gear pair at constant torque wrt position angle:

Table 3.5: Mesh stiffness of bevel gear pair at constant torque wrt position angle

Angular position (Degree)	$S = r_a * \theta, 10^{-5}$ m	$\theta = \frac{S}{r_a}, 10^{-2}$ rad	$K_m = \frac{K_t}{{r_{pb}}^2}$,10^6 N/m
15	1.4196	0.066693226	84.90
14	1.2468	0.058575031	96.66
13	1.2425	0.058373016	97.00
12	1.2465	0.058560937	96.69
11	1.2866	0.060444847	93.67
10	1.2669	0.059519335	95.13
9	1.2755	0.059923365	94.49
8	1.2733	0.059820009	94.65
7	1.2436	0.058424694	96.91
6	1.2443	0.058457580	96.86
5	1.2382	0.058171000	97.34
4	1.2406	0.058283753	97.15
3	1.2433	0.058410600	96.94
2	1.2512	0.058781744	96.32
1	1.2783	0.060054910	94.28
0	1.4201	0.066716716	84.87
-1	1.4217	0.066791884	84.77
-2	1.4224	0.066824771	84.73
-3	1.4146	0.066458324	85.20
-4	1.2433	0.058410600	96.94
-5	1.2380	0.058161604	97.35
-6	1.2410	0.058302545	97.12
-7	1.2703	0.059679068	94.88
-8	1.2653	0.059444166	95.25
-9	1.2541	0.058917987	96.10
-10	1.2381	0.058166302	97.34
-11	1.2386	0.058067644	97.30
-12	1.2381	0.058166302	97.34
-13	1.2413	0.058316639	97.09
-14	1.4205	0.066735508	84.84
-15	1.4238	0.066890543	84.65
-16	1.4212	0.066768394	84.80
-17	1.4221	0.066810677	84.75
-18	1.4250	0.066946919	84.58
-19	1.4161	0.066528795	85.11
-20	1.2451	0.058495164	96.80

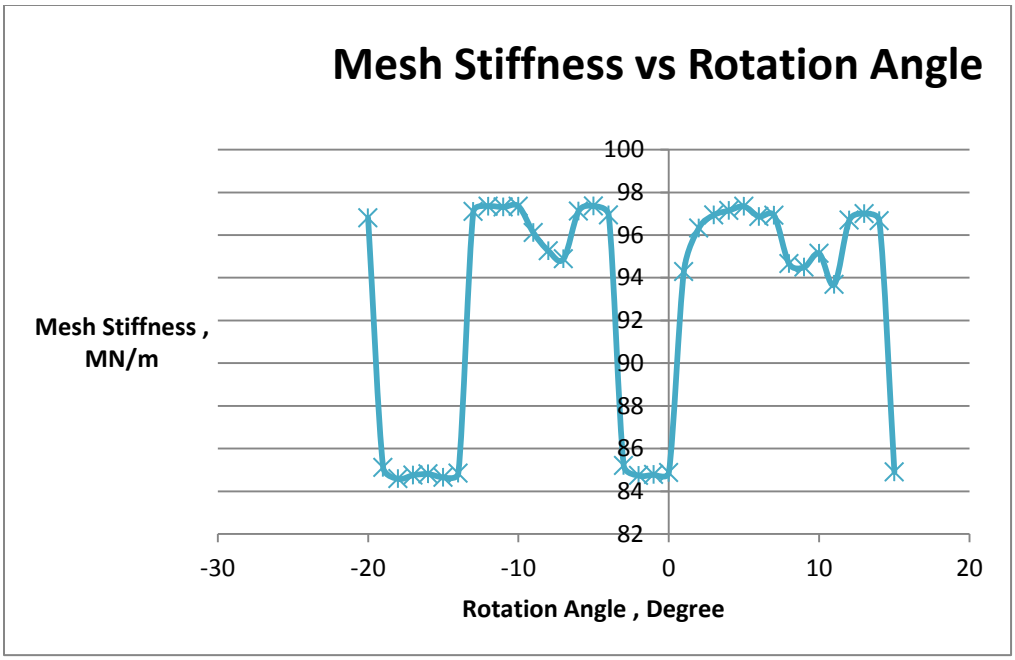

Figure 3.14: Mesh stiffness vs. Angular position (Both gears are of differ ent size)

From the figure 3.14 it is clear that value of average gear mesh stiffness for the bevel gear is low compared to spur gear having same pitch diameter.

3.2.4.2 Comparison

Obtained result compares with the one that calculated from the equation provided in the literature. Spott's (1985) provided an equation for the gear to calculate average mesh stiffness of gear pair.

Average gear mesh stiffness obtained:

1. Both gears are of same size and material:

$$K_m = 110.30 \text{ MN/m}$$

2. By using modify Spott's equation of average mesh stiffness:

$$K_m = \text{C. R.} * \frac{b}{9} * \frac{E_1 * E_2}{E_1 + E_2} = 104 \text{ MN/m}$$

Above result can modify Spott's equation of average gear mesh stiffness for bevel gear as:

$$K_m = 0.9 * \text{C. R.} * \frac{b}{9} * \frac{E_1 * E_2}{E_1 + E_2} \quad (3.17)$$

4 Modeling of Gear Disk

This chapter contains a modelling of gear disk in different coordinate systems used in helical and bevel gear system in later chapters as gear is assumed as a disk on the shaft.

4.1 Modelling of Gear Disk

The equations of motion of the simple rotor system are available in reference (Childs, 1993). This approach uses Lagrangian for the derivation of equations of motions. The Lagrangian formulation is given by equation 4.1.

$$\frac{d}{dt}\left(\frac{\partial L}{\partial \dot{q}^i}\right) - \frac{\partial L}{\partial q^i} = D_i \tag{4.1}$$

$$L = T - V \tag{4.2}$$

$$\{q\} = \{x, y, z, \theta_x, \theta_y, \theta_z\}^T \tag{4.3}$$

Where,

D = generalized forces

L = Lagrangian function

q = generalize coordinates

T = kinetic energy

V = potential energy

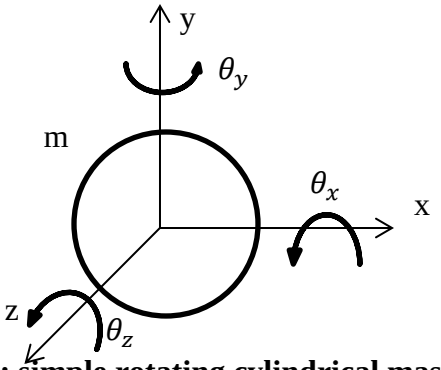

Figure 4.1: simple rotating cylindrical mass system

A single cylindrical mass contains 6 DOFs provides a most general model (as shown in fig. 4.1), applicable to any system. Rotating shaft in system may not have the same orientation. Some shafts may be vertical, or may be inclined at some angle with horizontal.

Equations 4.4 and 4.5 give the expressions for total kinetic energy (T) and potential energy (V):

$$T = \frac{1}{2}\left[m\left(\dot{x}^2 + \dot{y}^2 + \dot{z}^2\right) + I_t\left(\dot{\theta}_x{}^2 + \dot{\theta}_y{}^2\right) + I_p\dot{\theta}_z{}^2 + I_p\left(\Omega^2 - 2\Omega\dot{\theta}_y\theta_x\right)\right] \quad (4.4)$$

$$V = \frac{1}{2}\left[k_x x^2 + k_y y^2 + k_z z^2 + K_{\theta x}\theta_x{}^2 + K_{\theta y}\theta_y{}^2 + K_{\theta z}\theta_z{}^2\right] \quad (4.5)$$

Where,

I_t = transverse mass moment of inertia

I_p = polar mass moment of inertia

m = mass of cylindrical shape

K_q = rotational elastic stiffness about x, y, and z-axes

k_q = translational elastic stiffness about x,y. and z-axes

Ω = rotating speed of cylindrical mass

From the above equations, equations of motion for the 6-DOF system can be obtained as below.

$$m\ddot{x} + k_x x = F_x$$

$$\text{m}\ddot{\text{y}} + k_y y = F_y$$

$$\text{m}\ddot{\text{z}} + k_z z = F_z$$

$$I_t\ddot{\theta}_x + \Omega I_p\dot{\theta}_y + K_{\theta x}\theta_x = M_x \quad (4.6)$$

$$I_t\ddot{\theta}_y - \Omega I_p\dot{\theta}_x + K_{\theta y}\theta_y = M_y$$

$$I_p\ddot{\theta}_z + K_{\theta z}\theta_z = M_z$$

In form of matrix,

$$[M]\{\ddot{q}\} + [G]\{\dot{q}\} + [K]\{q\} = \{F\} \quad (4.7)$$

$$[M] = \begin{bmatrix} m & 0 & 0 & 0 & 0 & 0 \\ 0 & m & 0 & 0 & 0 & 0 \\ 0 & 0 & m & 0 & 0 & 0 \\ 0 & 0 & 0 & I_t & 0 & 0 \\ 0 & 0 & 0 & 0 & I_t & 0 \\ 0 & 0 & 0 & 0 & 0 & I_p \end{bmatrix}, \quad [K] = \begin{bmatrix} k_x & 0 & 0 & 0 & 0 & 0 \\ 0 & k_y & 0 & 0 & 0 & 0 \\ 0 & 0 & k_z & 0 & 0 & 0 \\ 0 & 0 & 0 & K_{\theta x} & 0 & 0 \\ 0 & 0 & 0 & 0 & K_{\theta y} & 0 \\ 0 & 0 & 0 & 0 & 0 & K_{\theta z} \end{bmatrix}$$

$$[G] = \begin{bmatrix} 0 & 0 & 0 & 0 & 0 & 0 \\ 0 & 0 & 0 & 0 & 0 & 0 \\ 0 & 0 & 0 & 0 & 0 & 0 \\ 0 & 0 & 0 & 0 & \Omega I_p & 0 \\ 0 & 0 & 0 & -\Omega I_p & 0 & 0 \\ 0 & 0 & 0 & 0 & 0 & 0 \end{bmatrix}$$

Where,

[M] = mass matrix

[K] = stiffness matrix

[G] = gyroscopic matrix

{F} = force/moment vector

The coupling between θ_x and θ_y represent the gyroscopic moment effect on the system. The terms used in gyroscopic effect is similar to damping, but it does not cause any energy loss as it is conservative. The gyroscopic effect on the system is directly proportional to its speed.

As the coordinates system used in another system may not be the same as the one used here so according to the coordinates system used, mass, stiffness and a gyroscopic matrix of the system will change.

Matrices for two other coordinates system used later in this work is shown in figure 4.2 and figure 4.4,

1.

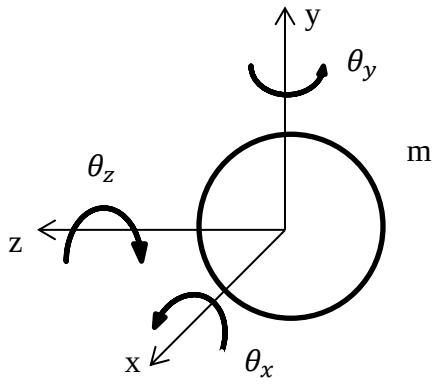

Figure 4.2 Coordinate system used later in jth gear of bevel gear system

$$[M] = \begin{bmatrix} m & 0 & 0 & 0 & 0 & 0 \\ 0 & m & 0 & 0 & 0 & 0 \\ 0 & 0 & m & 0 & 0 & 0 \\ 0 & 0 & 0 & I_p & 0 & 0 \\ 0 & 0 & 0 & 0 & I_t & 0 \\ 0 & 0 & 0 & 0 & 0 & I_t \end{bmatrix}, \quad [K] = \begin{bmatrix} k_x & 0 & 0 & 0 & 0 & 0 \\ 0 & k_y & 0 & 0 & 0 & 0 \\ 0 & 0 & k_z & 0 & 0 & 0 \\ 0 & 0 & 0 & K_{\theta x} & 0 & 0 \\ 0 & 0 & 0 & 0 & K_{\theta y} & 0 \\ 0 & 0 & 0 & 0 & 0 & K_{\theta z} \end{bmatrix}$$

$$[G] = \begin{bmatrix} 0 & 0 & 0 & 0 & 0 & 0 \\ 0 & 0 & 0 & 0 & 0 & 0 \\ 0 & 0 & 0 & 0 & 0 & 0 \\ 0 & 0 & 0 & 0 & 0 & 0 \\ 0 & 0 & 0 & 0 & 0 & \Omega I_p \\ 0 & 0 & 0 & 0 & -\Omega I_p & 0 \end{bmatrix}$$

2.

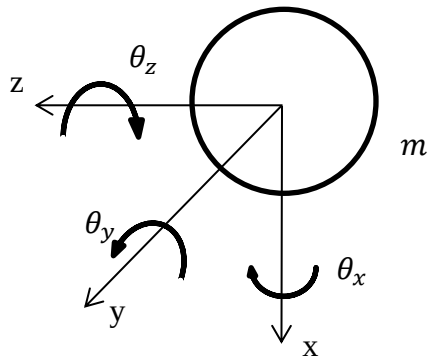

Figure 4.2 Coordinate system used later in ith gear of bevel gear system

$$[M] = \begin{bmatrix} m & 0 & 0 & 0 & 0 & 0 \\ 0 & m & 0 & 0 & 0 & 0 \\ 0 & 0 & m & 0 & 0 & 0 \\ 0 & 0 & 0 & I_t & 0 & 0 \\ 0 & 0 & 0 & 0 & I_p & 0 \\ 0 & 0 & 0 & 0 & 0 & I_t \end{bmatrix}, \quad [K] = \begin{bmatrix} k_x & 0 & 0 & 0 & 0 & 0 \\ 0 & k_y & 0 & 0 & 0 & 0 \\ 0 & 0 & k_z & 0 & 0 & 0 \\ 0 & 0 & 0 & K_{\theta x} & 0 & 0 \\ 0 & 0 & 0 & 0 & K_{\theta y} & 0 \\ 0 & 0 & 0 & 0 & 0 & K_{\theta z} \end{bmatrix}$$

$$[G] = \begin{bmatrix} 0 & 0 & 0 & 0 & 0 & 0 \\ 0 & 0 & 0 & 0 & 0 & 0 \\ 0 & 0 & 0 & 0 & 0 & 0 \\ 0 & 0 & 0 & 0 & 0 & -\Omega I_p \\ 0 & 0 & 0 & 0 & 0 & 0 \\ 0 & 0 & 0 & \Omega I_p & 0 & 0 \end{bmatrix}$$

When the finite element method applied to whole gear-shaft system it takes form same as equation 4.7.

$$[M]\{\ddot{q}\} + [D]\{\dot{q}\} + [K]\{q\} = \{F\} \tag{4.7}$$

$$[D] = [C] + \Omega[G]$$

[M], [G] and [K] are mass, gyroscopic and stiffness matrix in global coordinates system for Whole system of gear-shaft. These matrices are further broken into matrices of system components as follow.

$$\begin{aligned} [M] &= M_s + M_d \\ [G] &= G_s + G_d \\ [K] &= K_s + K_b + K_{mesh} \\ [C] &= C_s + C_b + C_{mesh} \end{aligned} \tag{4.8}$$

The subscript (s), designates the matrix corresponding to the rotor shaft. The subscript (d), designates the disk or gear. The subscript (b), designates a bearing matrix. The subscript (mesh), designates the matrix corresponds to gear-mesh. Appendix A lists all matrix formulation except for the mesh matrix.

5 Gear-Mesh Model Methodology with Application: Helical Gear

This chapter contains a methodology for deriving 12-DOF mesh stiffness matrix for helical and spur gear. This approach used technique proposed by Lao (1996) and it also includes some aspects presented by Choi (1993) and Blankenship (1995). Mesh stiffness matrix derived by resolving force and moments transmitted through gear. This chapter is reproduction of Stringer's (2008) work.

5.1 Gear-Mesh Model Methodology

5.1.1 Development of Gear Mesh Forcing Function

Figure 5.1 shows finite element representation of the gear-shaft system as suggested by Luo (1996).

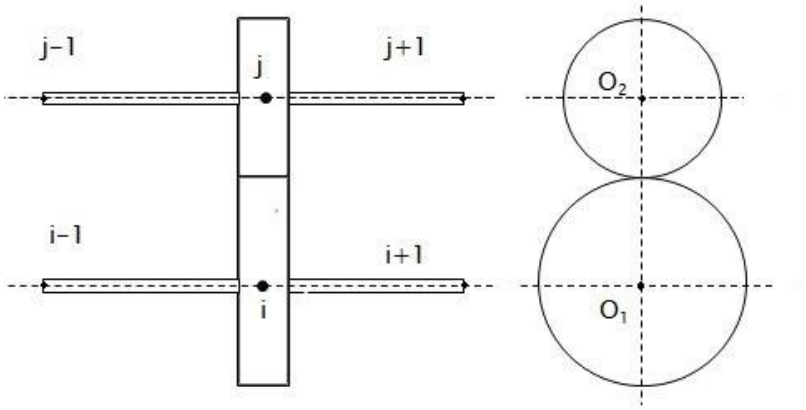

Figure 5.1: Finite element representation of a Gear Pair

The gear acts as a rigid disk on a flexible shaft. The two centers of gear O_1 and O_2 are assumed as a node i and j of the finite element analysis. A force and moment vector {F} can be modeled as function of a gear mesh stiffness matrix $[K]_{mesh}$ and displacement vector {q} acts on a node i and j.

$$\begin{Bmatrix} F_i \\ F_j \end{Bmatrix} = [K]_{mesh} \begin{Bmatrix} q_i \\ q_j \end{Bmatrix} = K_m \begin{bmatrix} [K_{ii}] & [K_{ij}] \\ [K_{ji}] & [K_{jj}] \end{bmatrix} \begin{Bmatrix} q_i \\ q_j \end{Bmatrix} \tag{5.1}$$

5.1.2 Geometry and Loading Conditions

The mesh is initially spring-mass-system, with spring along the line of action between two gears(as shown in fig. 5.2).The z-axis represents the axial direction of the gear. The line of action is a path of force transmission from one gear to another and is along a tangent line to both the gears.

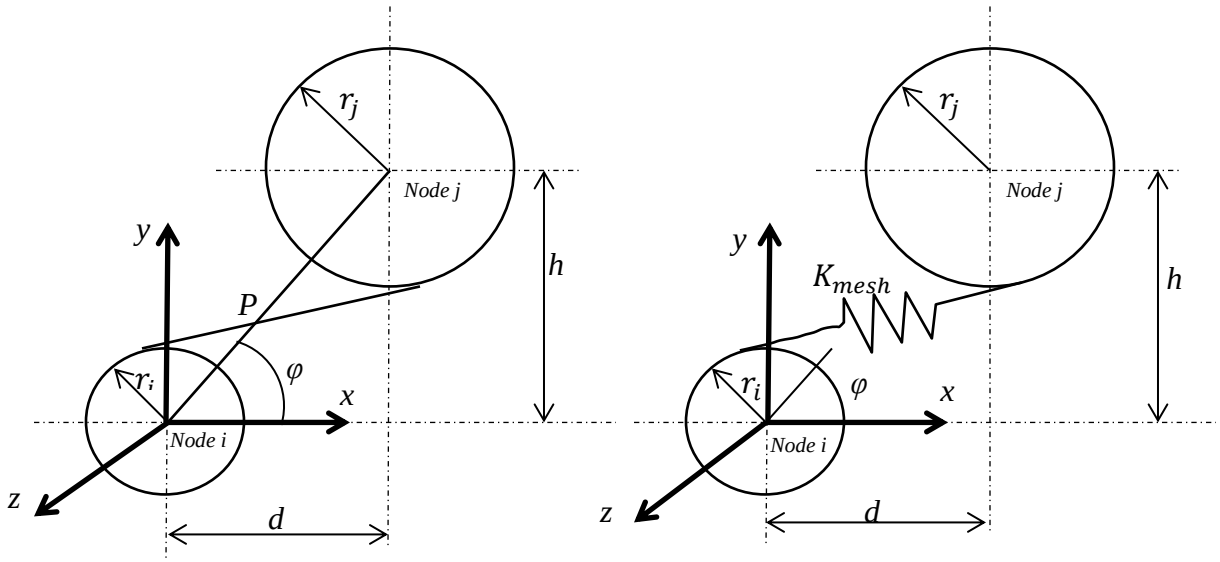

Figure 5.2: Gear-Mesh Spring-Mass Model (Stringer, 2008)

The intersection of the line of action and line connecting two centers of gears is defined as a pitch point, the effective point of force transmission between two gears. In spur gear, pitch point is a point of the concentrated load based on the uniform distribution of load along tooth width. In the case of helical gear load distribution is not uniform. Because of the inclination of the gear tooth amount of tooth contact during one mesh cycle is changing. From the beginning of mesh cycle, tooth contacts area increasing continuously until it reaches the point of the maximum contact area. Then contact area decreases during rest of cycle. Hence, contact load is maximum at the point of the maximum contact area. The primary objective of this analysis, the force transmission in helical gear is assumed to be at pitch point P.

The location of gear taken into consideration by height variable h. For example, gears might be employed horizontally (h=0), vertically ($h=r_i+r_j$) or any other orientation angle (φ). The height variable h is vertical distance between two centers of gears.

In this approach mesh stiffness is assume to be an average mesh stiffness derived from the experimental result or calculated using well-documented data.The value of average mesh stiffness of gear pair depends on materials of both gears. The geometry of the gear systems is related to mesh stiffness matrix by three variables: the helical angle (β), the orientation angle (φ), and the pressure angle (α_n). The orientation angle of the gear system is a function of height variable (h).

In many previous studies of the spur gear, the problem is two-dimensional because force act only in x-y plane and function of pressure angle (α_n). The problem becomes three dimensional while dealing with the helical gear. Force component is out of the x-y plane and is a function of both helical angle (β) and the pressure angle (α_n).

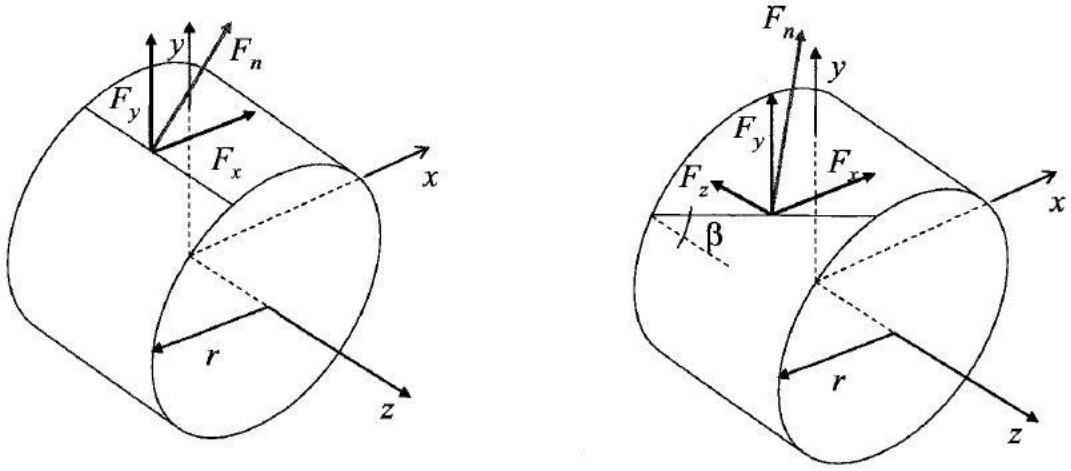

Figure 5.3: Spur (left) and Helical (right) Gear Force Contributions (Stringer, 2008)

In helical gear, three-dimensional force components are a function of direction cosine as illustrated in figure 5.4. The direction cosine angle can be written in the form of helical angle (β) and the pressure angle (α_n). The force components along x', y' and z' axes are determined by equations 5.2. The role of prime coordinates (x' ,y', and z') will discuss later.

$$\begin{aligned} F_{x'} &= F_n cos\phi_x \\ F_{y'} &= F_n cos\phi_y \\ F_{z'} &= F_n cos\phi_z \end{aligned} \tag{5.2}$$

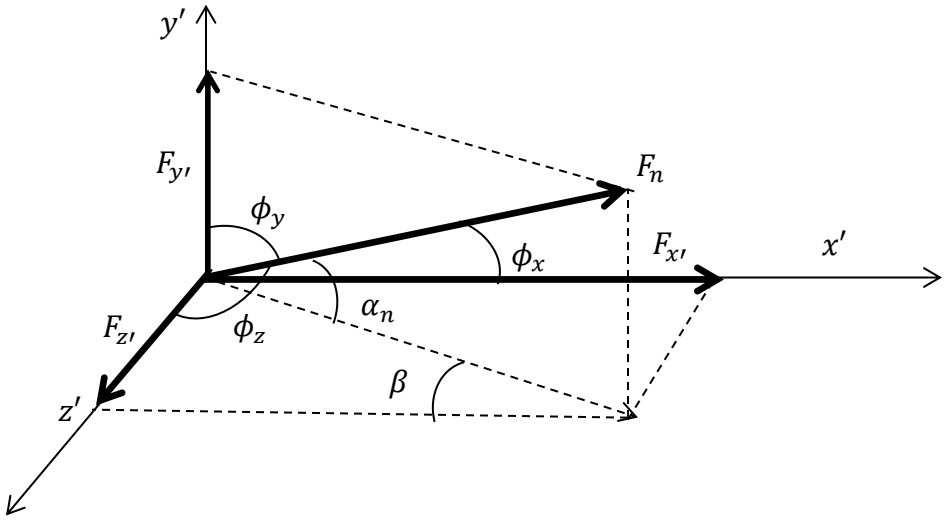

Figure 5.4 Mesh Force Component and Direction Cosines

Where,

$$cos\phi_x = cos\beta\ cos\alpha_n$$
$$cos\phi_y = sin\alpha_n \quad (5.3)$$
$$cos\phi_z = sin\beta\ cos\alpha_n$$

The equation relating the force vector to displacement vector is

$$\{F\}_{mesh} = -[K]_{mesh}\{u\}_{LOA} \quad (5.4)$$

The negative sign implies that forces and moments acting on the gear body are in the direction of positive displacement.In other word force function in global coordinates system can be brought to the left-hand side in the form of the stiffness matrix.

5.1.3 Gear-Mesh Coordinates System

The prime coordinate axes (x', y', and z') in figure 5.5 are local to pitch point. The prime coordinates axes are not necessary parallel with the global coordinate system. The prime coordinates depend on orientation angle (φ) of the gear pair. The pressure angle and helical angle fix the force vector on gear tooth. The geometry of tooth fixes the prime coordinates system at pitch point such that prime coordinate system is fixed and unchanging. The force vector must also be fixed in term of orientation angle to include the height of gears system. Suppose the

orientation angle of the gear system is allowed to vary such that orientation angle is allowed to sweep one full revolution, the prime coordinates axis appears to rotate about the center of the i^{th} gear. For example at φ = π/2 and φ = 3π/2, two coordinates systems are parallel to each other although the direction of axes between two value are reversed only z-axis remain parallel with global axes at any orientation.

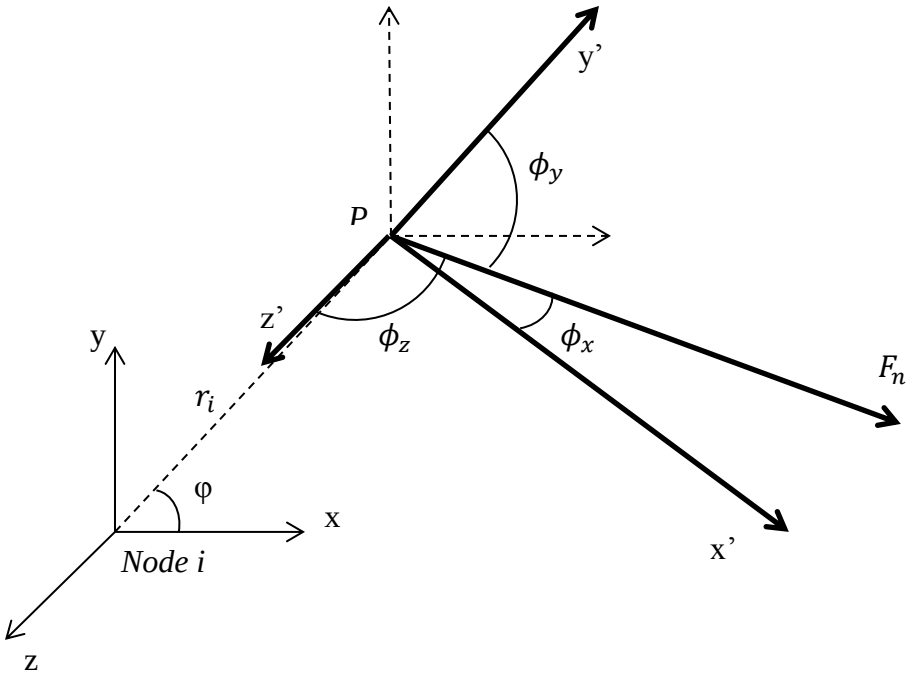

Figure 5.5: Relation of Local and Global Axes with φ (Stringer, 2008)

As seen in Figure 5.5, a force component in the direction of the prime coordinate axis x' has components in both x and y-direction of global coordinates system. Similarly the force component in the direction of prime coordinate axis y' has a component in both x and y-direction of global coordinates system.

5.1.4 Force and Moment Nodal Equations

The component of force acting on the node (i) in the direction of the global coordinate system are given by equation 5.5. The moment equation about the node (i) can be determined by multiplying the force components and moments arm about respective axes.

$$F_{xi} = F_{x'} sin\varphi + F_{y'} cos\varphi$$

$$F_{yi} = -F_{x'} cos\varphi + F_{y'} sin\varphi \quad (5.5)$$

$$F_{zi} = F_{z'}$$

Moment equations,

$$M_{xi} = F_{zi}\, r_i\, sin\varphi$$
$$M_{yi} = -F_{zi}\, r_i\, cos\varphi \quad (5.6)$$
$$M_{zi} = F_{yi}\, r_i cos\varphi - F_{xi}\, r_i\, sin\varphi$$

The force components acting on the node (j) are equal and opposite to those acting on the node (i) due to equilibrium condition of forces. The moments about the node (j) are equal and opposite to moments about the node (i) only if the gear ratio is unity. The forces and moments equation for node (j) can be written as,

$$F_{xj} = -F_{xi}$$
$$F_{yj} = -F_{yi} \quad (5.7)$$
$$F_{zj} = -F_{zi}$$
$$M_{xj} = F_{zj}\, r_j\, sin\varphi$$
$$M_{yj} = -F_{zj}\, r_j\, cos\varphi \quad (5.8)$$
$$M_{zj} = F_{yj}\, r_j cos\varphi - F_{xj}\, r_j\, sin\varphi$$

5.1.5 Displacement Method

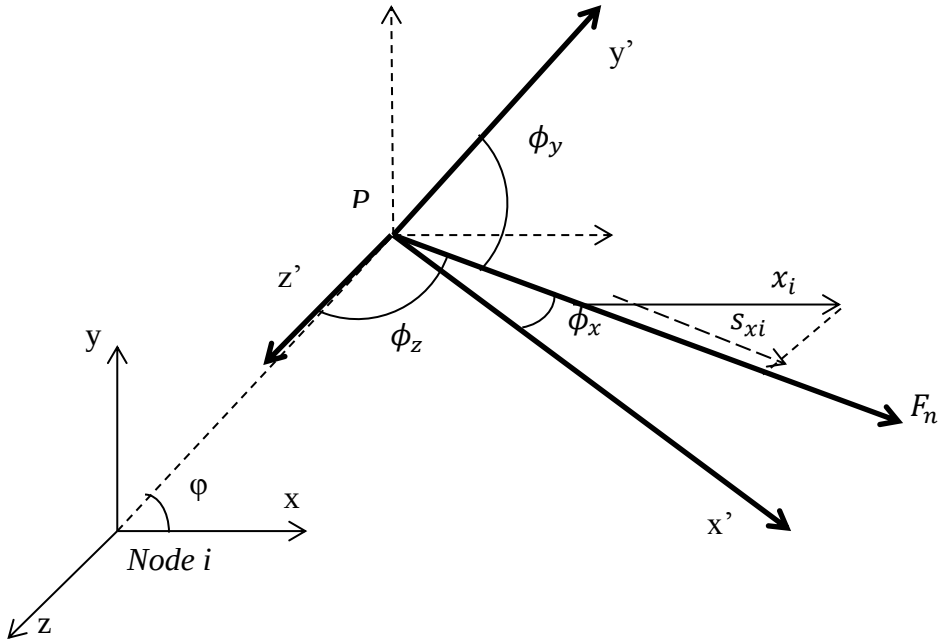

Figure 5.6: Contribution of x-displacement to the Line-of-Action (Stringer, 2008)

Each DOF contributes to shifting pitch point along the line of action of the gear pair. Summation of the contribution of all DOF will give a total shift of pitch point along the line of action. The effect of translation along the x-axis is considered in figure 5.6. A positive displacement of the node (i) or (j) along x-direction result in positive component along the line of action.

The effect of translational motion along the three axes will shift pitch point in the direction of motion. In the case of rotational displacement, a rotational motion about an axis will rotate pitch point in a circular arc about a respective axis. The circular arc represents motion in two directions. Figure 5.7 represent the effect of rotational motion on shifting pitch point.

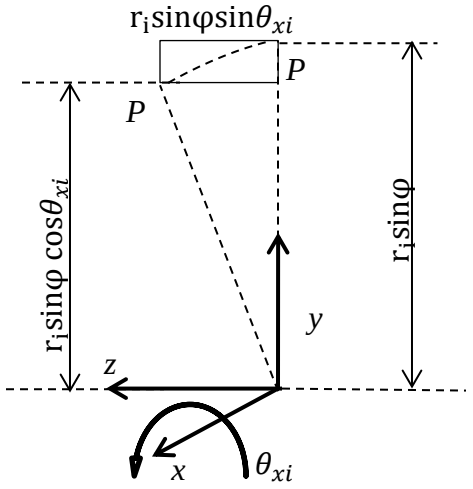

Figure 5.7: Contribution of rotational motion about x_i to rotate pitch point

The displacement method applied to each gear, resulting in 12-DOF displacement model. The pitch point displacement can be resolve in global coordinates through two coordinates transformation. The pressure angle and helical angle fix the components to the prime coordinates system located on the pitch circle, and the orientation angle fixes the prime coordinate system to global coordinates system. The displacement method resulting equation 5.9 to 5.11.

$$s_{xi} = x_i\left(sin\varphi cos\phi_x + cos\varphi cos\phi_y\right)$$
$$s_{xj} = x_j\left(sin\varphi cos\phi_x + cos\varphi cos\phi_y\right) \quad (5.9)$$

$$s_{yi} = y_i\left(sin\varphi cos\phi_y - cos\varphi cos\phi_x\right)$$
$$s_{yj} = y_j\left(sin\varphi cos\phi_y - cos\varphi cos\phi_x\right) \quad (5.10)$$

$$s_{zi} = z_i cos\phi_z$$
$$s_{zj} = z_j cos\phi_z \quad (5.11)$$

the rotational motion displacement is presented regarding (x), (y), and (z)

For rotation about (x):

$$y_i = r_i sin\varphi(cos\theta_{xi} - 1)$$
$$y_j = r_j sin\varphi(1 - cos\theta_{xj}) \quad (5.12)$$

$$z_i = r_i sin\varphi sin\theta_{xi}$$
$$z_j = -r_j sin\varphi sin\theta_{xj} \quad (5.13)$$

For rotation about (y):

$$x_i = r_i cos\varphi(cos\theta_{yi} - 1)$$
$$x_j = r_j cos\varphi(1 - cos\theta_{yj}) \quad (5.14)$$

$$z_i = -r_i cos\varphi sin\theta_{yi}$$
$$z_j = r_j cos\varphi sin\theta_{yj} \quad (5.15)$$

For rotation about (z):

$$x_i = -r_i cos\varphi + r_i \cos(\varphi + \theta_{zi})$$
$$x_j = r_j cos\varphi - r_j \cos(\varphi + \theta_{zj}) \quad (5.16)$$

$$y_i = -r_i sin\varphi + r_i \sin(\varphi + \theta_{zi})$$
$$y_j = r_j sin\varphi - r_j \sin(\varphi + \theta_{zj}) \quad (5.17)$$

Because of the assumption of small angle equation 5.12 to 5.17 can be written as below,

For rotation about (x):

$$z_i = r_i \theta_{xi} sin\varphi$$
$$z_j = -r_j \theta_{xj} sin\varphi \quad (5.18)$$

For rotation about (y):

$$z_i = -r_i\theta_{yi}cos\varphi$$
$$z_j = r_j\theta_{yj}cos\varphi \tag{5.19}$$

For rotation about (z):

$$x_i = -r_i\theta_{zi}sin(\varphi)$$
$$x_j = r_j\theta_{zj}sin(\varphi) \tag{5.20}$$

$$y_i = r_i\theta_{zi}cos(\varphi)$$
$$y_j = -r_j\theta_{zj}\cos(\varphi) \tag{5.21}$$

Substitution of equation 5.18 to 5.21 into translational displacement equation 5.9 to 5.11 yields following displacement equations:

$$s_{\theta xi} = r_i\theta_{xi}sin\varphi\ cos\phi_z$$
$$s_{\theta xj} = -r_j\theta_{xj}sin\varphi\ cos\phi_z \tag{5.22}$$

$$s_{\theta yi} = -r_i\theta_{yi}cos\varphi\ cos\phi_z$$
$$s_{\theta yj} = r_j\theta_{yj}cos\varphi\ cos\phi_z \tag{5.23}$$

$$\begin{aligned} s_{\theta zi} = &-r_i\theta_{zi}si\,n(\varphi)\left(sin\varphi cos\phi_x + cos\varphi cos\phi_y\right) \\ &+ r_i\theta_{zi}\cos(\varphi)\left(sin\varphi cos\phi_y - cos\varphi cos\phi_x\right) \\ s_{\theta zj} = &\ r_j\theta_{zj}sin(\varphi)\left(sin\varphi cos\phi_x + cos\varphi cos\phi_y\right) \\ &- r_j\theta_{zj}\cos(\varphi)\left(sin\varphi cos\phi_y - cos\varphi cos\phi_x\right) \end{aligned} \tag{5.24}$$

The displacement equation can be assembled which described relative motion due to the displacement of the node (i) and (j). For translational component this equation is,

$$u_{xyz} = \left(s_{xj} - s_{xi}\right) + \left(s_{yj} - s_{yi}\right) + \left(s_{zj} - s_{zi}\right) \tag{5.25}$$

Due to the effect of force coupling, angular displacement term must be treated differently. For the derivation of equation 5.18 to 5.21, a positive angular displacement was assumed about each axis. In reality, angular displacement is negatively coupled. A positive displacement of (θ_{xi})

results in negative displacement of (θ_{xj}) and vice versa. Hence, angular relative displacement equation takes the form,

$$u_\theta = \left(-s_{\theta xj} - s_{\theta xi}\right) + \left(-s_{\theta yj} - s_{\theta yi}\right) + \left(-s_{\theta zj} - s_{\theta zi}\right) \tag{5.26}$$

Total displacement along the line-of-action can be written as;

$$u_{LOA} = \left(s_{xj} - s_{xi}\right) + \left(s_{yj} - s_{yi}\right) + \left(s_{zj} - s_{zi}\right) + \left(-s_{\theta xj} - s_{\theta xi}\right) + \left(-s_{\theta yj} - s_{\theta yi}\right) + \left(-s_{\theta zj} - s_{\theta zi}\right) \tag{5.27}$$

The force along the line-of-action,

$$F_{mesh_{LOA}} = -K u_{LOA}$$

$$F_n = K_m u_{LOA} \tag{5.28}$$

Where,

K = component of mesh stiffness matrix

K_m = Average value of mesh stiffness

5.1.6 Influence Coefficient Method

Each element of mesh stiffness matrix can be calculated by assuming only one component of displacement vector {q} has a unit displacement, and all other components of the displacement vector $\{q_i\}$ and $\{q_j\}$ are zero. Then put the value of F_n in terms of force vector component in equation 5.28. The negative value of force vector component is represented the respective element of mesh stiffness matrix. This is a fundamental principle of influence coefficient method. The mesh stiffness matrix can be assembled by applying a unit displacement for each variable in $\{q_i\}$ and zero displacements in all other variables in $\{q_j\}$ vector. By applying each of six different unit displacement in $\{q_i\}$ will yield a 6×12 matrix. Similarly, using the same method to each of the variables in $\{q_j\}$ yields another 6×12 matrix. By a combination of this two 6×12 matrix final 12×12 mesh stiffness matrix obtained.

Mesh stiffness matrix can be written as,

$$[K]_{mesh} = K_m \begin{bmatrix} [K_{ii}] & [K_{ij}] \\ [K_{ji}] & [K_{jj}] \end{bmatrix} \tag{5.29}$$

The element of the four submatrices in Equation 5.29 are presented in Appendix B

5.1.7 Insertion into the Finite Element Model

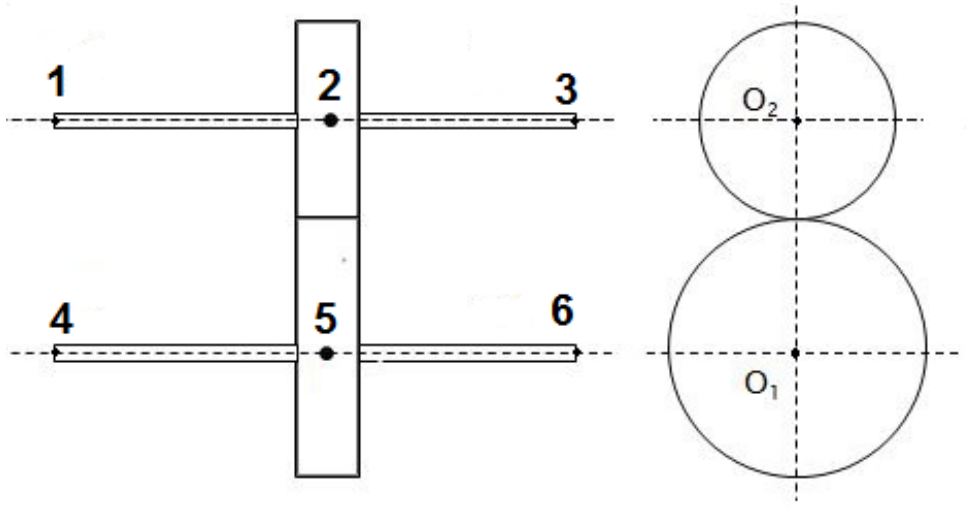

Figure 5.8: Finite Element Representation of Coupled Shaft

The mesh stiffness matrix is implemented into a finite element analysis in the following way. The node of the shaft is generally numbered sequentially for ease of analysis. However, couple node of shafts is usually non-sequential as shown in figure 5.8. Mesh coupling between node 2 and 5, results in mesh model

$$[K]_{mesh}\begin{Bmatrix} q_2 \\ q_5 \end{Bmatrix} = \begin{bmatrix} [k_{2,2}]_{mesh} & [K_{2,5}]_{mesh} \\ [K_{5,2}]_{mesh} & [K_{5,5}]_{mesh} \end{bmatrix}\begin{Bmatrix} q_2 \\ q_5 \end{Bmatrix} \tag{5.30}$$

While assembling global matrix, mesh stiffness matrix "breaks apart" to place the corresponding sub-matrices in the appropriate blocks of the global matrix. For figure 5.8 the mesh stiffness matrix substitute in global matrix as follows,

$$[K]^{(G)} = \begin{bmatrix} [k_{1,1}{}^{(1)}] & [k_{1,2}{}^{(1)}] & 0 & 0 & 0 & 0 \\ [k_{2,1}{}^{(1)}] & [k_{2,2}{}^{(1)} + k_{2,2}{}^{(2)}] + [k_{2,2}]_{mesh} & [k_{2,3}{}^{(2)}] & 0 & [K_{2,5}]_{mesh} & 0 \\ 0 & [k_{3,2}{}^{(2)}] & [k_{3,3}{}^{(2)}] & 0 & 0 & 0 \\ 0 & 0 & 0 & [k_{4,4}{}^{(3)}] & [k_{4,5}{}^{(3)}] & 0 \\ 0 & [K_{5,2}]_{mesh} & 0 & [k_{5,4}{}^{(3)}] & [k_{5,5}{}^{(3)} + k_{5,5}{}^{(4)}] + [K_{5,5}]_{mesh} & [k_{5,6}{}^{(4)}] \\ 0 & 0 & 0 & 0 & [k_{6,5}{}^{(4)}] & [k_{6,6}{}^{(4)}] \end{bmatrix} \tag{5.31}$$

5.2 Application

5.2.1 Approach and System Parameter

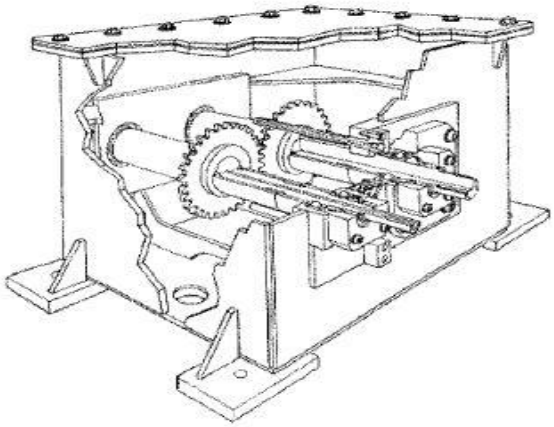

Figure 5.9: NASA Glenn Research Center Spur Gear Test Ring (Lim,1991)

The application selected for this methodology is a basic spur gear shaft pair system at NASA Glenn Research Center as shown in figure 5.9. This application is chosen because of the ease of availability of system parameters from the literature.

This system consists two spur gear on a two identical shafts connected to the gear box by two rolling element bearing per shaft. The parameter of shaft and gears are provided in Table 5.1, as documented in Singh (1990).

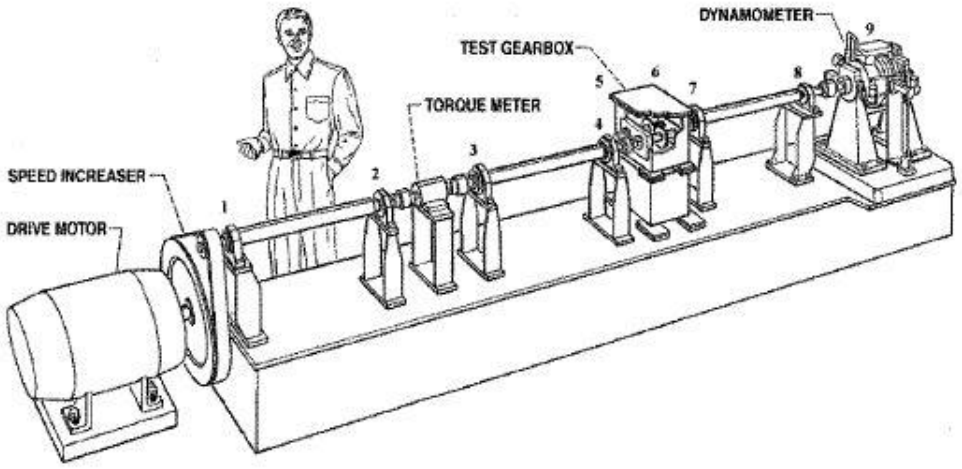

Figure 5.10: Gear Noise Test Ring – NASA Glenn Research Center (Lim, 1991)

Table 5.1: Spur Gear Application System Parameter

Materials Parameters	
Youngs's Modulus (E) (N/m^2)	2.03E11
Shear Modulus (G) (N/m^2))	8.0E10
Poisson's Ratio (υ)	0.27
Density (ρ) (kg/m^3)	7750
Shaft Parameters	
Length (L_s) (m)	0.254
Mass (M_s) (kg)	1.96
Rigidity (EI) ($N\text{-}m^2$)	18576
Outer Diameter (d_o) (m)	0.037
Inner Diameter (d_i) (m)	0.01
Gear Parameters	
Mass (M_g) (kg)	1.84
Moment of inertia (I_t) ($kg\text{-}m^2$)	1.8E-3
Polar mass moment of inertia (I_p) ($kg\text{-}m^2$)	3.6E-3
Diameter (d_g) (m)	0.089
Normal Pressure Angle (α_n) (deg)	20
Helical Angle (β) (deg)	0
Orientation Angle (φ) (deg)	0
Average mesh stiffness (K_m) (N/m)	1.0E10
Number of teeth	28
Bearing Parameters	
k_{xx}, k_{yy} (N/m)	1.0E9

In this analysis, two results have been compared and analyzed. The first one is one of the rotating gear shafts as a single system, with gear acting as a rigid disk only. The second one is of complete gear shafts system.Node numbearing for the analysis of the system is considered as shown in figure 5.11.

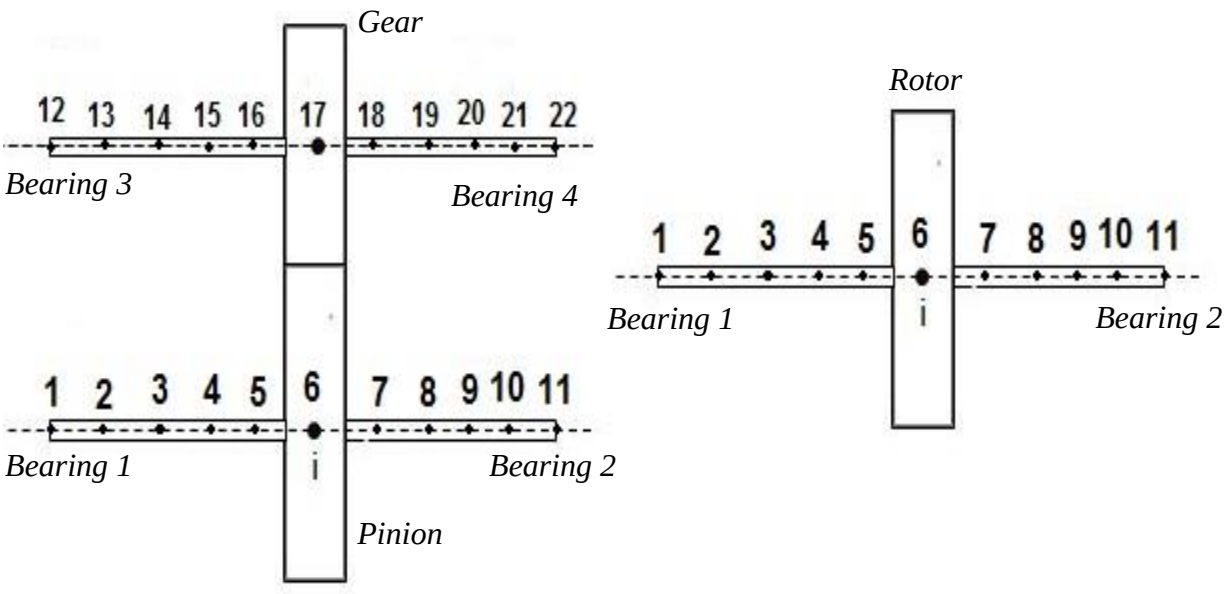

Figure 5.11: Node Numbering of Complete Gear System and Single Shaft of Gear System

5.2.2 Results: Single Shaft System

First, ten natural frequency of the single shaft system with their corresponding descriptions is shown in Table 5.2.

Table 5.2: Natural Frequencies (Hz) of Single Rotor Shaft

Frequency No.	Mode	Natural Frequency
1	1st Torsional, 1st Axial	0
2	1st Lateral	612
3	2nd Lateral	2508,2524
4	3rd Lateral	5430,5446
5	2nd Torsional	6350,6598
6	4th Lateral	9682,9684
7	2nd Axial	10014,10115
8	3rd Axial	13211
9	5th Lateral	15547,15915
10	3rd Torsional	19681,19768

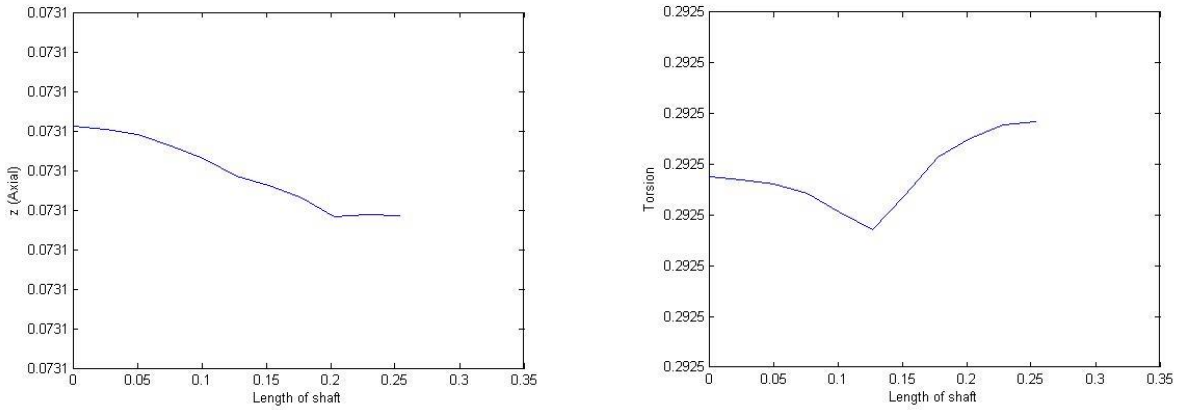

Figure 5.12: 1st Axial (left) and 1st Torsional (right) Mode Shapes- at 0 Hz

The mode shape for the first ten natural frequencies is plotted in figure 5.12 through figure 5.21 for the rotating speed of 1000 rpm. At 0 rpm, the mode shapes are planer and shaft behave as a vibrating beam. At 1000 rpm mode shapes are no longer planer, the orbital mode shape is proof for that.

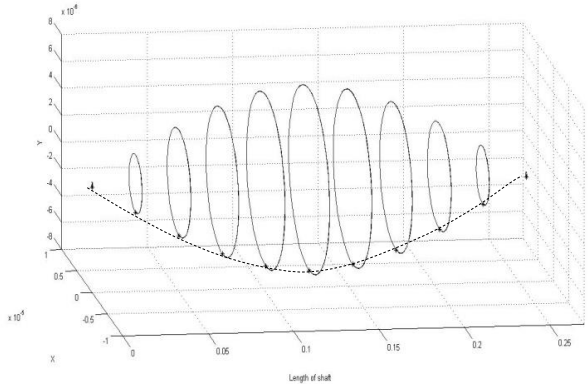

Figure 5.13: 1st Lateral Mode Shape - 612 Hz

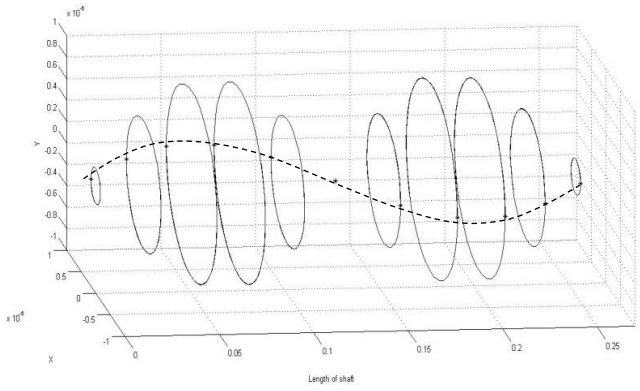

Figure 5.14: 2nd Lateral Mode Shape – 2508 Hz

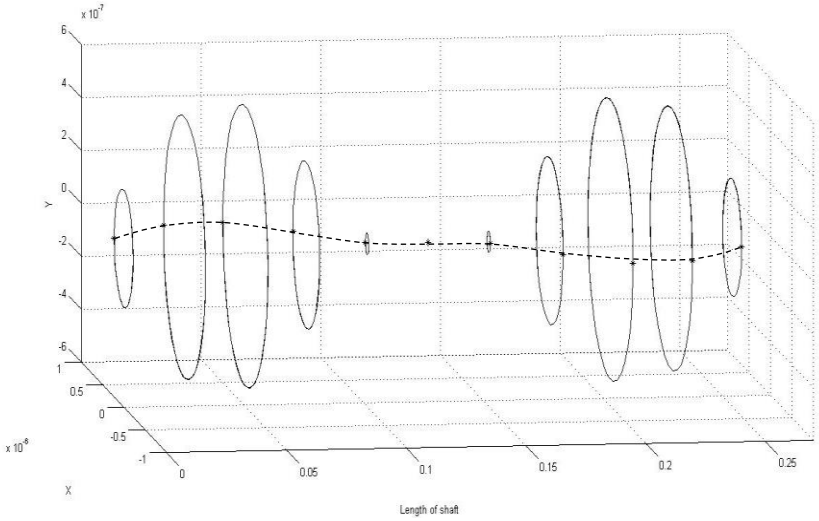

Figure 5.15: 3rd Lateral Mode Shape – 5430 Hz

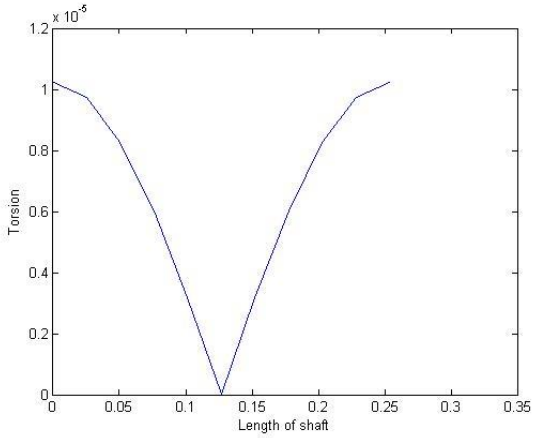

Figure 5.16: 2nd Torsional Mode Shape – 6350 Hz

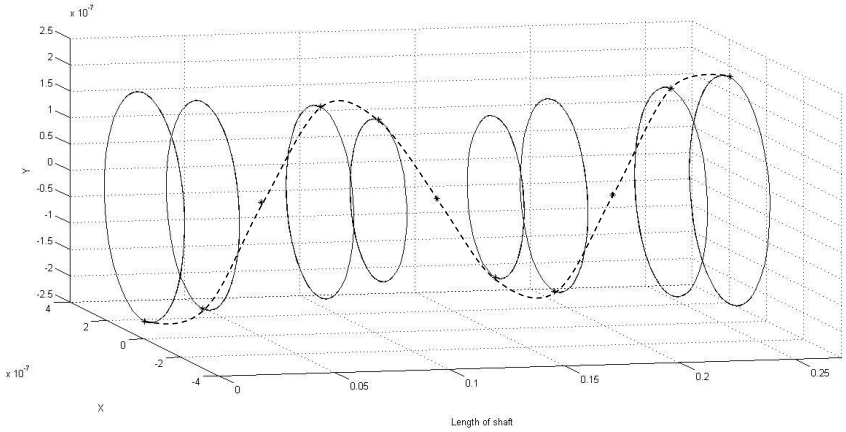

Figure 5.17: 4th Lateral Mode Shape – 9682 Hz

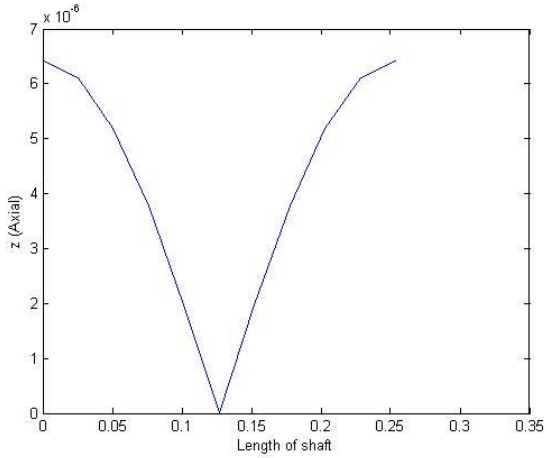

Figure 5.18: 2nd Axial Mode Shape – 10115 Hz

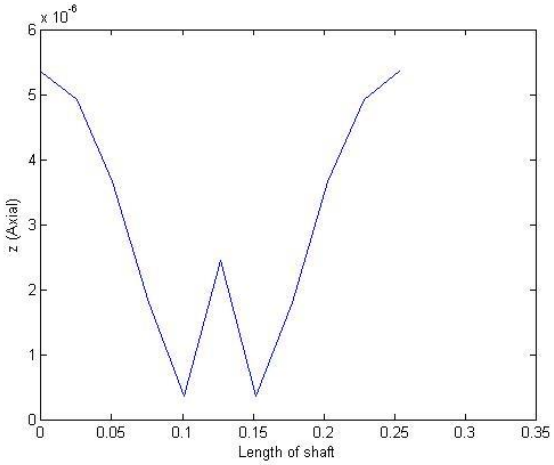

Figure 5.19: 3rd Axial Mode Shape: 13211 Hz

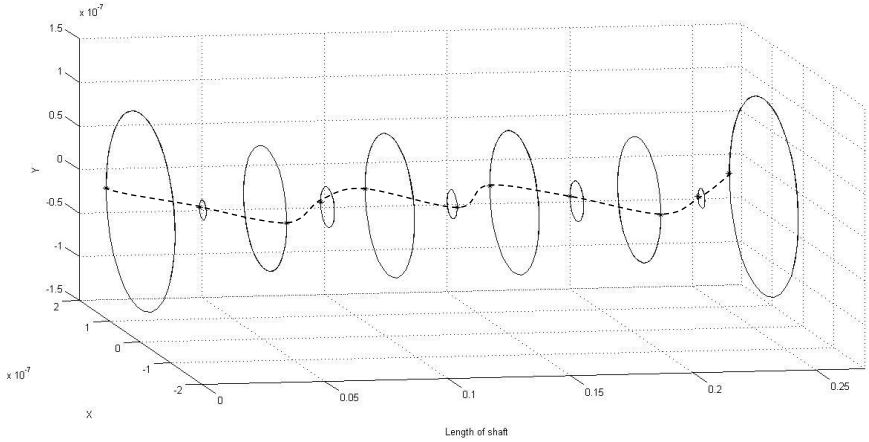

Figure 5.20: 5th Lateral Mode Shape: 15915 Hz

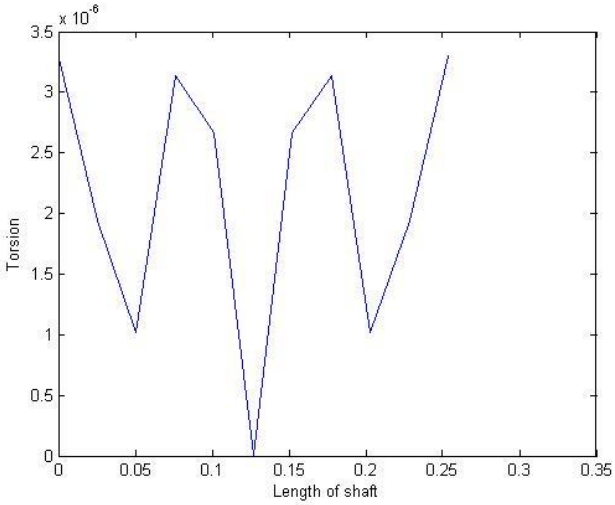

Figure 5.21: 3rd Torsional Mode Shape: 19681 Hz

The effect of the rotation speed on the natural frequencies is very small because the natural frequencies of the system are quite large, and length of the shaft is small, only 0.254 m. Hence, one would expect the natural frequencies is free from the rotational speed of the shaft.

5.2.3 Results: Dual Shaft System

Table 5.3 lists the natural frequencies of dual shaft system and compare it with natural frequencies of the single-shaft system.

Table 5.3: Comparision of Natural Frequencies of Single and Dual Shaft System

Frequency no.	Mode	Single Shaft	Gear Pair
1	1st Axial, 1st Torsional	0	0
2	Coupled, 1st Lateral	-	463
3	1st Lateral	612	612
4	Coupled, 2nd Lateral	-	1546
5	2nd Lateral	2508,2524	2514,2530
6	3rd Lateral	5430, 5446	5454
7	2nd Torsional	6350,6598	6350
8	4th Lateral	9682,9684	9737,9738
9	Coupled, 3rd Lateral	-	10079,10084
10	2nd Axial	10014,10115	10115
11	3rd Axial	13211	13211
12	5th Lateral	15547,15915	15708
13	Coupled, 4th Lateral	-	16082,16084
14	3rd Torsional	19681,19768	19768

For comparison of single and dual shaft system, first two mode shape of single and dual shaft system at a rotation speed of 1000 rpm shown in figure 5.22 and figure 5.23.

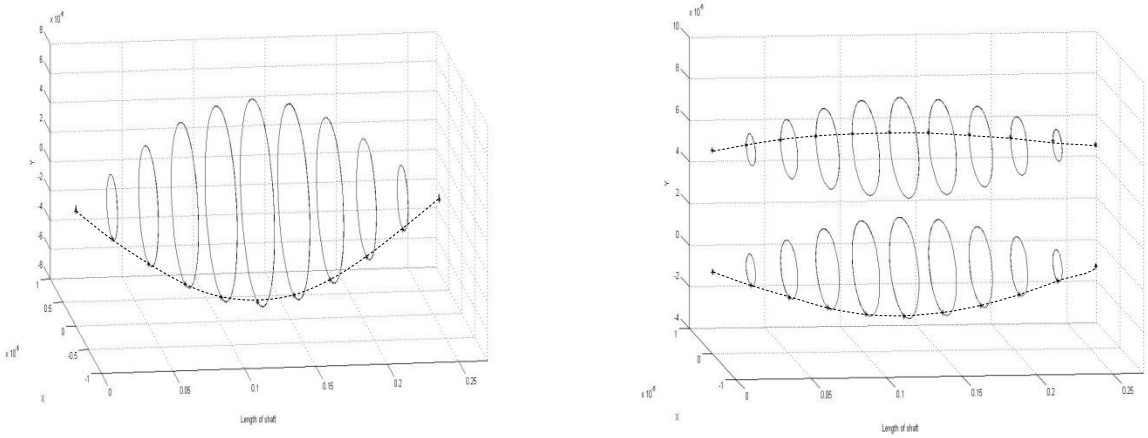

Figure 5.22: Comparison of 1st Lateral Mode Shape – 612 Hz

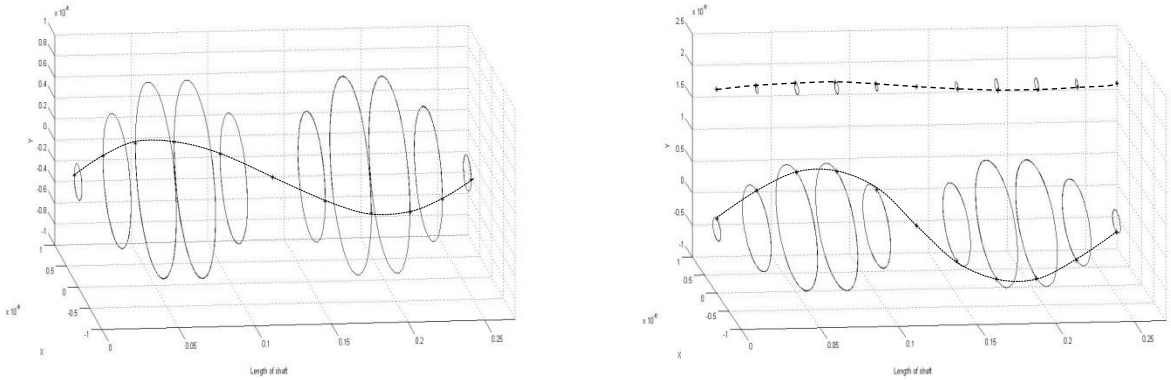

Figure 5.23: Comparison of 2nd Lateral Mode Shape – 2508(left) and 2514(right) Hz

Additionally coupled lateral-torsional mode shape arise from the gear-mesh. Figure 5.24 through figure 5.27 shows couple mode shape at a rotational speed of 1000 rpm.

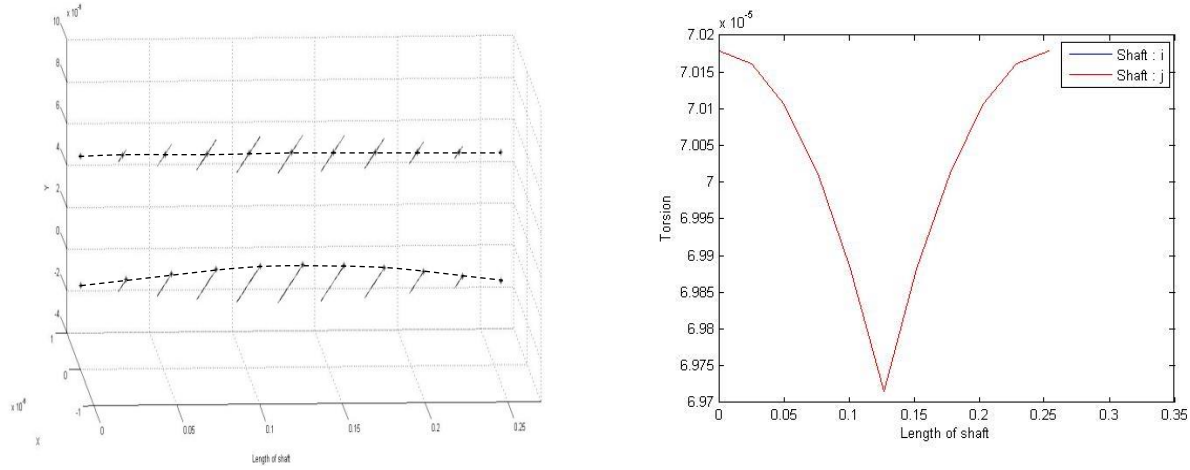

Figure 5.24: Coupled,1st Lateral-Torsional Mode shape – 463 Hz

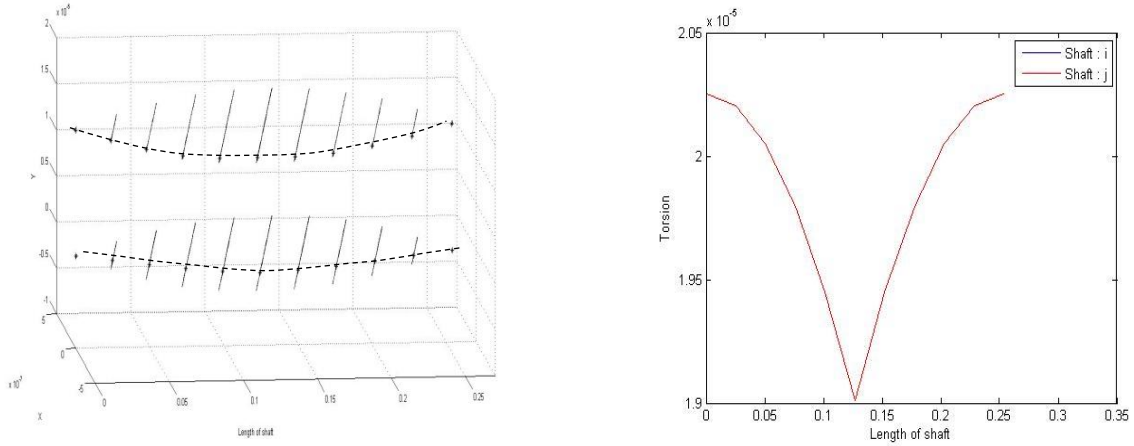

Figure 5.25: Coupled, 2nd Lateral-Torsional Mode Shape – 1546 Hz

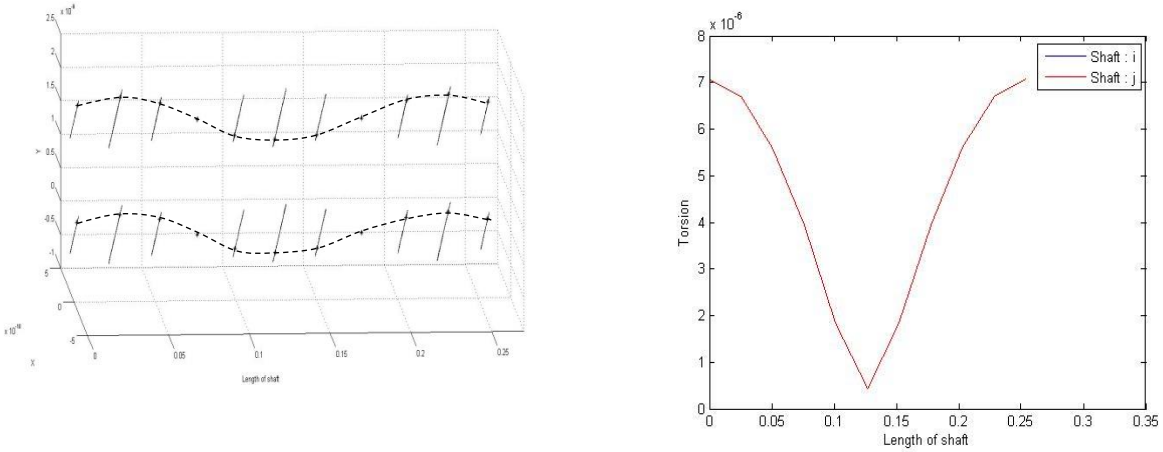

Figure 5.26: Coupled, 3rd Lateral-Torsional Mode shape -10084 Hz

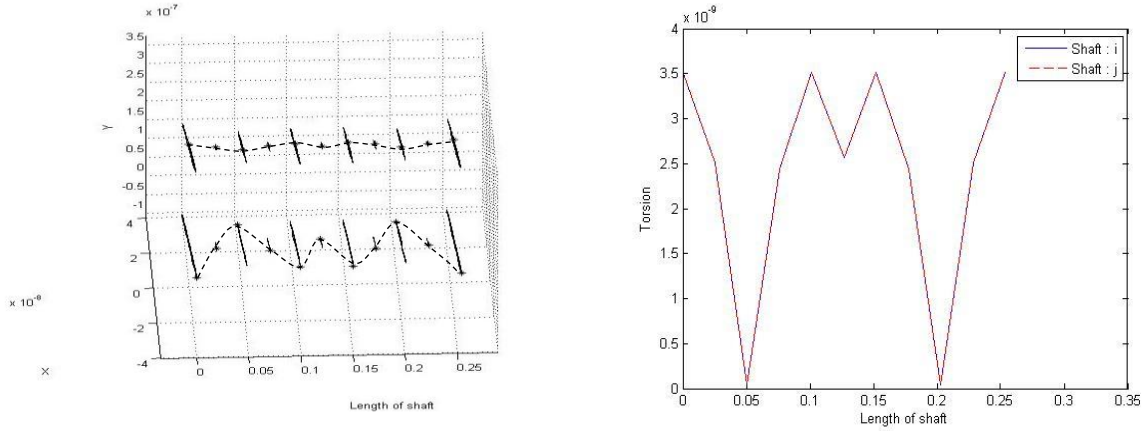

Figure 5.27: Coupled, 4th Lateral-Torsional Mode Shape – 16084 Hz

5.2.4 Observation

Comparison between single and dual shaft system, the following observation are noted.

1. The uncoupled natural frequencies of dual shaft system are the same as the single shaft system.
2. Coupled natural frequencies of dual shaft system identify coupled modes of vibration between the lateral and torsional DOFs.
3. Shapes of coupled modes are those characterizing odd-numbered lateral modes of vibration.
4. The magnitude of torsional coupling increases as the frequency increases.

5.2.5 Validation

The result in Table 5.2 and Table 5.3 is validated with the result with the previous study by Stringer (2008).

Comparison of first few natural frequencies of single-shaft and dual shaft system with Stringer's work:

Natural frequencies shown in table 5.4 and table 5.5 are having small difference with the original natural frequencies obtained priviously.

Table 5.4: Comparision of Natural Frequency of Single Shaft System

Natural Freq. No.	Natural freq. obtained by Stringer (2008)	Calculated	Difference (%)
1st	0	0	0
2nd	684	612	10.52
3rd	2838,2858	2508,2524	11.76
4th	6677	5446	18.43
5th	7138	6350	11.03

Table 5.5: Comparison of Natural Frequency of Dual Shafts System

Natural Freq. No.	Natural freq. obtained by Stringer (2008)	Calculated	Difference (%)
1st	0	0	0
2nd	505	463	8.31
3rd	684	612	10.52
4th	2090	1546	26.02
5th	2838,2858	2514,2530	11.76
6th	6677	5454	18.43
7th	6706	6350	11.03

6 Gear-Mesh Model Methodology with Application: Bevel Gear

This chapter contains a methodology for deriving 12-DOF mesh stiffness matrix for bevel gear system. This approach used technique proposed by Lao (1996) and it also includes some aspects presented by Choi (1993) and Blankenship (1995) for helical gear. A technique used for this work was proposed by Stringer (2008), but the orientation angle employed in this work is a new concept applied to a three-dimensional model of bevel gear system.

6.1 Gear-Mesh Model Methodology

6.1.1 Development of Gear Mesh Forcing Function

Figure 6.1 shows simple geometry of straight bevel gear

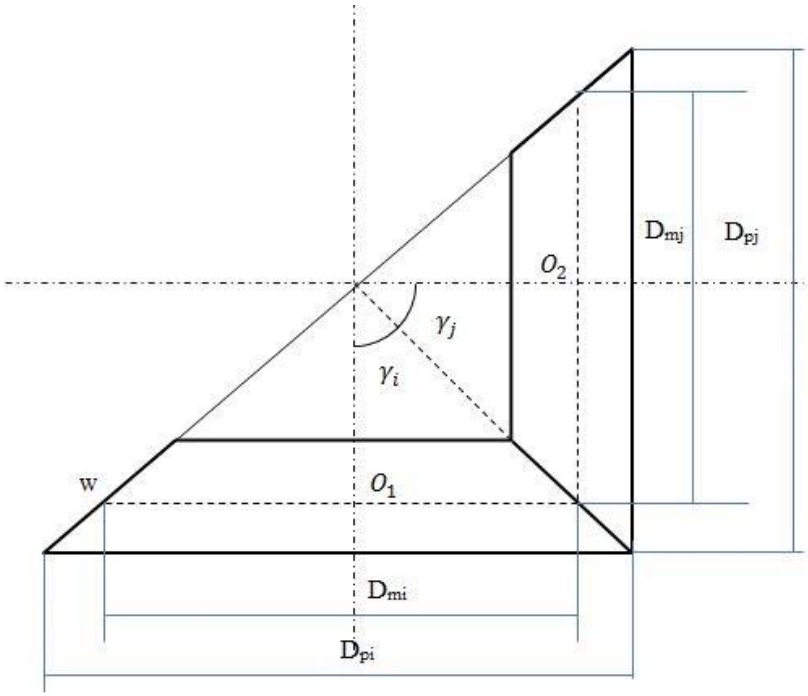

Figure 6.1: Simple Geometry of Straight Bevel Gear

Where,

$\gamma_i + \gamma_j = 90^{\circ}$

γ_i = pitch angle of ith gear

γ_j = pitch angle of ith gear

D_{mi} , D_{mj} = mean diameter of i[th] and j [th] gear respectively

D_{pi} , D_{pj} = pitch circle diameter of i[th] and j [th] gear respectively

O_1 , O_2 = center of i[th] and j [th] gear respectively

w = Tooth face width

Figure 6.2 Shows finite element representation of bevel gear pair.

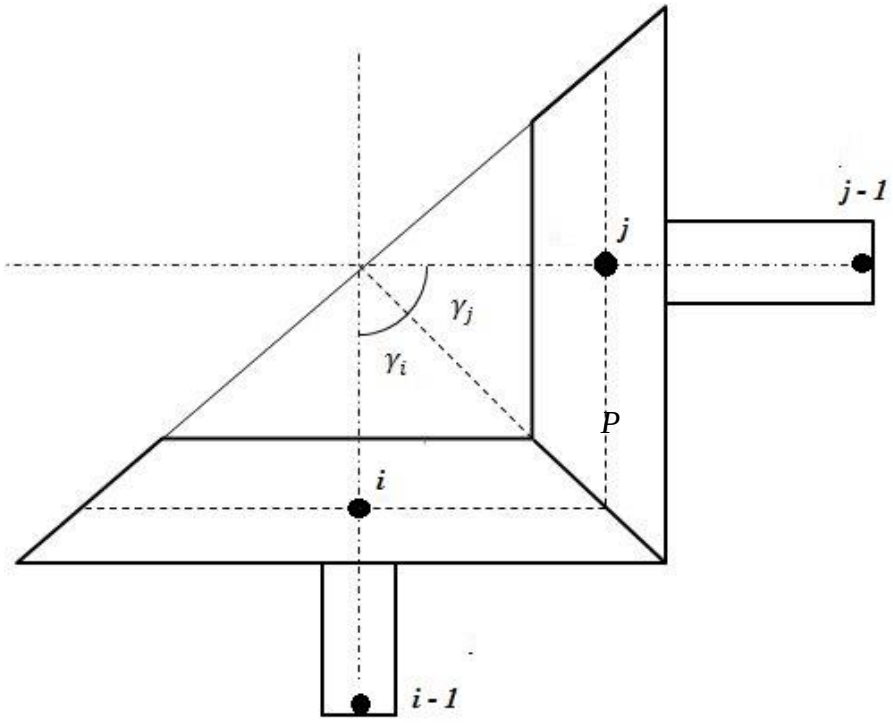

Figure 6.2: Finite Element Representation of Bevel Gear Pair

Two gears are assumed as a rigid disk on a flexible shaft. Two centers of bevel gears are considered as a node i and j of finite element analysis. A force and moment vector {F} can be modeled as function of a bevel gear mesh stiffness matrix $[K]_{mesh}$ and displacement vector {q} acts on a node i and j.

$$\begin{Bmatrix} F_i \\ F_j \end{Bmatrix} = [K]_{mesh} \begin{Bmatrix} q_i \\ q_j \end{Bmatrix} = K_m \begin{bmatrix} [K_{ii}] & [K_{ij}] \\ [K_{ji}] & [K_{jj}] \end{bmatrix} \begin{Bmatrix} q_i \\ q_j \end{Bmatrix} \quad (6.2)$$

6.1.2 Loading and Direction Cosine

Figure 6.3: shows forces on ith bevel gear.

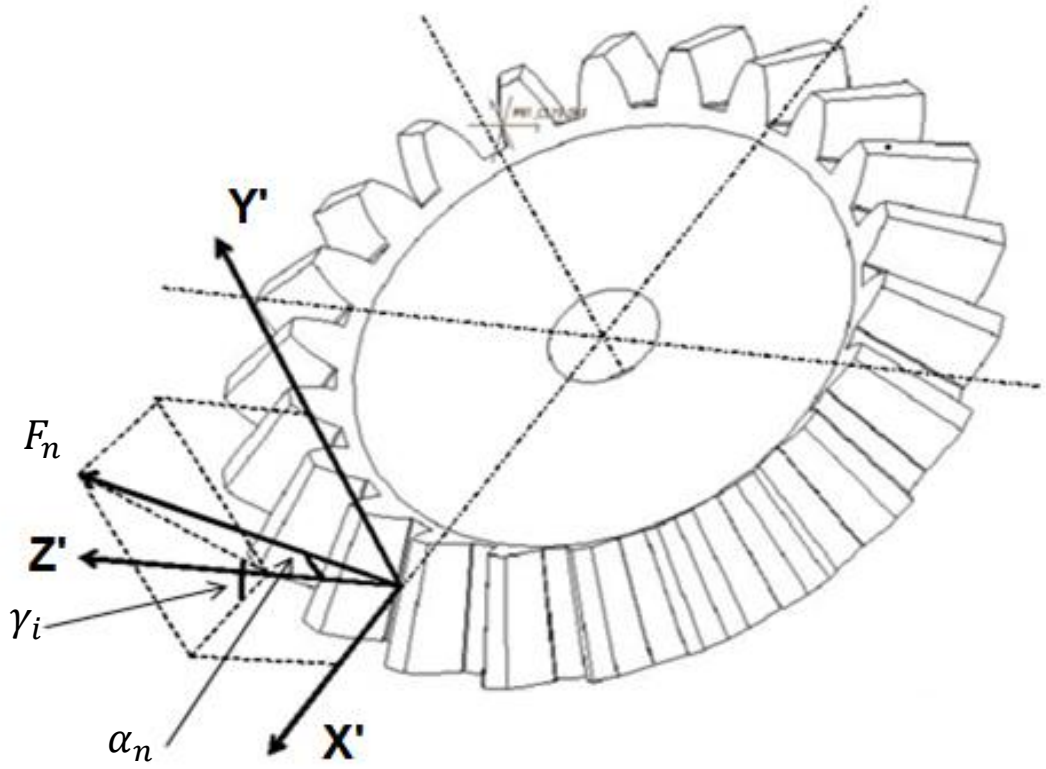

Figure 6.3: Force Contribution in Bevel Gear

In bevel gear, three-dimensional force components are a function of direction cosine as illustrated in figure 6.4. The direction cosine angle can be written in the form of pitch angle of gear (γ_i) and the normal pressure angle (α_n). The force components along X', Y' and Z' axes are determined by equations 6.2. The role of prime coordinates (X', Y', and Z') will discuss later.

$$\begin{aligned} F_{X'} &= F_n cos\phi_x \\ F_{Y'} &= F_n cos\phi_y \\ F_{Z'} &= F_n cos\phi_z \end{aligned} \tag{6.2}$$

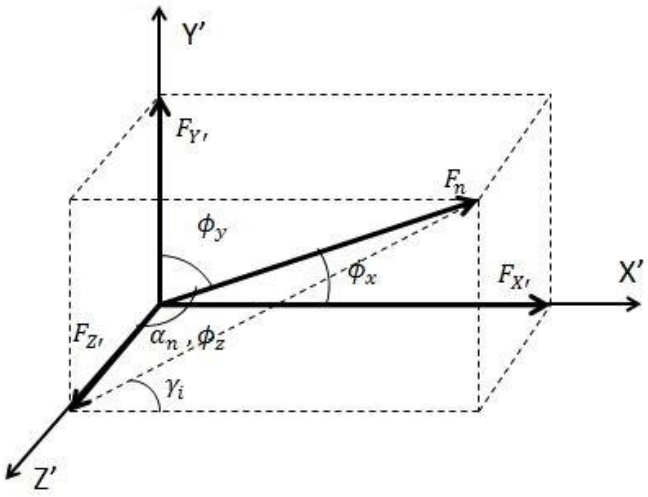

Figure 6.4: Mesh Force Components and Direction Cosine for Bevel Gear

Where,

$$cos\phi_x = sin\alpha_n \, cos\gamma_i$$
$$cos\phi_y = sin\alpha_n \, sin\gamma_i \quad (6.3)$$
$$cos\phi_z = cos\alpha_n$$

The equation relating the force vector to displacement vector is

$$\{F\}_{mesh} = -[K]_{mesh}\{u\}_{LOA} \quad (6.4)$$

The negative sign implies that forces and moments acting on the gear body are in the direction of positive displacement.In other word force function in global coordinates system can be brought to the left-hand side in the form of the stiffness matrix.

6.1.3 Gear Mesh Coordinates System and Orientation Angles

The prime coordinate axes (X', Y' and Z') are local to pitch point and not necessarily parallel with the global coordinate system. The prime coordinate system depends on two orientation angle θ_1 and θ_2.The normal pressure angle (α_n) and the pitch angle of gear (γ_i) fix the force vector on gear tooth. The geometry of tooth fix the prime coordinate system on the effective point of force transmission (P) such that prime coordinate system is fixed and unchanging. To consider orientation of both gear two orientation angles θ_1 and θ_2 are used. The first orientation

angle θ_1 define the position of the j^{th} gear with respect to initial position of the i^{th} bevel gear. The second orientation angle defines the position of i^{th} bevel gear with respect to new position of j^{th} bevel gear. Figure 6.5 shows assumed initial position of i^{th} and j^{th} bevel gear and figure 6.6 shows coordinates system at initial position of bevel gear system.

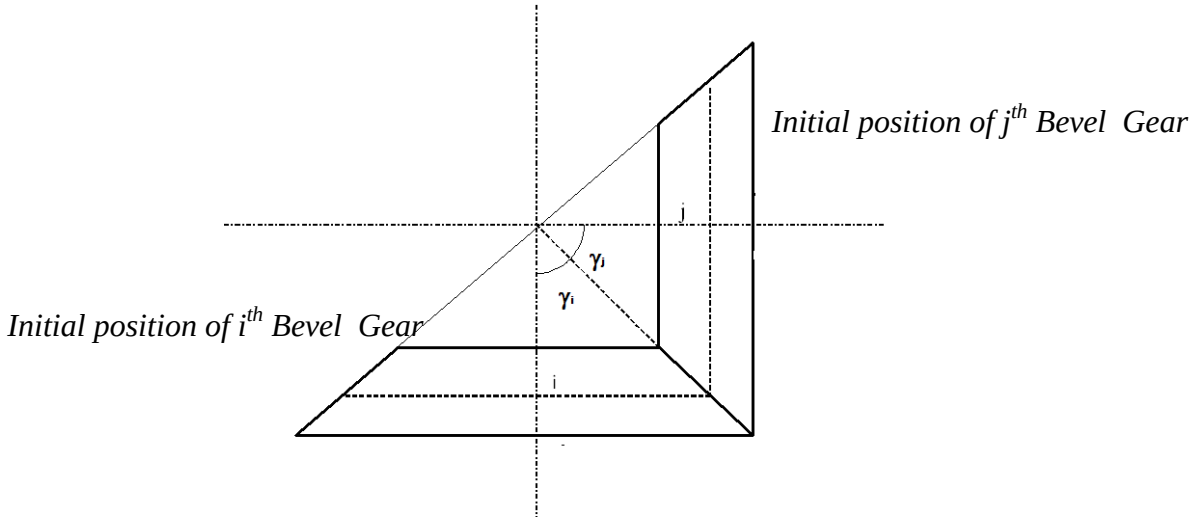

Figure 6.5: Initial Position of i^{th} and j^{th} Bevel Gear

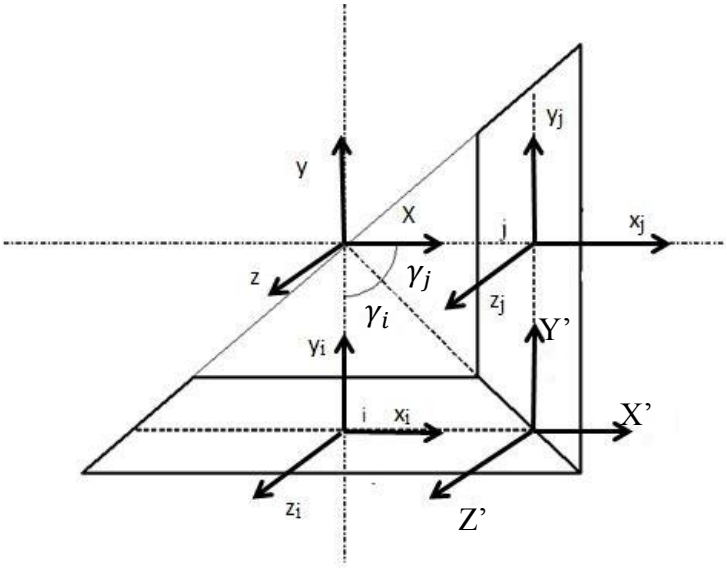

Figure 6.6: Coordinate System at Initial Position

Another two coordinates systems (x_i, y_i, z_i and x_j, y_j, z_j) are assumed as a center of the each gear and always parallel to the global coordinate system (X, Y, and Z).

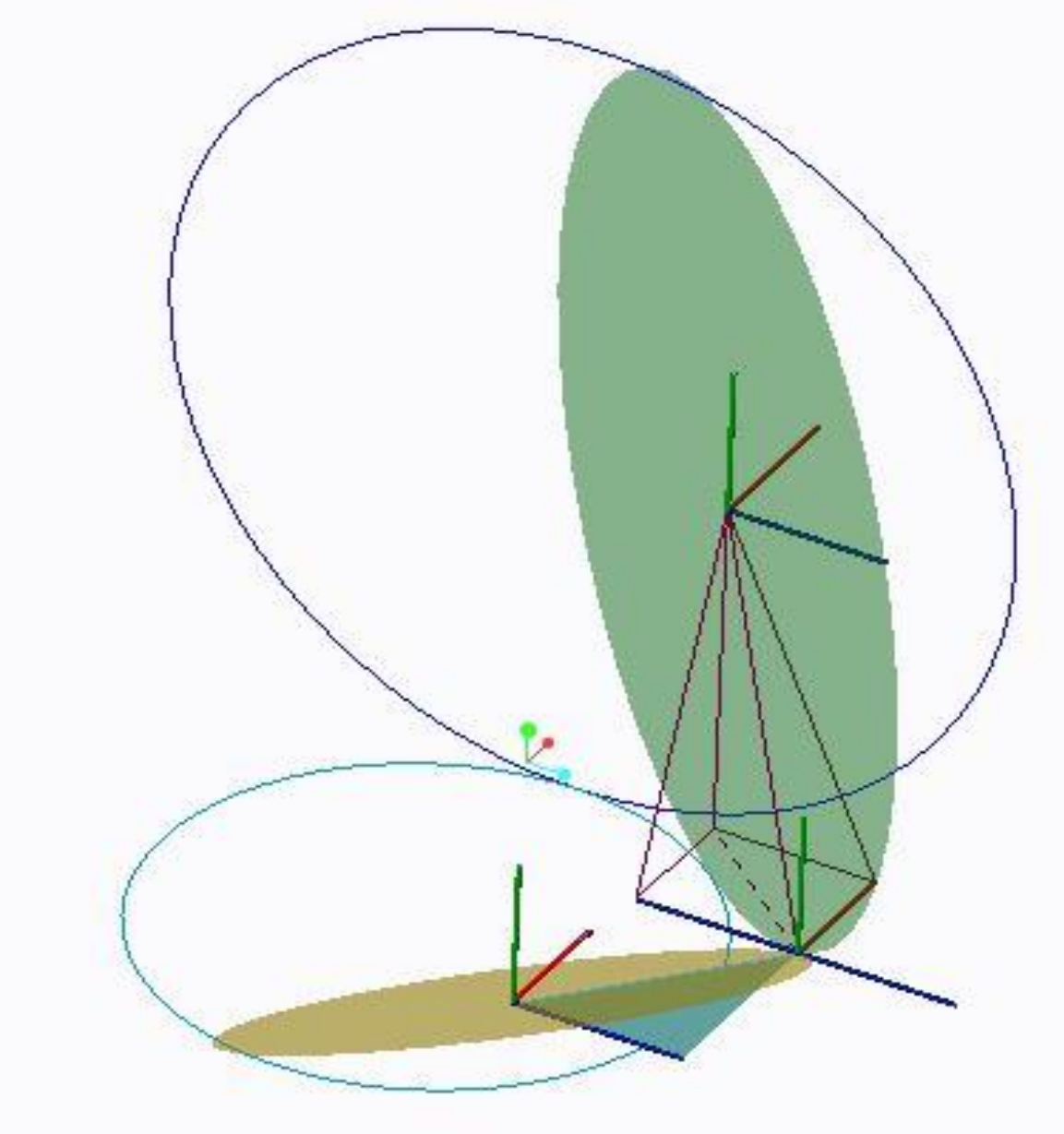

Figure 6.7: Effect of Orientation Angle on Bevel Gear

Figure 6.8 explain the axes systems in figure 6.7. As seen in Figure 6.8, a force component in the direction of the prime coordinate axis X' has components in X, Y, and Z - the direction of global coordinates system. Similarly, the force component in the direction of prime coordinate axis Y' has a component in X, Y, and Z-direction of global coordinates system. Unlike in helical gear system, the force components in the direction of prime coordinate axis Z' also have a component in X, Y, and Z-direction.

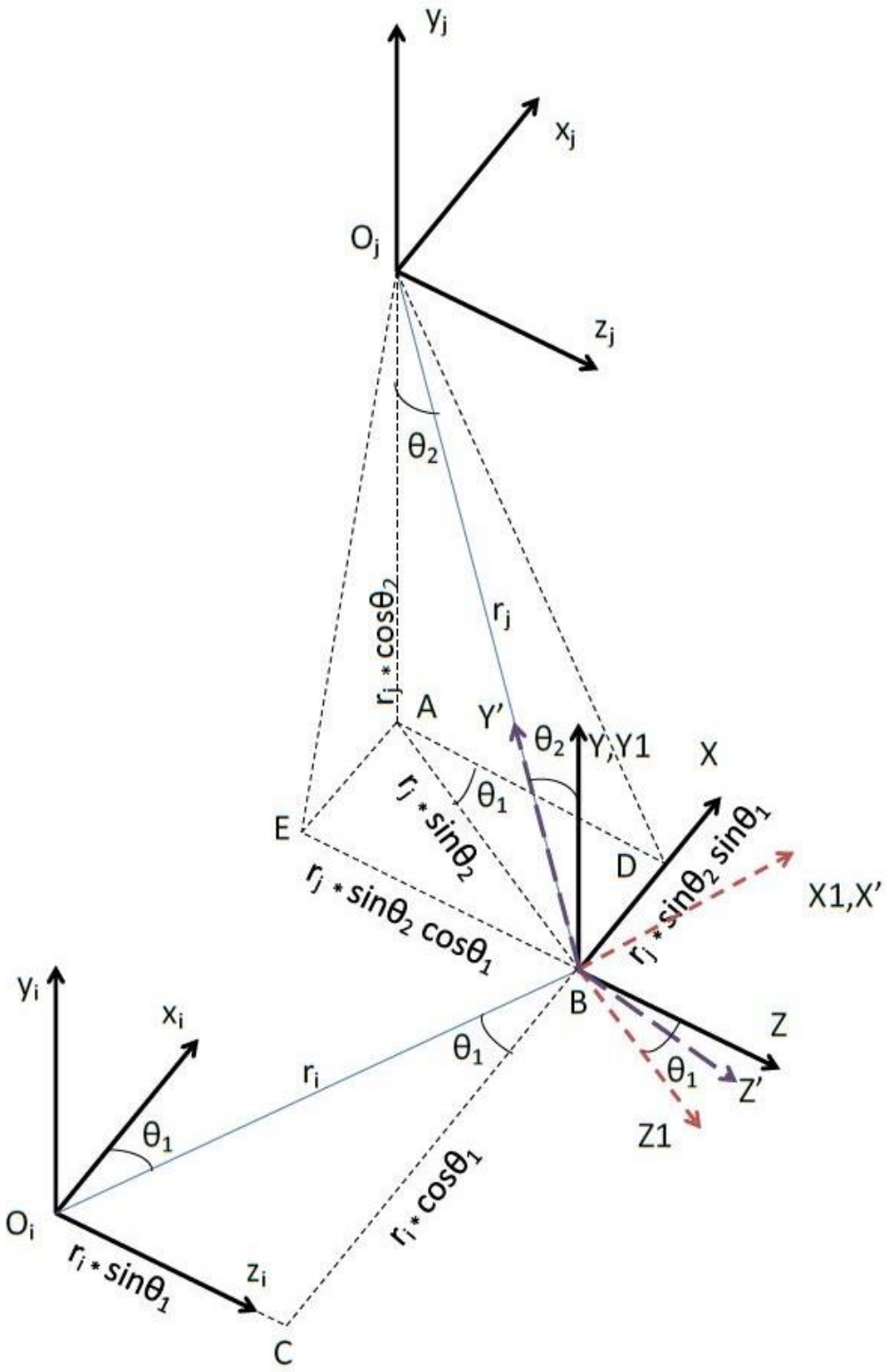

Figure 6.8: Local and Global Axes Relation with Orientation Angles

O_j is the center of gear j, and O_i is the center of gear i. The plane of gear j is O_jAB and plane of gear i is perpendicular to line O_jB and passing through line O_iB which makes an angle of θ_2 with plane O_iCB.

Some bevel gear system arrangements are shown at a different-different orientation angle to understand orientation angles clearly. In figure 6.9 blue and white gears represent j^{th} and i^{th} gear respectively. Each and every figure in figure 6.9 contains two figure in which top and bottom show front and top view of systems respectively.

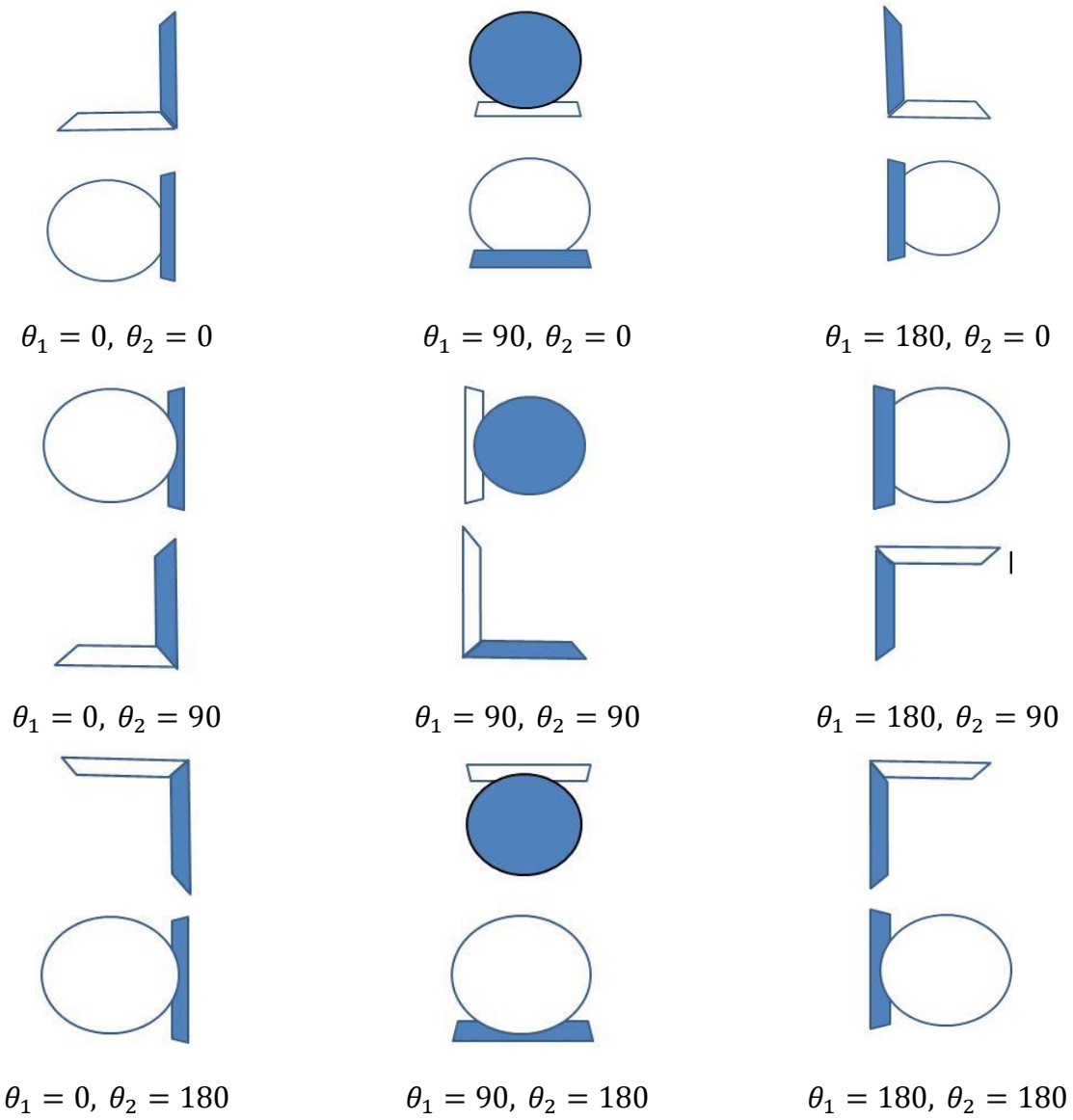

Figure 6.9: Gear Systems at Differents Orientation Angles

6.1.4 Nodal Forces and Moments Equations

The forces at the point P in global coordinate system can be written in matrix form as below,

$$\begin{Bmatrix} F_X \\ F_Y \\ F_Z \end{Bmatrix} = \begin{bmatrix} cos\theta_1 & 0 & -sin\theta_1 \\ 0 & 1 & 0 \\ sin\theta_1 & 0 & cos\theta_1 \end{bmatrix} \begin{bmatrix} 1 & 0 & 0 \\ 0 & cos\theta_2 & sin\theta_2 \\ 0 & -sin\theta_2 & cos\theta_2 \end{bmatrix} \begin{Bmatrix} F_{X'} \\ F_{Y'} \\ F_{Z'} \end{Bmatrix} \tag{6.5}$$

The component of force acting on the node (i) in the direction of the global coordinate system are given by equation 6.6. The moment equation about the node (i) can be determined by multiplying the force components and moments arm about respective axes.

$$\begin{aligned} F_{xi} &= F_X \\ F_{yi} &= F_Y \\ F_{zi} &= F_Z \end{aligned} \tag{6.6}$$

Moment equations,

$$\begin{aligned} M_{xi} &= -F_{yi}\, r_i\, sin\theta_1 \\ M_{yi} &= F_{xi}\, r_i\, sin\theta_1 - F_{zi}\, r_i\, cos\theta_1 \\ M_{zi} &= F_{yi}\, r_i\, cos\theta_1 \end{aligned} \tag{6.7}$$

The force components acting on the node (j) are equal and opposite to those acting on the node (i) due to equilibrium condition of forces. The moments about the node (j) are not equal and opposite to moments about the node (i).

$$\begin{aligned} F_{xj} &= -F_{xi} \\ F_{yj} &= -F_{yi} \\ F_{zj} &= -F_{zi} \end{aligned} \tag{6.8}$$

$$\begin{aligned} M_{xj} &= F_{yj}\, r_j\, sin\theta_2\, cos\theta_1 + F_{zj}\, r_j\, cos\theta_2 \\ M_{yj} &= -F_{xj}\, r_j\, sin\theta_2\, cos\theta_1 - F_{zj}\, r_j\, sin\theta_2 sin\theta_1 \\ M_{zj} &= F_{yj}\, r_j\, sin\theta_2 sin\theta_1 - F_{xj}\, r_j\, cos\theta_2 \end{aligned} \tag{6.9}$$

6.1.5 Displacement Method

Each DOF contributes to shifting point P along the line of action of the gear pair. Summation of the contribution of all DOF will give a total shift of point P along the line of action.

The effect of translational motion along the three axes will shift point P in the direction of motion. The component of each displacement along the direction of F_n can be determined using the same matrix that used earlier to find the component of F_n in global coordinate system. In the case of rotational displacement, a rotational motion about an axis will rotate pitch point in a circular arc about a respective axis. The circular arc represents motion in two directions.

$$\begin{Bmatrix} x_i \\ y_i \\ z_i \end{Bmatrix} = \begin{bmatrix} cos\theta_1 & 0 & -sin\theta_1 \\ 0 & 1 & 0 \\ sin\theta_1 & 0 & cos\theta_1 \end{bmatrix} \begin{bmatrix} 1 & 0 & 0 \\ 0 & cos\theta_2 & sin\theta_2 \\ 0 & -sin\theta_2 & cos\theta_2 \end{bmatrix} \begin{Bmatrix} x'_i \\ y'_i \\ z'_i \end{Bmatrix}$$

$$\begin{Bmatrix} x_i \\ y_i \\ z_i \end{Bmatrix} = [A] * [B] \begin{Bmatrix} x'_i \\ y'_i \\ z'_i \end{Bmatrix}$$

$$\begin{Bmatrix} x'_i \\ y'_i \\ z'_i \end{Bmatrix} = [B]^{-1}[A]^{-1} \begin{Bmatrix} x_i \\ y_i \\ z_i \end{Bmatrix} \tag{6.10}$$

From above equation we can find the displacement of contact point along X', Y' and Z' axis due to the displacement of node i (gear i)along X, Y and Z axis that is x_i, y_i, and z_i . Then, by using direction cosine s_{xi}, s_{yi}, and s_{zi} along the line of action can be determined. Using MATLAB program, we can find s_{xi},$s_{yi,}$ and s_{zi} as below,

$$\begin{aligned} s_{xi} &= x_i\left(cos\theta_1 cos\phi_x - cos\phi_z cos\theta_2 sin\theta_1 + cos\phi_y sin\theta_2 sin\theta_1\right) \\ s_{xj} &= x_j\left(cos\theta_1 cos\phi_x - cos\phi_z cos\theta_2 sin\theta_1 + cos\phi_y sin\theta_2 sin\theta_1\right) \end{aligned} \tag{6.11}$$

$$\begin{aligned} s_{yi} &= y_i\left(cos\phi_y cos\theta_2 + cos\phi_z sin\theta_2\right) \\ s_{yj} &= y_j\left(cos\phi_y cos\theta_2 + cos\phi_z sin\theta_2\right) \end{aligned} \tag{6.12}$$

$$s_{zi} = z_i\left(cos\phi_x sin\theta_1 + cos\phi_z cos\theta_2 cos\theta_1 - cos\phi_y cos\theta_1 sin\theta_2\right)$$
$$s_{zj} = z_j\left(cos\phi_x sin\theta_1 + cos\phi_z cos\theta_2 cos\theta_1 - cos\phi_y cos\theta_1 sin\theta_2\right) \quad (6.13)$$

Rotational motion displacement is presented in figure 6.10 through figure 6.15 regarding (X), (Y) and (Z)

For i[th] bevel gear,

- Rotational motion about x_i by θ_{xi}

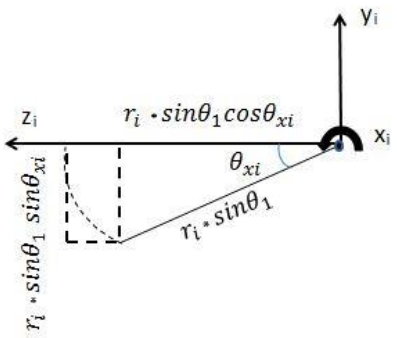

Figure 6.10: Rotational Motion About x_i

$$y_i = -r_i\, sin\theta_1 sin\theta_{xi}$$
$$z_i = r_i\, sin\theta_1(cos\theta_{xi} - 1) \quad (6.14)$$

- Rotational motion about y_i by θ_{yi}

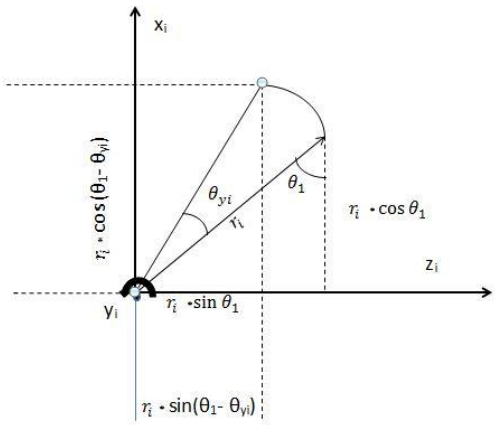

Figure 6.11: Rotational Motion About y_i

$$x_i = r_i\,(\cos\theta_1\, cos\theta_{yi} + \sin\theta_1\, sin\theta_{yi} - \cos\theta_1)$$
$$z_i = r_i\,(\sin\theta_1\, cos\theta_{yi} - \cos\theta_1\, sin\theta_{yi} - \sin\theta_1) \quad (6.15)$$

- Rotational motion about z_i by θ_{zi}

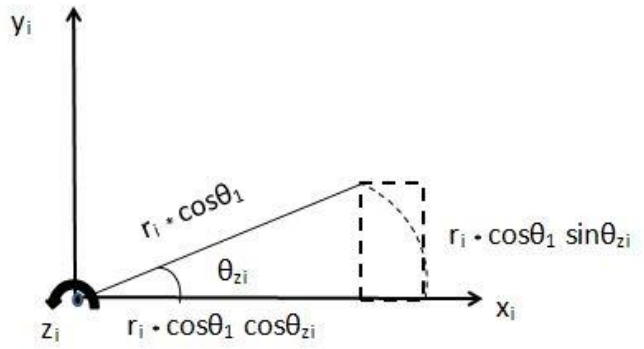

Figure 6.12: Rotational Motion About z_i

$$x_i = r_i\, cos\theta_1(cos\theta_{zi} - 1)$$
$$y_i = r_i\, cos\theta_1\, sin\theta_{zi} \quad (6.16)$$

For j[th] bevel gear,

- Rotational motion about x_j by θ_{xj}

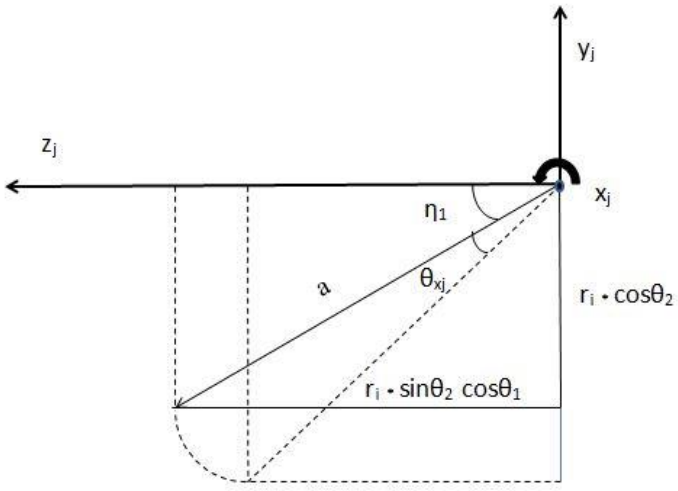

Figure 6.13: Rotational Motion About x_j

$$y_j = -\,\mathrm{a}\,(\,\sin\eta_1\,cos\theta_{xj} + cos\eta_1 sin\theta_{xj}) + a\,sin\eta_1$$
$$z_j = \mathrm{a}\,(\,\cos\eta_1\,cos\theta_{xj} - sin\eta_1 sin\theta_{xj}) - a\,cos\eta_1 \qquad (6.17)$$

Where,

$\eta_1 = tan^{-1}\left(\frac{r_j cos\theta_2}{r_j sin\theta_2 cos\theta_1}\right)$

a = $r_j\sqrt{cos^2\theta_2 + sin^2\theta_2 cos^2\theta_1}$

- Rotational motion about y_j by θ_{yj}

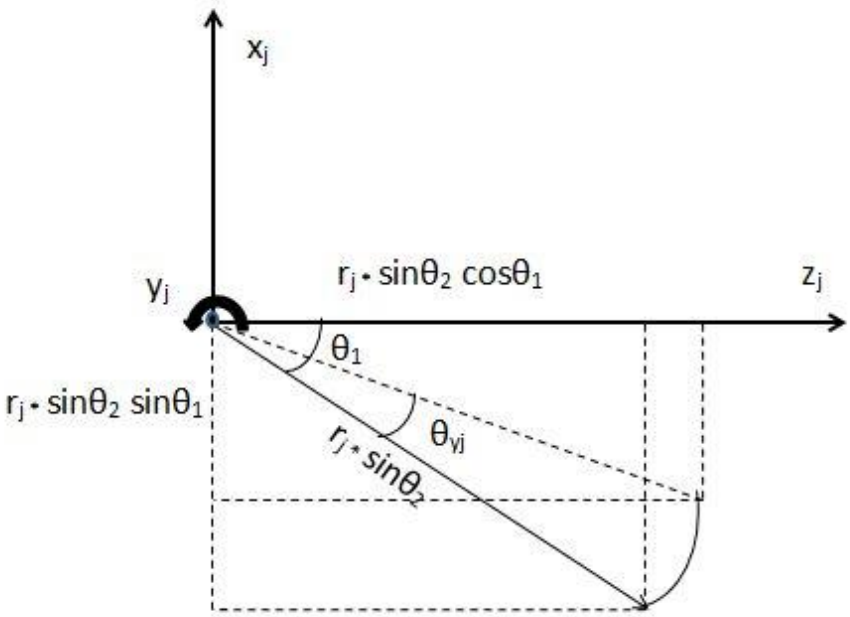

Figure 6.14: Rotational Motion About y_j

$$x_j = -\,r_j\,\sin\theta_2(sin\theta_1 cos\theta_{yj} - cos\theta_1 sin\theta_{yj}) + r_j\,sin\theta_2 sin\theta_1$$
$$z_j = r_j\,\sin\theta_2(cos\theta_1 cos\theta_{yj} + sin\theta_1 sin\theta_{yj}) - r_j\,sin\theta_2 cos\theta_1 \qquad (6.18)$$

- Rotational motion about z_j by θ_{zj}

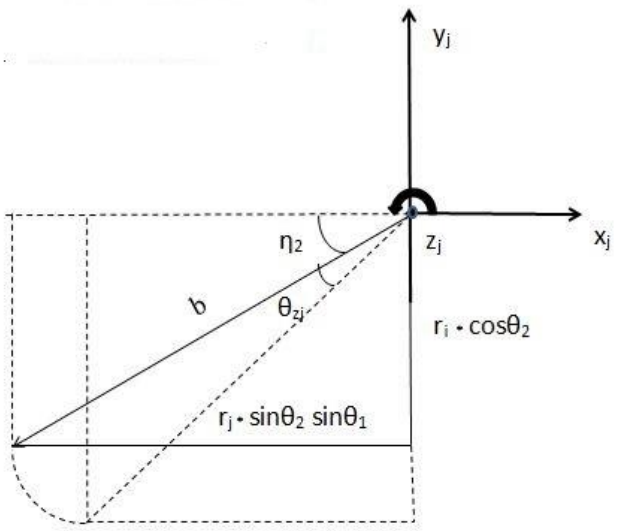

Figure 6.15: Rotational Motion About z_j

$$y_j = -\,\mathrm{b}\,(\sin\eta_2\, cos\theta_{zj} + cos\eta_2 sin\theta_{zj}) + b\, sin\eta_2$$
$$x_j = -\mathrm{b}\,(\cos\eta_2\, cos\theta_{zj} - sin\eta_2 sin\theta_{zj}) + b\, cos\eta_1 \qquad (6.19)$$

Where,

$$\eta_2 = tan^{-1}\left(\frac{r_j cos\theta_2}{r_j sin\theta_2 sin\theta_1}\right)$$

$$\mathrm{b} = r_j\sqrt{cos^2\theta_2 + sin^2\theta_2 sin^2\theta_1}$$

Because of the assumption of small angle equation 6.14 to 6.19 can be written as below,

For rotation about x_i

$$y_i = -r_i\,\theta_{xi} sin\theta_1$$
$$z_i = 0 \qquad (6.20)$$

For rotation about y_i

$$x_i = r_i\,\theta_{yi}\sin\theta_1$$
$$z_i = -r_i\,\theta_{yi}\cos\theta_1 \qquad (6.21)$$

For rotation about z_i

$$x_i = 0$$
$$y_i = r_i\,\theta_{zi}\,cos\theta_1 \tag{6.22}$$

For rotation about x_j

$$y_j = -a\,\theta_{xj} cos\eta_1$$
$$z_j = -a\,\theta_{xj} sin\eta_1 \tag{6.23}$$

For rotation about y_j

$$x_j = r_j\theta_{yj} sin\theta_2 cos\theta_1$$
$$z_j = r_j\theta_{yj} sin\theta_2 sin\theta_1 \tag{6.24}$$

For rotation about z_j

$$y_j = -b\,\theta_{zj} cos\eta_2$$
$$z_j = b\,\theta_{zj} sin\eta_2 \tag{6.25}$$

Substitution of equation 6.20 to 6.25 into translational displacement equation 6.11 to 6.13 yields following displacement equations:

$$s_{\theta xi} = -r_i\theta_{xi} sin\theta_1\left(cos\phi_y cos\theta_2 + cos\phi_z sin\theta_2\right)$$
$$s_{\theta yi} = r_i\theta_{yi}\left(cos\phi_y sin\theta_2 - cos\phi_z cos\theta_2\right)$$
$$s_{\theta zi} = r_i\theta_{zi} cos\theta_1\left(cos\phi_y cos\theta_2 + cos\phi_z sin\theta_2\right) \tag{6.26}$$

$$s_{\theta xj} = a\,\theta_{xj} cos\eta_1\left(cos\phi_y cos\theta_2 + cos\phi_z sin\theta_2\right)$$
$$- a\,\theta_{xj} sin\eta_1\left(cos\phi_x sin\theta_1 + cos\phi_z cos\theta_2 cos\theta_1 - cos\phi_y cos\theta_1 sin\theta_2\right)$$
$$s_{\theta yj} = r_j\theta_{yj}(cos\phi_x\, sin\theta_2)$$
$$s_{\theta zj} = -b\,\theta_{zj} cos\eta_2\left(cos\phi_y cos\theta_2 + cos\phi_z sin\theta_2\right)$$
$$+ a\,\theta_{zj} sin\eta_2\left(cos\theta_1 cos\phi_x - cos\phi_z cos\theta_2 sin\theta_1 + cos\phi_y sin\theta_2 sin\theta_1\right) \tag{6.27}$$

The displacement equation can be assembled which described relative motion due to the displacement of the node (i) and (j). For translational component this equation is,

$$u_{xyz} = \left(s_{xj} - s_{xi}\right) + \left(s_{yj} - s_{yi}\right) + \left(s_{zj} - s_{zi}\right) \tag{6.28}$$

Due to the effect of force coupling, angular displacement term must be treated differently. For the derivation of equation 6.20 to 6.25, a positive angular displacement was assumed about each axis. In reality, angular displacement is negatively coupled. A positive displacement of (θ_{xi}) results in negative displacement of (θ_{xj}) and vice versa. Hence, angular relative displacement equation takes the form

$$u_\theta = \left(-s_{\theta xj} - s_{\theta xi}\right) + \left(-s_{\theta yj} - s_{\theta yi}\right) + \left(-s_{\theta zj} - s_{\theta zi}\right) \tag{6.29}$$

Total displacement along the line-of-action can be written as;

$$u_{LOA} = \left(s_{xj} - s_{xi}\right) + \left(s_{yj} - s_{yi}\right) + \left(s_{zj} - s_{zi}\right) + \left(-s_{\theta xj} - s_{\theta xi}\right) + \left(-s_{\theta yj} - s_{\theta yi}\right) + \left(-s_{\theta zj} - s_{\theta zi}\right) \tag{6.30}$$

The force along the line-of-action,

$$F_{mesh_{LOA}} = -Ku_{LOA}$$
$$F_n = K_m u_{LOA} \tag{6.31}$$

Where,

K = component of mesh stiffness matrix

K_m = Average value of mesh stiffness

6.1.6 Influence Coefficient Method

Bevel gear mesh stiffness matrix can be determined using influence coefficient method as explained earlier in chapter 5. The mesh stiffness matrix can be assembled by applying a unit displacement for each variable in $\{q_i\}$ and zero displacements in all other variables in $\{q_j\}$ vector. By applying each of six different unit displacement in $\{q_i\}$ will yield a 6×12 matrix. Similarly, using the same method to each of the variables in $\{q_j\}$ yields another 6×12 matrix. By a combination of this two 6×12 matrix final 12×12 mesh stiffness matrix obtained.

Mesh stiffness matrix can be written as,

$$[K]_{mesh} = K_m \begin{bmatrix} [K_{ii}] & [K_{ij}] \\ [K_{ji}] & [K_{jj}] \end{bmatrix} \tag{6.32}$$

The element of the four submatrices in Equation 6.32 are presented in Appendix C

6.1.7 Insertion into the Finite Element Model

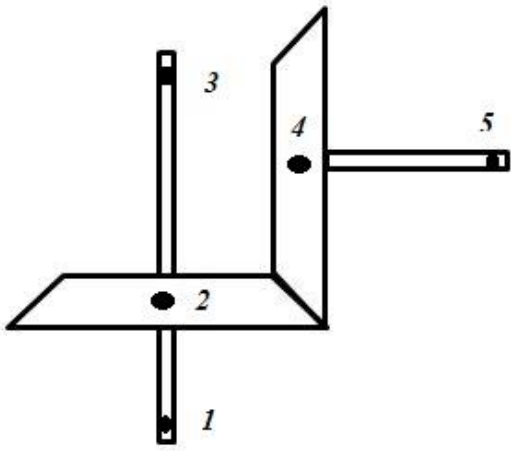

Figure 6.16: Finite Element Representation of Coupled Shaft

The mesh stiffness matrix is implemented into a finite element analysis in the following way. The node of the shaft is generally numbered sequentially for ease of analysis. However, couple node of shafts is usually non-sequential as shown in figure 6.16. Mesh coupling between node 2 and 4, results in mesh model,

$$[K]_{mesh}\begin{Bmatrix} q_2 \\ q_4 \end{Bmatrix} = \begin{bmatrix} [k_{2,2}]_{mesh} & [K_{2,4}]_{mesh} \\ [K_{4,2}]_{mesh} & [K_{4,4}]_{mesh} \end{bmatrix}\begin{Bmatrix} q_2 \\ q_4 \end{Bmatrix} \tag{6.33}$$

While assembling global matrix, mesh stiffness matrix "breaks apart" to place the corresponding sub-matrices in the appropriate blocks of the global matrix. For figure 6.16 the mesh stiffness matrix substitute in global matrix as follows,

$$[K]^{(G)} = \begin{bmatrix} [k_{1,1}{}^{(1)}] & [k_{1,2}{}^{(1)}] & 0 & 0 & 0 \\ [k_{2,1}{}^{(1)}] & [k_{2,2}{}^{(1)} + k_{2,2}{}^{(2)}] + [k_{2,2}]_{mesh} & [k_{2,3}{}^{(2)}] & [K_{2,4}]_{mesh} & 0 \\ 0 & [k_{3,2}{}^{(2)}] & [k_{3,3}{}^{(2)}] & 0 & 0 \\ 0 & [K_{4,2}]_{mesh} & 0 & [k_{4,4}{}^{(3)}] + [K_{4,4}]_{mesh} & [k_{4,5}{}^{(3)}] \\ 0 & 0 & 0 & [k_{5,4}{}^{(3)}] & [k_{5,5}{}^{(3)}] \end{bmatrix} \tag{6.34}$$

6.2 Application

6.2.1 System and System Parameter

A system selected for the analysis purpose is simple rotor-bearing system geared by bevel gears as shown in figure 6.17. This system is chosen because of the availability of the system parameters. Two journal bearing supports each rotor. There are two identical 360˚ cylindrical bearing 1 and 2. Two five–pad tilting-pad bearing 3 and 4. A rigid axial support is located at bearing 1 to constain axial movement of the rotor 1. For system shown in Figure 6.17 θ_1=180 and θ_2= 0.

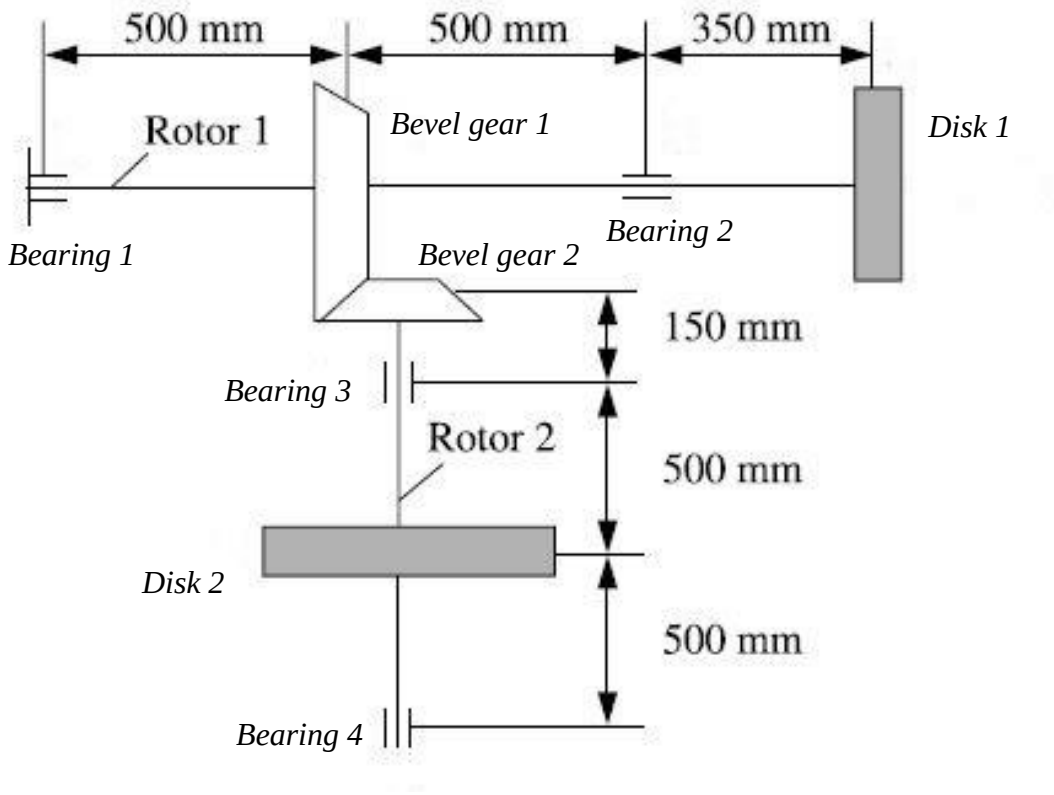

Figure 6.17: A Rotor-Bearing System Geared by Bevel Gear (M. Li (2001))

The eight coefficient of stiffness and damping can be calculated under the assumption of the small bearing. In this analysis, two results have been compared and analyzed. The first one is one of the rotating gear shafts as a single system, with gear acting as a rigid disk only. The second one is of complete gear shafts system.

Table 6.1: The Bevel Gear System Parameters

Materials Parameters	
Youngs's Modulus (E) (N/m²)	2.06E11
Shear Modulus (G) (N/m²))	7.8E10
Poisson's Ratio (υ)	0.3
Density (ρ) (kg/m³)	7800
Shaft Parameters	
Length of Rotor 1 (L_1) (m)	1.350
Length of Rotor 2 (L_2) (m)	1.150
Outer Diameter (d_o) (m)	0.1
Inner Diameter (d_i) (m)	0.0
Gear Parameters	
Radius of Bevel Gear 1 (m)	0.30
Radius of Bevel Gear 2 (m)	0.10
Mass of Bevel Gear 1 (kg)	600.0
Mass of Bevel Gear 2 (kg)	40.0
Transverse Mass Moment of Inertia of Gear 1 (kg-m²)	15.0
Polar Mass Moment of Inertia of Gear 1 (kg-m²)	25.0
Transverse Mass Moment of Inertia of Gear 2 (kg-m²)	0.05
Polar Mass Moment of Inertia of Gear 2 (kg-m²)	0.072
Pitch Angle of Gear 1 (δ_1) (deg)	71.57
Pitch Angle of Gear 2 (δ_2) (deg)	18.43
Average Mesh stiffness (K_m)(N/m)	1.0E8
Disk Parameters	
Mass of Disk 1 (kg)	300.0
Mass of Disk 2 (kg)	600.0
Transverse Mass Moment of Inertia of Disk 1 (kg-m²)	12.0
Polar Mass Moment of Inertia of Disk 1 (kg-m²)	20.0
Transverse Mass Moment of Inertia of Disk 2 (kg-m²)	15.0
Polar Mass Moment of Inertia of Disk 2 (kg-m²)	25.0
Bearing Parameter	
L/D Ratio	0.5
Clearance Ratio (ψ)	0.002
Dynamic Viscosity (μ) (N-s/m²)	0.021

The node numbering for the analysis of the bevel gear system shown in figure 6.17 is considered as shown in figure 6.18.

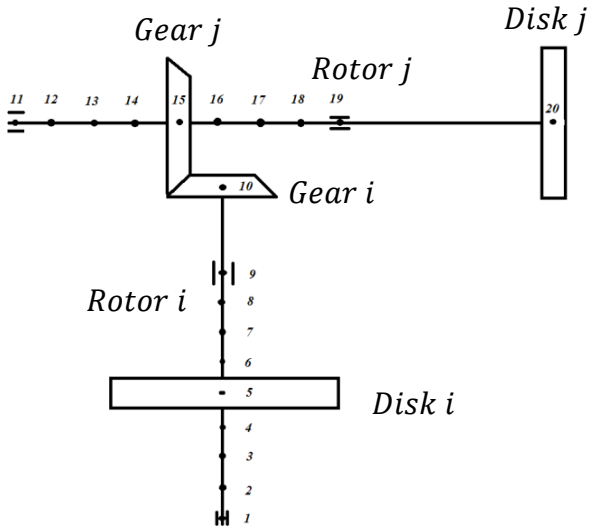

Figure 6.18: Node Numbering For Bevel Gear System

6.2.2 Result of Single Shaft System: ROTOR 1 / ROTOR j

First, ten natural frequency of the single shaft system with their corresponding descriptions is shown in Table 6.2.

Table 6.2: Natural Frequencies (Hz) of Single Rotor 1/ Rotor j

Frequency No.	Mode	Natural Frequency
1	1st Axial, 1st Torsional	0
2	1st Lateral	23.87
3	2nd Lateral	33.42
4	2nd Torsional	44.56
5	3rd Lateral	57.29
6	4th Lateral	63.66
7	5th Lateral	124.14
8	6th Lateral	144.83
9	7th Lateral	162.33
10	8th Lateral	173.47

The mode shape for the first ten natural frequencies is plotted in figure 6.19 through figure 6.28 for the rotating speed of 1500 rpm of rotor 1. At 0 rpm, the mode shapes are planer and shaft

behave as a vibrating beam. At 1500 rpm mode shapes are no longer planer, the orbital mode shape is proof for that.

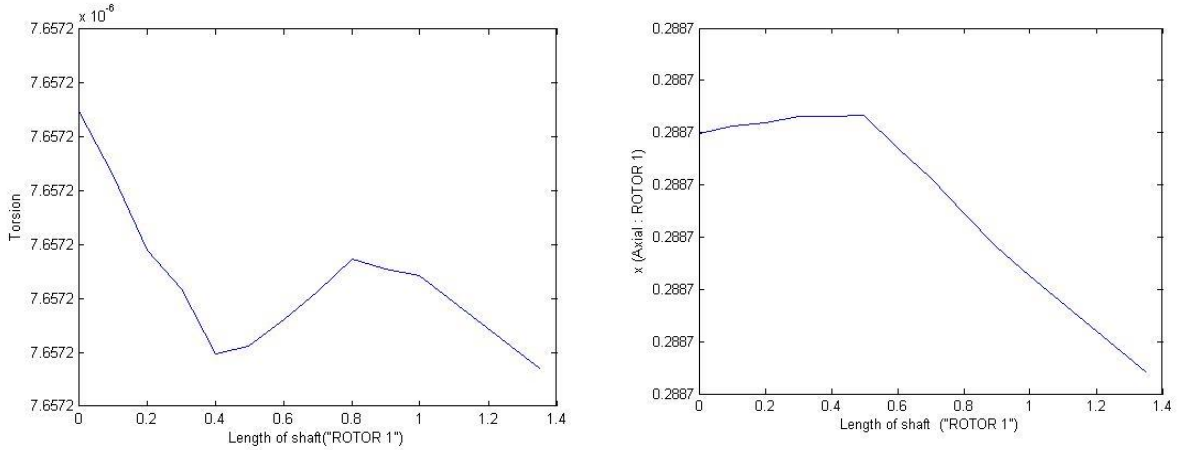

Figure 6.19: 1st Torsional (left) and 1st Axial (right) Mode Shape: 0 Hz

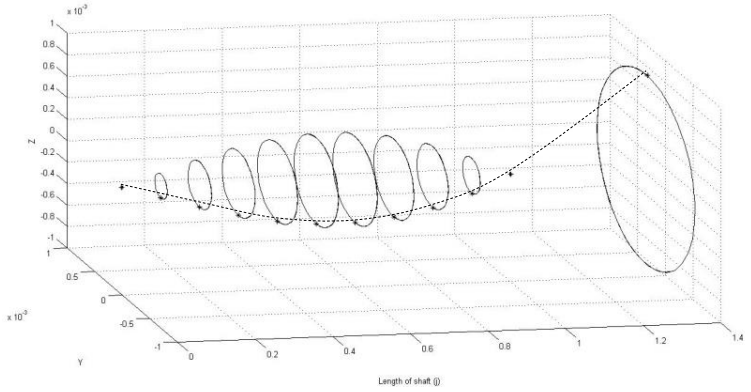

Figure 6.20: 1st Lateral Mode Shape: 23.87 Hz

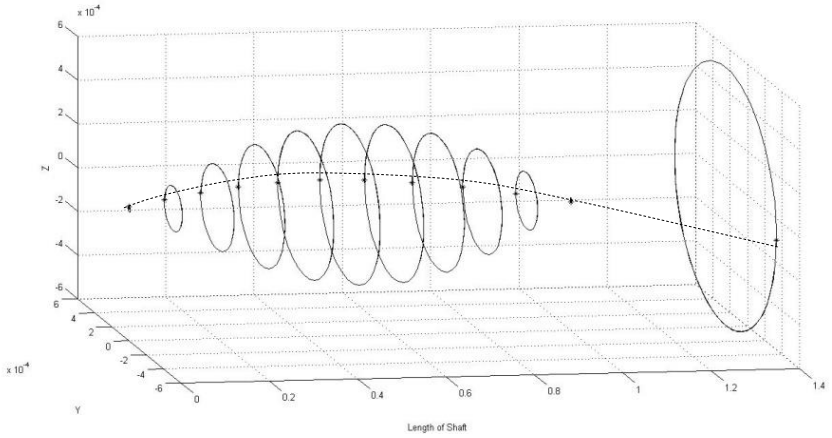

Figure 6.21: 2nd Lateral Mode Shape: 33.42 Hz

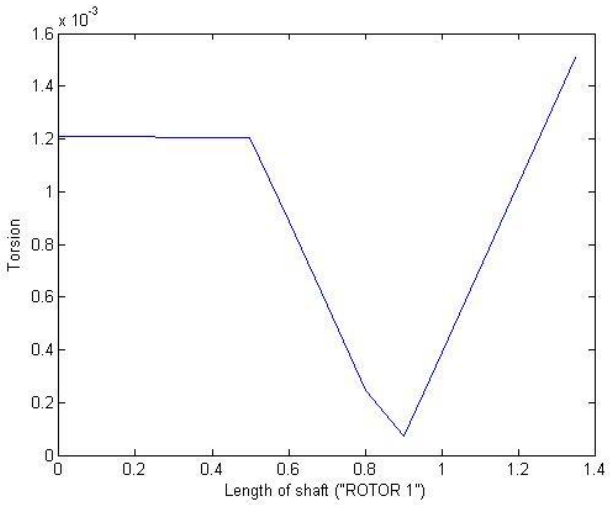

Figure 6.22: 2nd Torsional Mode Shape: 44.56 Hz

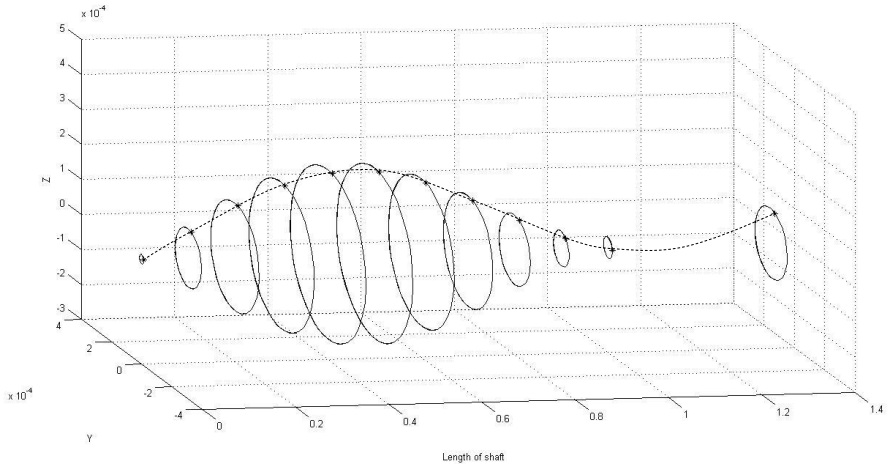

Figure 6.23: 3rd Lateral Mode Shape: 57.29 Hz

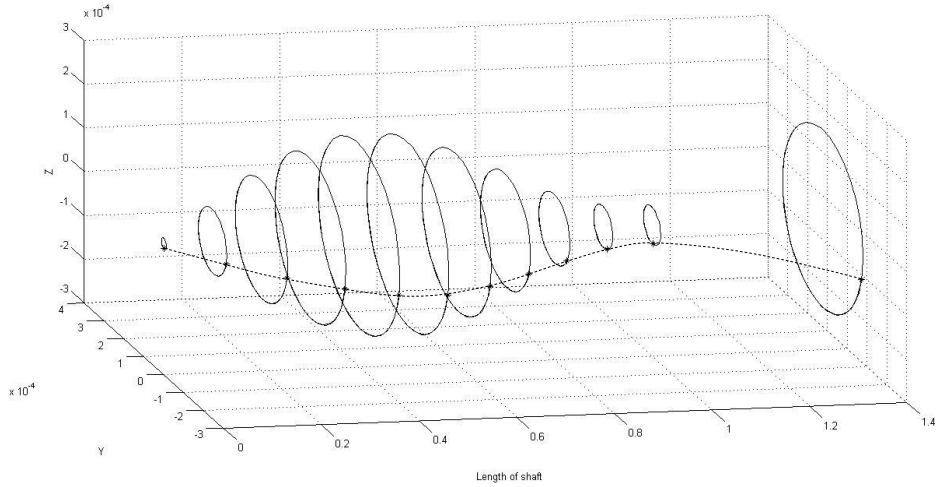

Figure 6.24: 4th Lateral Mode Shape: 63.66 Hz

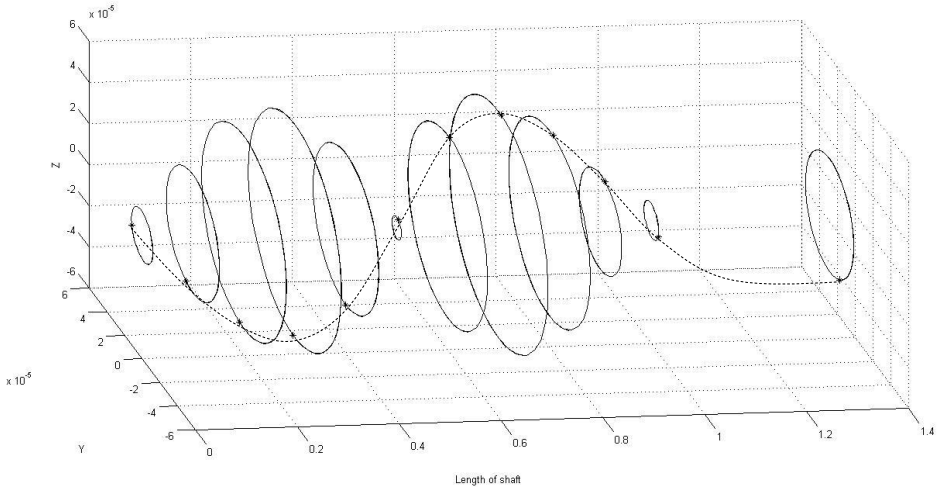

Figure 6.25: 5th Lateral Mode Shape: 124.14 Hz

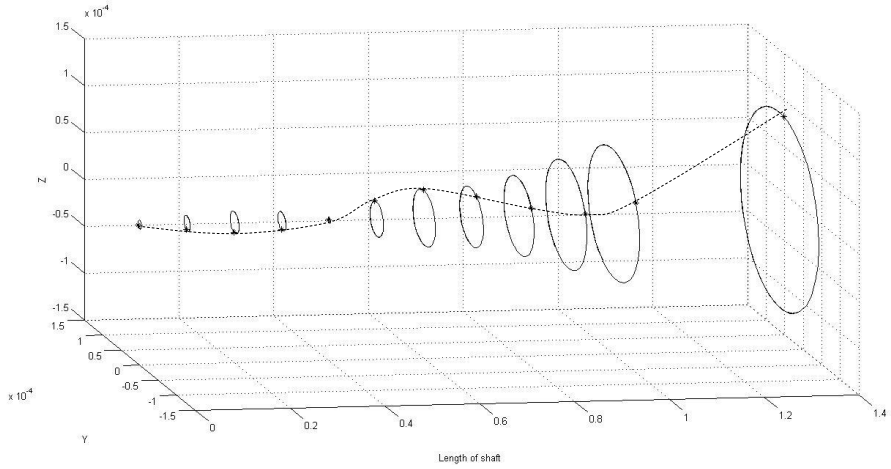

Figure 6.26: 6th Lateral Mode Shape: 144.83 Hz

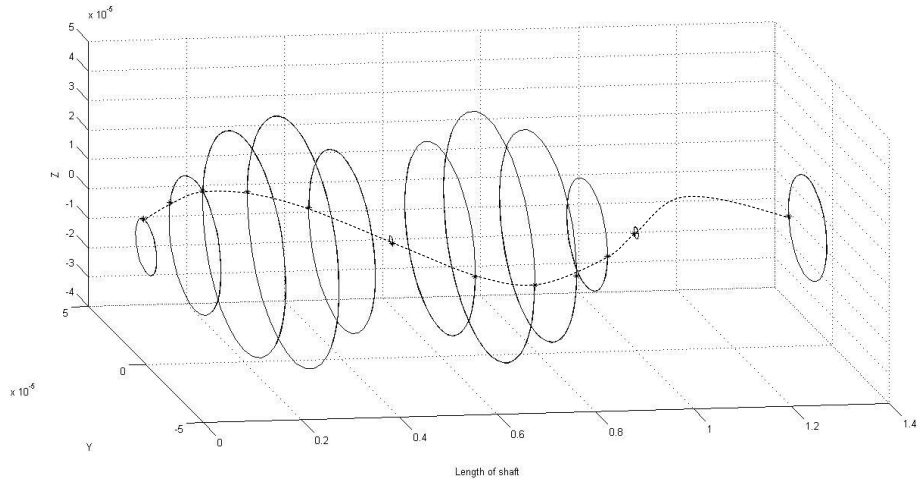

Figure 6.27: 7th Lateral Mode Shape: 162.33 Hz

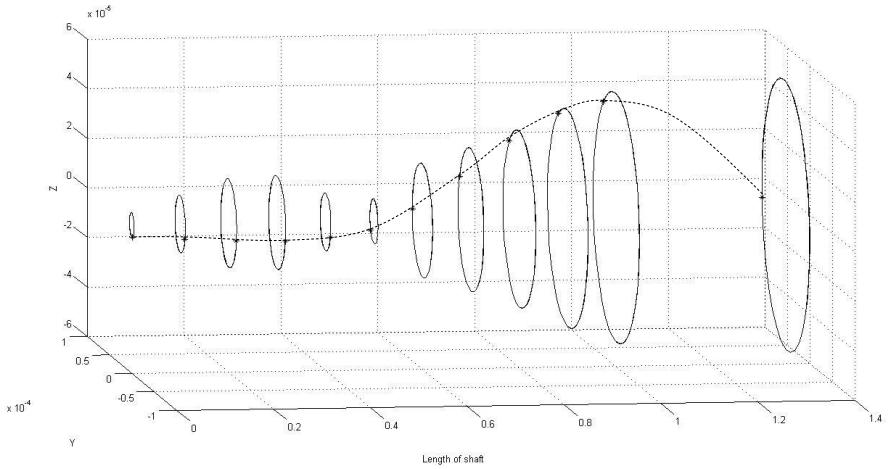

Figure 6.28: 8th Lateral Mode Shape: 173.47 Hz

6.2.3 Result of Single Shaft System: ROTOR 2 / ROTOR i

First, Twelve natural frequency of the single shaft system with their corresponding descriptions is shown in Table 6.3.

Table 6.3: Natural Frequencies (Hz) of Single Rotor 2/ Rotor i

Frequency No.	Mode	Natural Frequency
1	1st Axial	0
2	1st Lateral	45,47
3	2nd Lateral	95
4	3rd Lateral	206
5	4th Lateral	286
6	5th Lateral	302
7	6th Lateral	366
8	7th Lateral	716
9	8th Lateral	986
10	9th Lateral	1575
11	1st Torsional	1591
12	10th Lateral	1718

The mode shape for the first ten natural frequencies is plotted in figure 6.29 through 6.40 for the rotating speed of 1500 rpm of rotor 1.

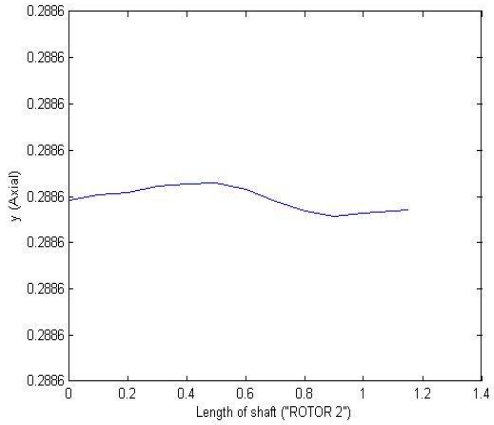

Figure 6.29: 1st Axial Mode: 0 Hz

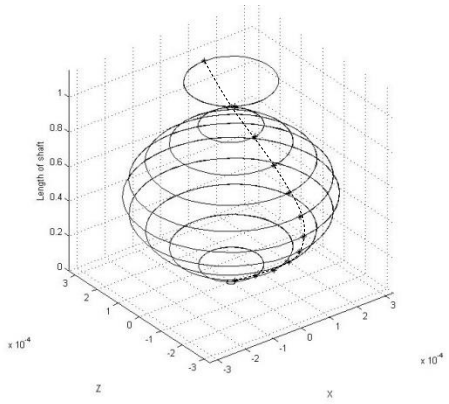

Figure 6.30: 1st Lateral Mode: 45 Hz

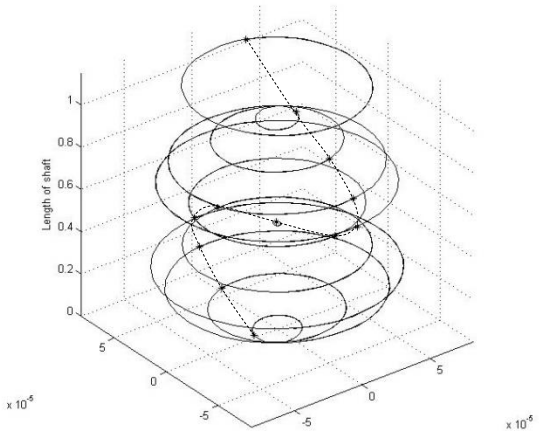

Figure 6.31: 2nd Lateral Mode: 95 Hz

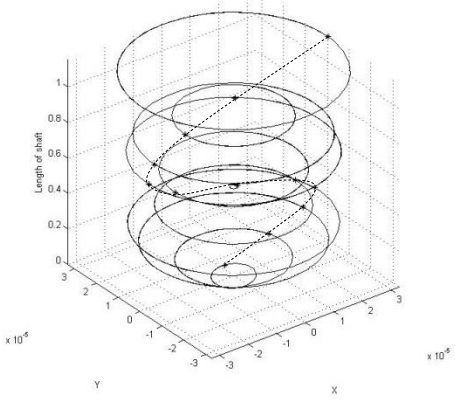

Figure 6.32: 3rd Lateral Mode: 206 Hz

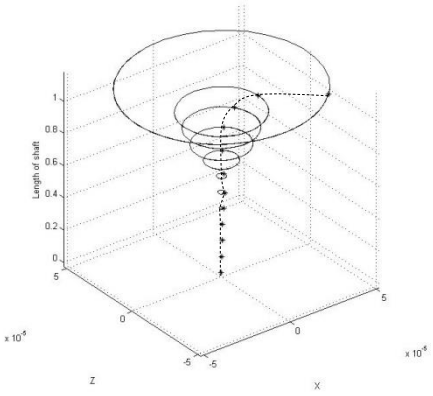

Figure 6.33: 4th Lateral Mode: 286 Hz

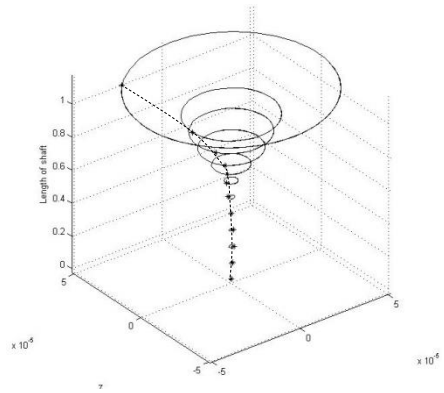

Figure 6.34: 5th Lateral Mode: 302 Hz

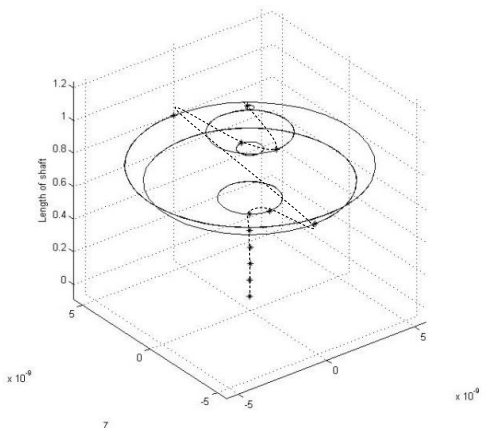

Figure 6.35: 6th Lateral Mode: 366 Hz

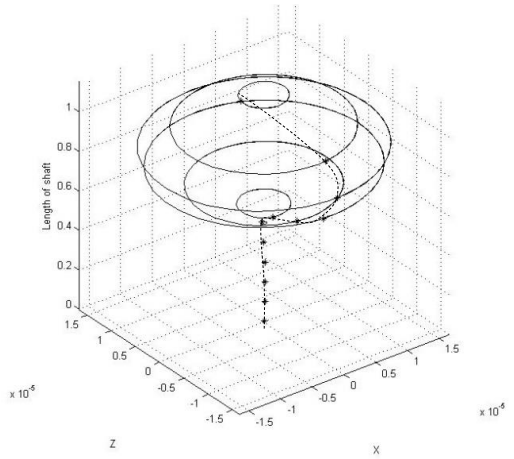

Figure 6.36: 7th Lateral Mode: 716 Hz

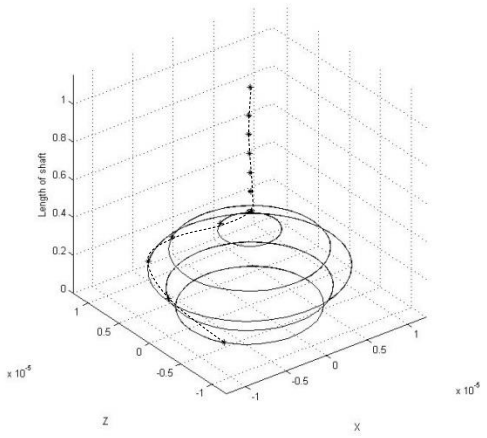

Figure 6.37: 8th Lateral Mode: 986 Hz

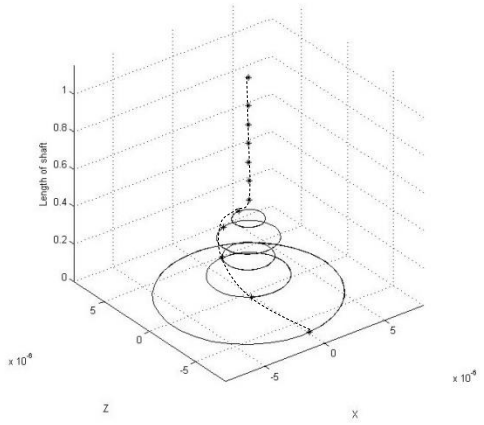

Figure 6.38: 9th Lateral Mode: 1575 Hz

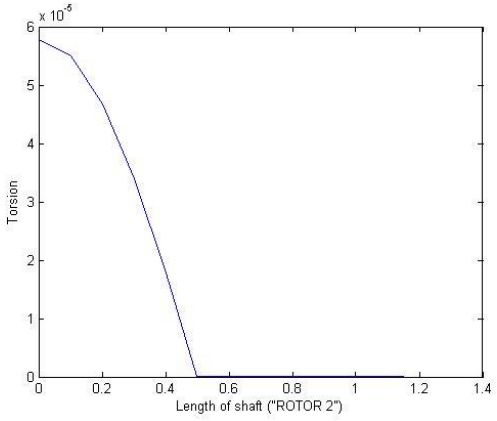

Figure 6.39: 1st Torsional Mode: 1591 Hz

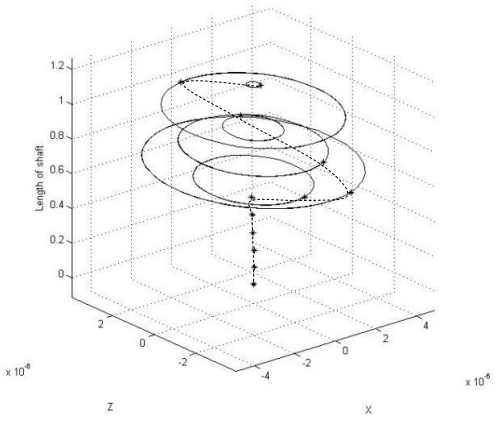

Figure 6.40: 10th Lateral Mode: 1718 Hz

6.2.4 Result of Coupled System

Table 6.4 shows natural frequency of the dual shaft system and comparison with natural frequencies of the single-shaft system.

Table 6.4: Natural Frequencies of Coupled System (Hz)

Frequency No.	Mode	Natural Frequency		
		Rotor 1	**Rotor 2**	**Coupled System**
1	1st Axial , 1st Torsional	0	0	0
2	1st Lateral	23.87		22.28
3	Coupled, 1st Lateral			28.64
4	2nd Lateral	33.42		35.01
5	3rd Lateral	44.56	45,47	43.29, 43.60
6	4th Lateral	57.29		55.70
7	5th Lateral	63.66		62.07
8	Coupled, 2nd Lateral			84.35
9	6th Lateral		95	93.90
10	7th Lateral	124.14		125.73
11	8th Lateral	144.83		146.42
12	9th Lateral	162.33		163.92
13	10th Lateral	173.47		173.47
14	11th Lateral		206	211.67
15	12th Lateral		286,302	311.94, 316.71

For Comparison of single and dual shaft system, Mode shape at first individual natural frequencies of the single-shaft system compared with mode shape of dual shaft system at the corresponding natural frequency.

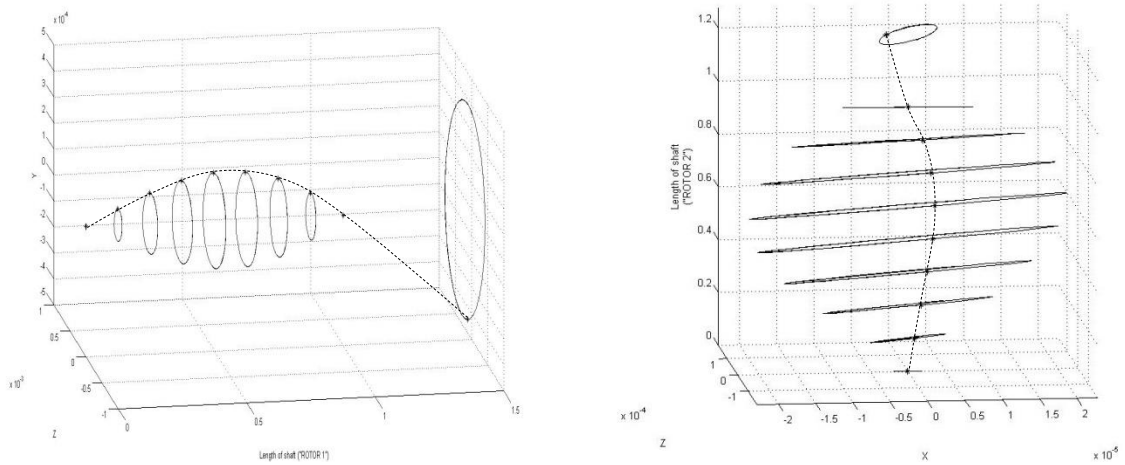

Rotor 1 Rotor 2

Figure 6.41: 1st Lateral Mode Shape of Coupled System: 22.28 Hz

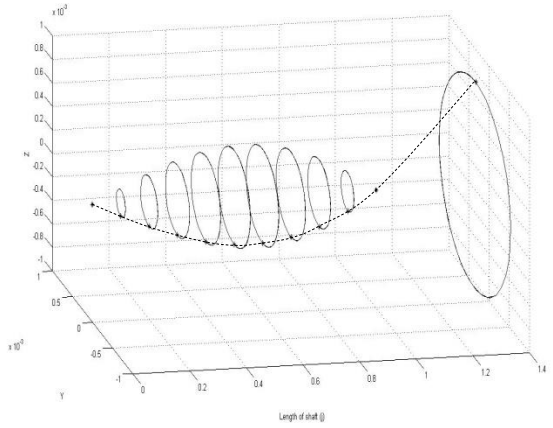

Figure 6.42: 1st Lateral Mode Shape Single Rotor1: 23.87 Hz

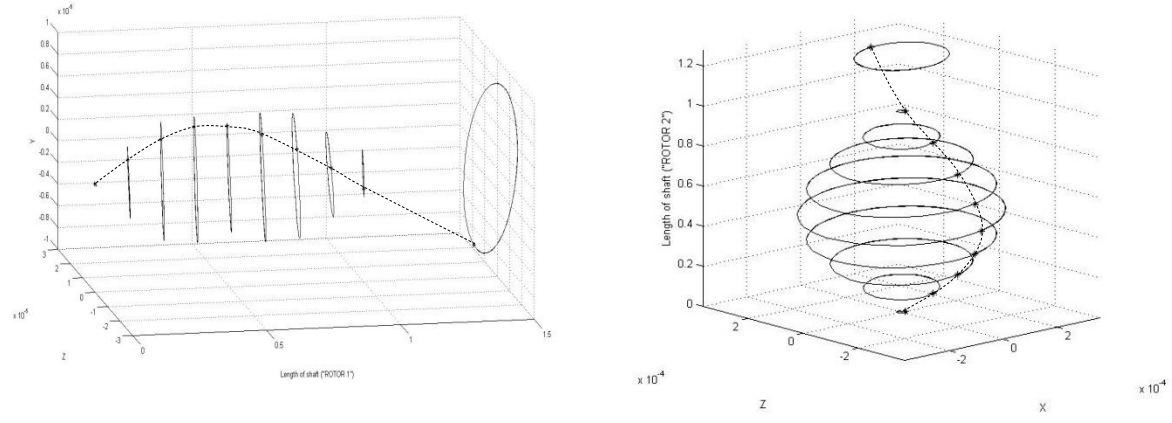

Rotor 1 Rotor 2

Figure 6.43: 3rd Lateral Mode Shape of Coupled System: 43.60 Hz

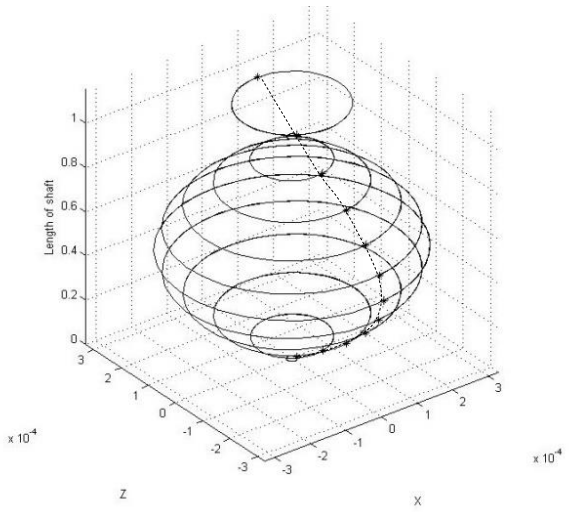

Figure 6.44: 1st Lateral Mode Shape of Single Rotor 2: 45 Hz

Figure 6.41 and figure 6.43 explain that mode shape of dual shaft system at frequencies which close to individual natural frequencies of a particular single shaft system having same mode shape of that particular shaft in dual shaft system as in single shaft system. For example, Mode shape of coupled shaft system is shown in figure 6.41 in which mode shape of rotor one has same mode shape as in single shaft system illustrated in figure 6.42 because natural frequency 22.28 Hz of the dual-shaft system is close to the natural frequency 23.87 Hz of the single-shaft system: rotor one. Figure 6.45 through figure 6.57 present remaining mode shape of the coupled system.

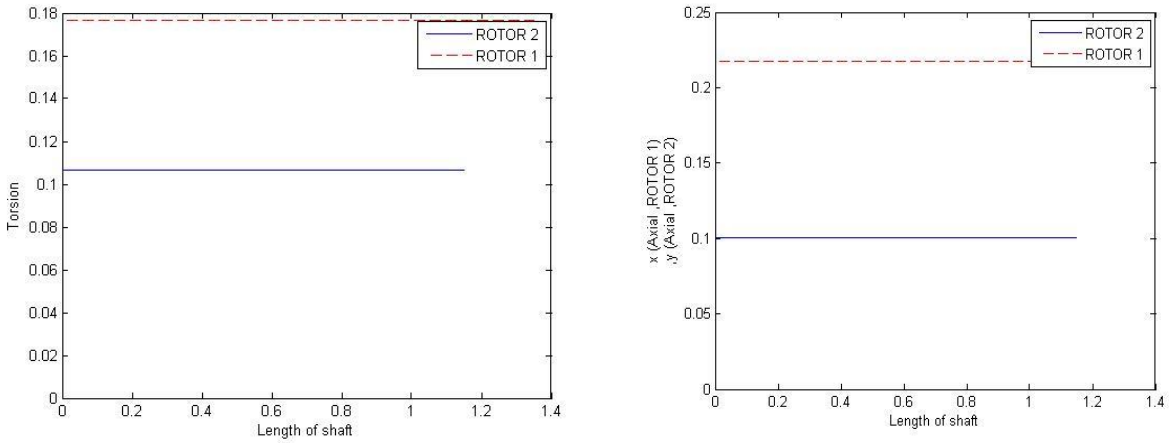

Figure 6.45: 1st Axial (right) and 1st Torsional Mode Shape, 0 Hz

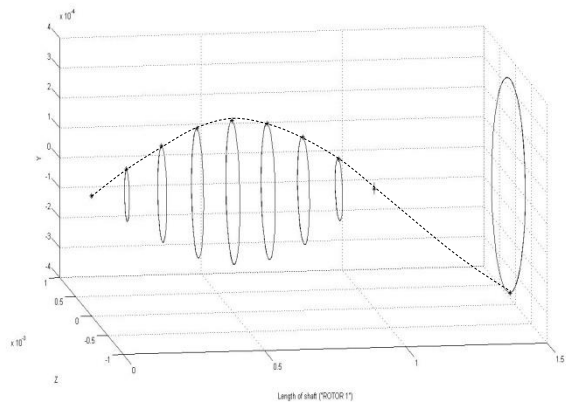

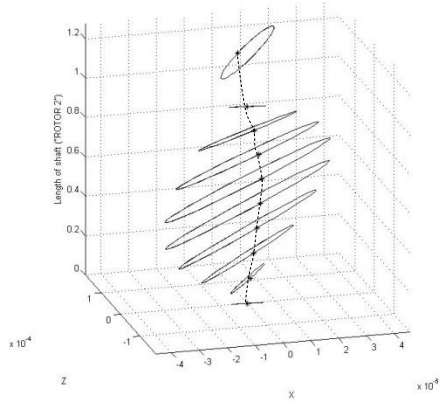

Rotor 1 Rotor 2

Figure 6.46: 2nd Lateral Mode Shape: 35.01 Hz

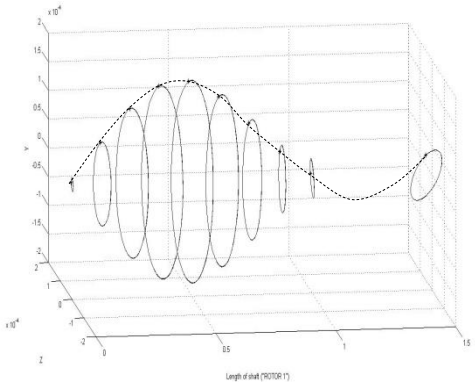

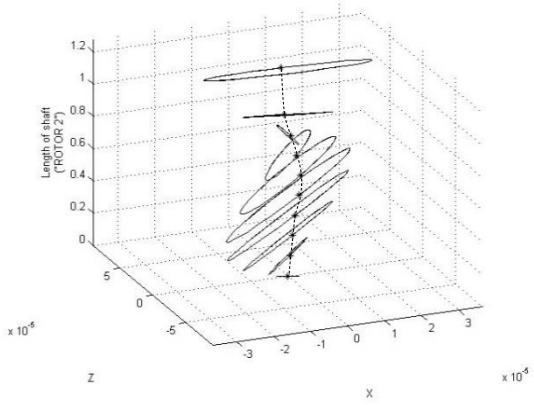

Rotor 1 Rotor 2

Figure 6.47: 4th Lateral Mode Shape: 55.70 Hz

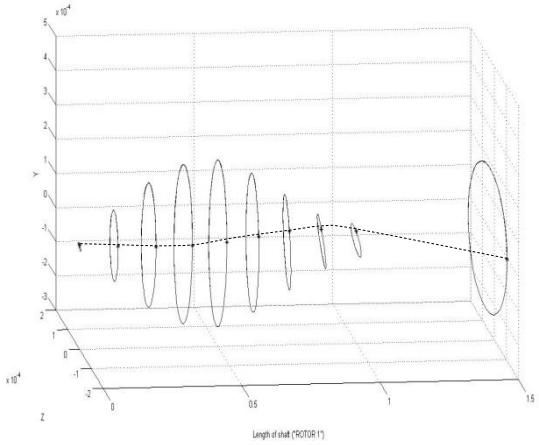

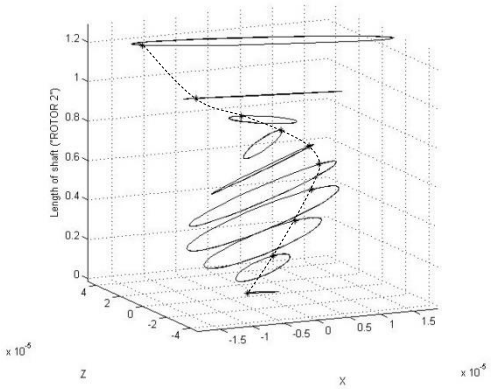

Rotor 1 Rotor 2

Figure 6.48: 5th Lateral Mode Shape: 62.07 Hz

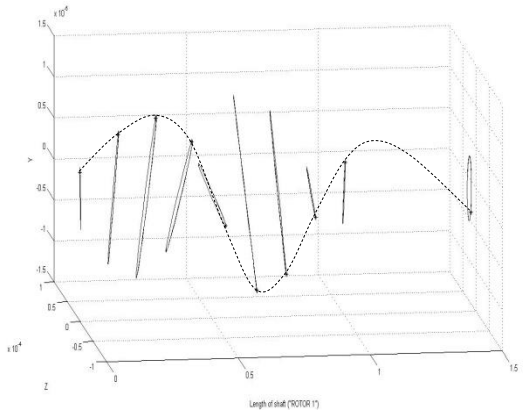

Rotor 1

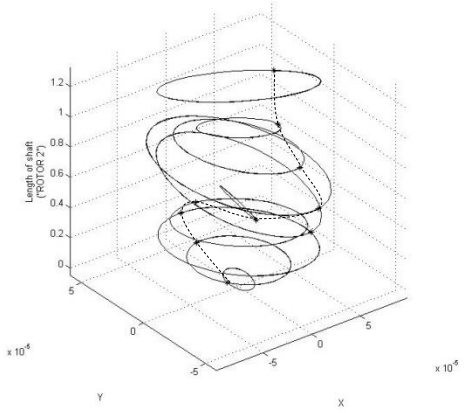

Rotor 2

Figure 6.49: 6th Lateral Mode Shape: 93.90 Hz

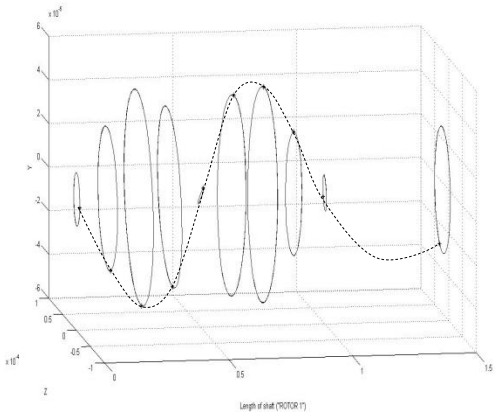

Rotor 1

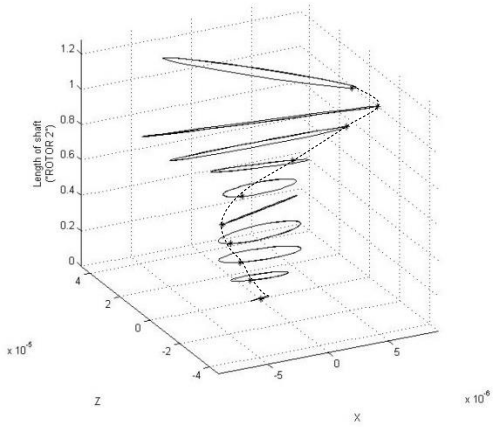

Rotor 2

Figure 6.50: 7th Lateral Mode Shape: 125.73 Hz

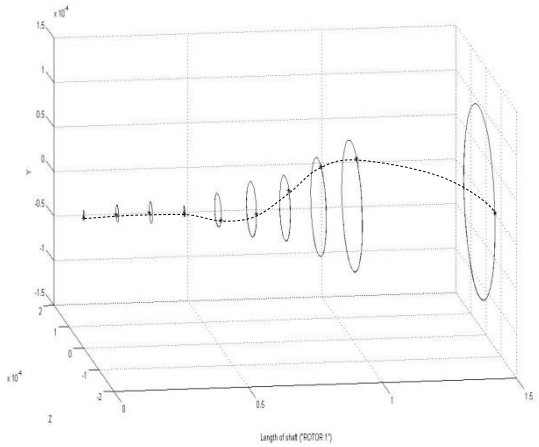

Rotor 1

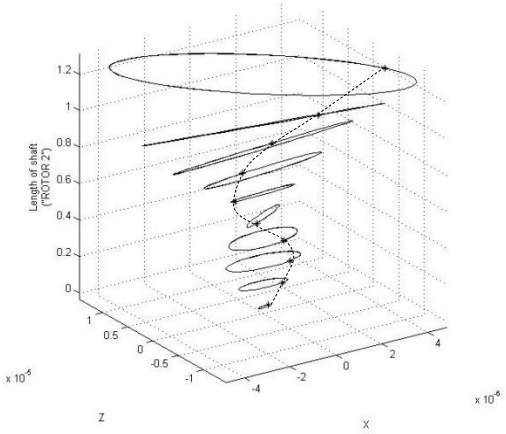

Rotor 2

Figure 6.51: 8th Lateral Mode Shape: 146.42 Hz

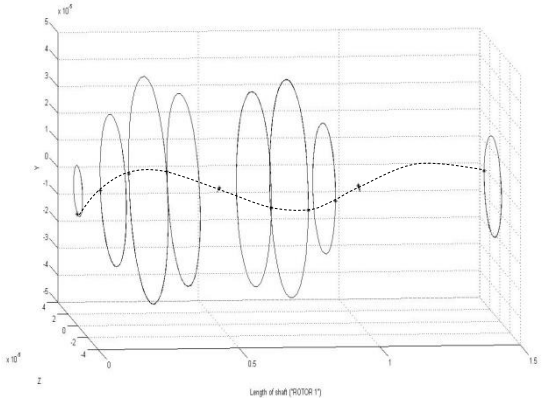

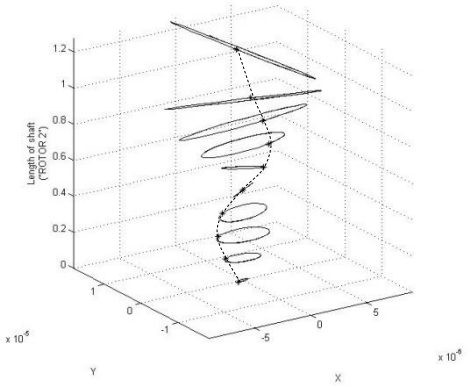

Rotor 1 Rotor 2

Figure 6.52: 9th Lateral Mode Shape: 163.92 Hz

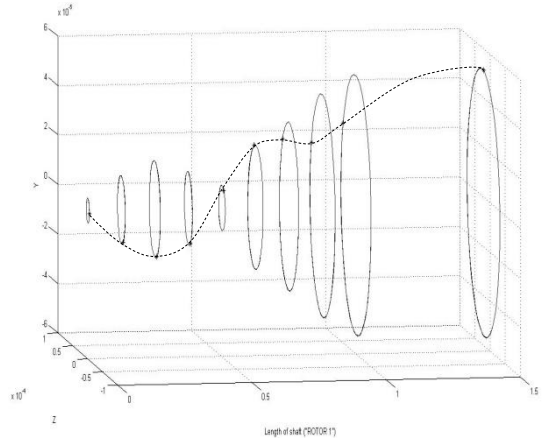

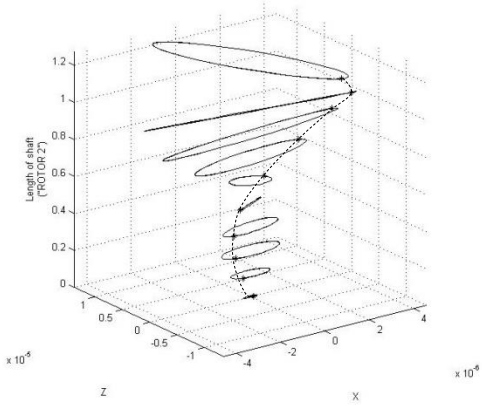

Rotor 1 Rotor 2

Figure 6.53: 10th Lateral Mode Shape: 173.47 Hz

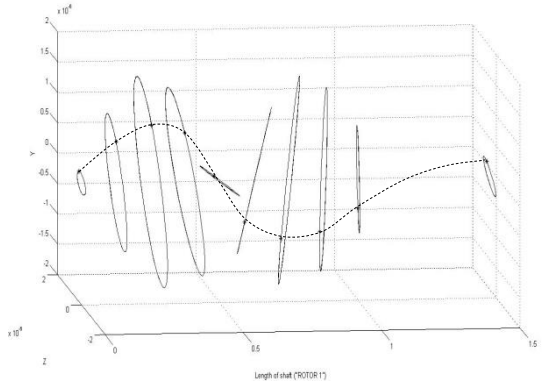

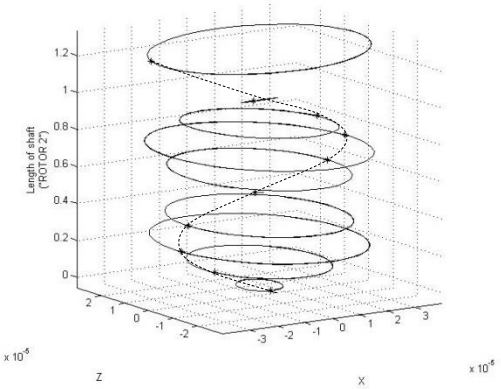

Rotor 1 Rotor 2

Figure 6.54: 11th Lateral Mode Shape: 211.67 Hz

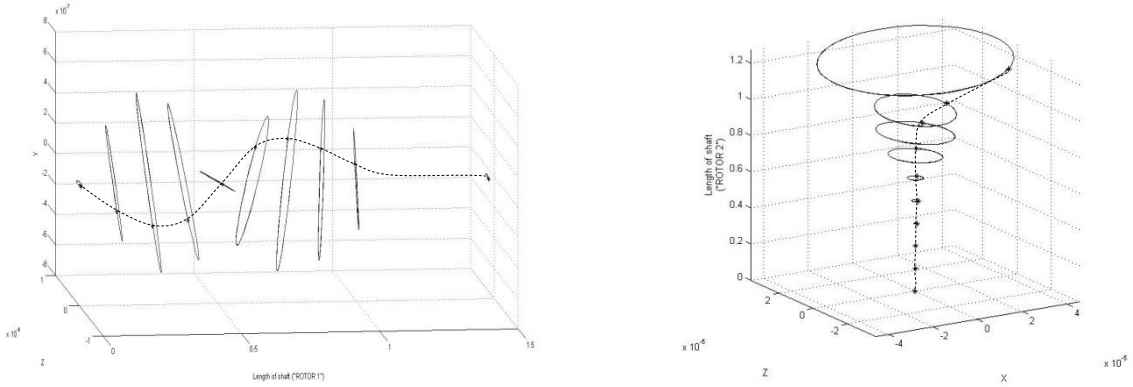

Rotor 1 Rotor 2

Figure 6.55: 12th Lateral Mode Shape: 311.94 Hz

Coupled Mode Shapes:

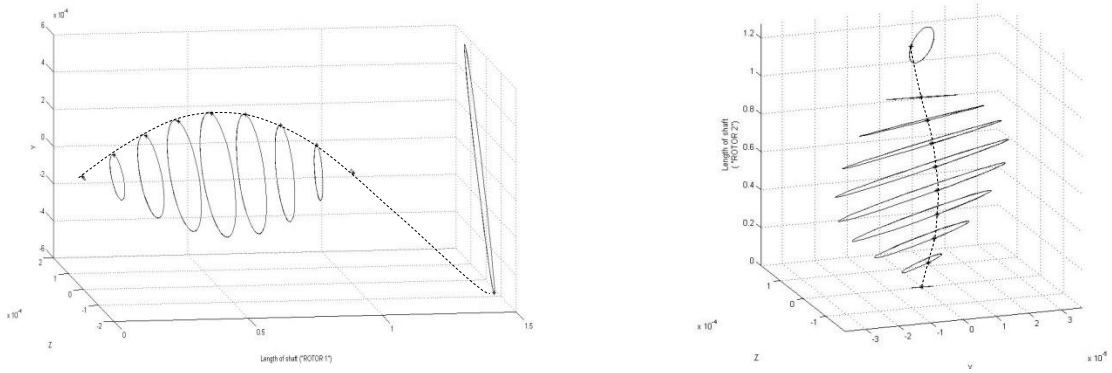

Rotor1 Rotor 2

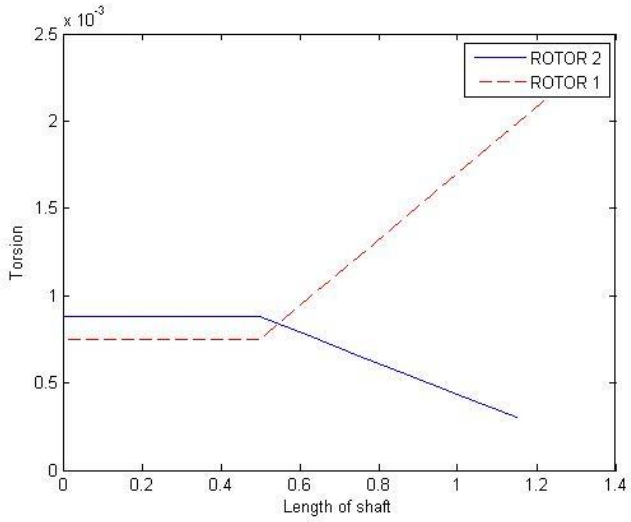

Figure 6.56: Coupled, 1st Lateral- Torsional Mode Shape: 28.64 Hz

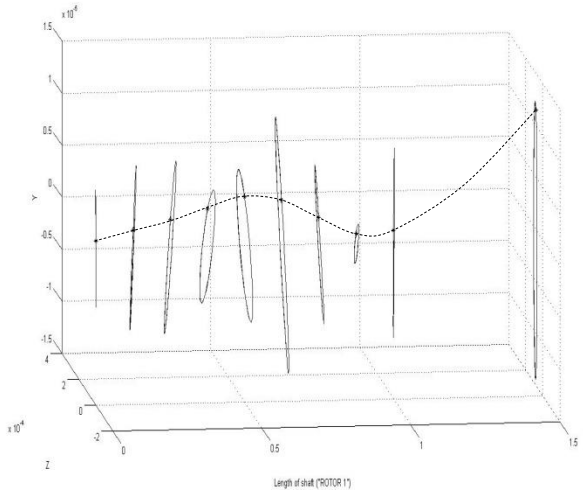

Rotor 1

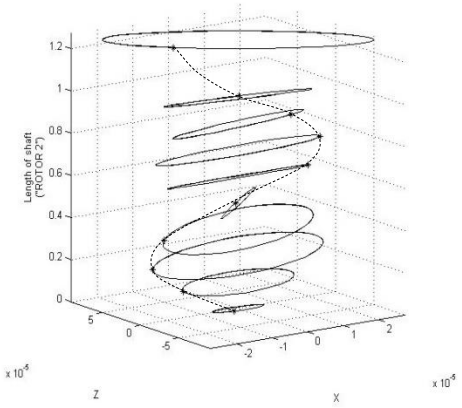

Rotor 2

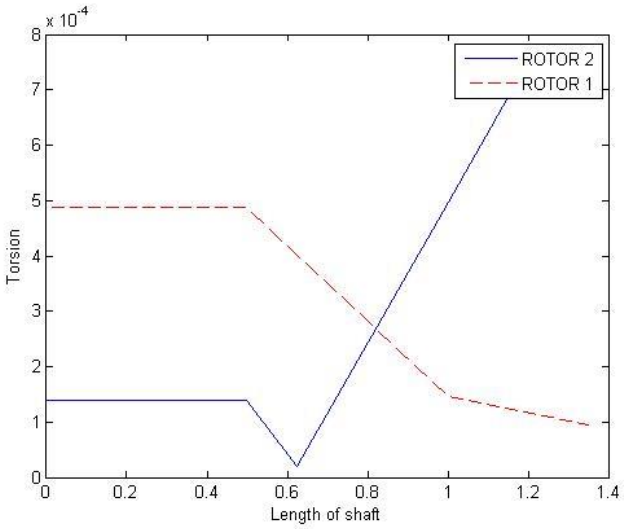

Figure 6.57: Coupled, 2nd Lateral- Torsional Mode Shape: 84.35 Hz

6.2.5 Validation

The results of bevel gear system in Table 6.2, 6.3 and 6.4 is validated with the previous study by M. Li and H.Y. Hu (2001).

Comparison of first few natural frequencies of single and dual shaft system is shown in Table 6.5, 6.6 and 6.7

From the table 6.5,6.6 and 6.7 it can be varified that method developed for the bevel gear mesh gives approximate same result as difference between is vary less between obtained natural frequencies and natural frequncies obtained priviously by M. Li.

Table 6.5: Comparison of Natural Frequencies (Hz) of Rotor 1

Natural Frequency No.	Natural freq. obtained by M. Li (2001)	Calculated	Difference (%)
1st	24.6	23.87	2.96
2nd	35.28	33.42	5.27
3rd	-	44.56	-
4th	58.18	57.29	1.52

Table 6.6: Comparison of Natural Frequencies (Hz) of Rotor 2

Natural Frequency No.	Natural freq. obtained by M. Li (2001)	Calculated	Difference (%)
1st	44.91	45	0.2
2nd	44.96	45	0.08
3rd	87.33	95	8.07

Table 6.7: Comparison of Natural Frequencies (Hz) Dual Shaft System

Natural Frequency No.	Natural freq. obtained by M. Li (2001)	Calculated	Difference (%)
1st	23.31	22.28	4.41
2nd	29.05	28.64	3.49
3rd	37.75	35.01	7.25
4th	44.9	43.29	3.58
5th	45.1	43.60	3.32
6th	55.78	55.70	0.14
7th	58.35	62.07	6.42

7 Conclusions and Recommendations

This research has presented a comprehensive set of methodologies for conducting geared rotor dynamic analysis of a complex system using a finite element modeling approch.

7.1 Conclusions

Following are some primary conclusion from this research.

1. The derivation of 12-DOF mesh stiffness matrix was presented for coupling two node of the finite element analysis. This matrix can incorporate both linear and non-linear mesh stiffness coefficient values into model.
2. This model is able to provide the contribution of all DOFs of the gear pair to a global coordinates system.
3. Helical gear gear-mesh model uncoupled lateral, torsional and axial frequencies of the dual shaft system are same as the single shaft system.
4. The coupling between two gear-shafts can be identified as coupled natural frequencies. This coupled natural frequency gives a couple mode of vibration between the lateral and torsional DOFs.
5. Magnitude of the coupled vibration is increases with increases in frequencies.
6. Uncoupled natural frequencies of coupled system will provide same mode shape of that particular shaft as in single shaft system of that particular shaft.
7. Magnitude of the torsional vibration largely depends on the mass moment of inertia of the rotor disk or gear's itself.
8. Meshing stiffness of the gear depends on the number of mashing pair in contact at a time, when one pair of teeth are in contact at that time mesh stiffness of gear pair decreases but as number of pair in contact increases the mesh stiffness value of gear pair increases.
9. Average value of the gear mesh stiffness is largely depends upon materials parameter of meshing gears.

7.2 Limitation

1. This model does not include effect of the sliding action or friction, and all force are assumed to operate at the pitch point along the LOA.

2. This model can’t be used for a shafts where the shaft axis are in relative motion to one another such as epicyclic gear train.

7.3 Recommendations

1. The combine tooth stiffness and elastohydrodynamic (EHD) stiffness effects on mesh stiffness. Both the stiffness of tooth and EHD determine the mesh stiffness. By including both more sophisticated model can be develop.
2. Further effect of non-linear mesh stiffness can be analyzed for the both helical and bevel geared system.
3. Inclusion of the backlash and transmission error would give more robust model.
4. This work can be extended to the epicyclic gear train.

References

[1]. A. Kahraman, H. Ozguven, D. Houser and J. Zakrajsek, "Dynamic Analysis of Geared Rotors by Finite Elements", *Journal of Mechanical Design*, vol. 114, no. 3, p. 507, 1992.

[2]. B. Kishor and S. Gupta, "On Dynamic Gear Tooth Loading Due to Coupled Torsional-Lateral Vibrations in a Geared Rotor-Hydrodynamic Bearing System", *J. Tribol.*, vol. 111, no. 3, p. 418, 1989.

[3]. C. Lee, "Nonlinear contact Analysis of mashing gear", M. tech, California Polytechnic State University, San Luis Obispo, 2009.

[4]. D. Stringer, "Gear rotor dynamic methodologies for advancing prognostic modeling capabilities in rotary wing transmission system", Ph. D., University of Virginia, Charlottesville, VA, 2008.

[5]. G. Wesley Blankenship and R. Singh, "Dynamic force transmissibility in helical gear pairs", *Mechanism and Machine Theory*, vol. 30, no. 3, pp. 323-339, 1995.

[6]. I. Howard, S. Jia and J. Wang, "The Dynamic Modelling of a Spur Gear In Mesh Including Friction and a Crack", *Mechanical Systems and Signal Processing*, vol. 15, no. 5, pp. 831-853, 2001.

[7]. J. Kaplan, S. Dousti and P. Allaire, "Rotor dynamics modeling of geared and geared system", in *Turbine Technical Conference and Exposition*, San Antonio, Texas, USA, 2013, pp. 1-10.

[8]. J. Lin and R. Parker, "Mesh Stiffness Variation Instabilities in Two-Stage Gear Systems", *J. Vib. Acoust.*, vol. 124, no. 1, p. 68, 2002.

[9]. J. Przemieniecki, *Theory of Matrix Structure Analysis*. New York: Dover Publications Inc., 1968.

[10]. J. Rao, J. Chang and T. Shiau, "Couple Bending-Torsion Vibration of Geared Rotors", in *Proceedings of the 1995 Design Engineering Technical Conferences*, Boston, 1995.

[11]. J. rao, *Rotor Dynamics*, 3rd ed. New Age Publisher, INDIA, 1996.

[12]. J. Wang and I. Howard, "Finite Element Analysis of High Contact Ratio Spur Gears in Mesh", *J. Tribol.*, vol. 127, no. 3, p. 469, 2005.

[13]. K. Werff, "Kinematics and Dynamic Analysis of Mechanisms - A Finite Element Approach", Ph. D., Delft University of Technology (Netherlands), 1977.

[14]. L. Wang, G. Wang and Z. Wang, "Equivalent Conversion Calculation of Straight Bevel Gear's Mesh Stiffness", *AMR*, vol. 381, pp. 67-71, 2011.

[15]. L. Yinong, L. Guiyan and Z. Ling, "Influence of Asymmetric Mesh Stiffness on Dynamics of Spiral Bevel Gear Transmission System", *Mathematical Problems in Engineering*, vol. 2010, pp. 1-13, 2010.

[16]. M. Li and H. Hu, "Dynamic Analysis of a Spiral Bevel-Geared Rotor-Bearing System", *Journal of Sound and Vibration*, vol. 259, no. 3, pp. 605-624, 2003.

[17]. M. Li, H. Hu, P. Jiang and L. Yu, "Coupled Axial–Lateral–Torsional Dynamics of a Rotor–Bearing System Geared by Spur Bevel Gears", *Journal of Sound and Vibration*, vol. 254, no. 3, pp. 427-446, 2002.

[18]. M. Spott, *Design of Machine Element*, 6th ed. Englewood Cliffs: NJ: Prentice- Hall, Inc., 1985.

[19]. S. Choi, J. Glienicke, D. Han and K. Urlichs, "Dynamic Gear Loads Due to Coupled Lateral, Torsional and Axial Vibrations in a Helical Geared System", *J. Vib. Acoust.*, vol. 121, no. 2, p. 141, 1999.

[20]. S. Ebrahimi and P. Eberhard, "Rigid-elastic modeling of meshing gear wheels in multibody systems", *Multibody System Dynamics*, vol. 16, no. 1, pp. 55-71, 2006.

[21]. S. Jones, "Finite Element for the Analysis of rotor dynamics system that includes Gyroscopic Effects", Ph. D., Brunel University, 2005.

[22]. S. Ratan, *Theory of Machines*, 3rd ed. New Delhi: Tata McGrow Hill Education Private Limited, 2012.

[23]. S. Wadkar and S. Kajale, "Theoretical Evaluation of Effect of Gear Parameters on Mesh Stiffness Variations", in *Proceeding of the 14th international conference on mechanical engineering in knowledge edge*, Delhi, 2005, pp. 148-153.

[24]. Singh, R., D. Houser, and A. Kahraman, "Non-Linear Dynamic Analysis of Geared Systems", Washington, D.C., 1990, NASA CR 4338. AVSCOM TR 90-C-020.

[25]. T. Kiekbusch, D. Sappok, B. Sauer and I. Howard, "Calculation of the Combined Torsional Mesh Stiffness of Spur Gears with Two- and Three-Dimensional Parametrical FE Models", *SV-JME*, vol. 57, no. 11, pp. 810-818, 2011.

[26]. T. Lim and R. Singh, "Vibration transmission through rolling element bearings. Part III: Geared rotor system studies", *Journal of Sound and Vibration*, vol. 151, no. 1, pp. 31-54, 1991.

[27]. *Theory Reference For the Mechanical APDL and Mechanical Application*, 12th ed. ANSYS Inc., 2009.

[28]. W. Cleghorn and B. Tabarrok, "Finite element formulation of a tapered Timoshenko beam for free lateral vibration analysis", *Journal of Sound and Vibration*, vol. 152, no. 3, pp. 461-470, 1992.

[29]. Y. Wang, H. Cheung and W. Zhang, "Finite element modelling of geared multi-body system", *Communications in Numerical Methods in Engineering*, vol. 18, no. 11, pp. 765-778, 2002.

[30]. Z. Luo, X. Sun and J. Fawcett, "Coupled torsional-lateral-axial vibration analysis of a geared shaft system using substructure synthesis", *Mechanism and Machine Theory*, vol. 31, no. 3, pp. 345-352, 1996.

Appendix A: Finite Element Matrix Equations

This equation presents the matrices used in equation 4.8, with exception of the gear-mesh matrix. The matrices are found from variety of sources, but mainly from ANSYS theory references (2009).

A.1 12-DOF Matrices

In equation 4.8,assuming shaft itself having no damping. Only the mass, stiffness, and gyroscopic matrices are presented for different coordinates system used in helical and bevel gear system. Subscript (h) designates matrices used in helical gear system. Subscript bi and bj used to designate matrices for i^{th} and j^{th} shaft of bevel gear system.

Two primary parameters for both shaft mass and stiffness matrices are the shape factor (κ), and the transverse shear factor (Φ).

For solid shaft,

$$\kappa = \frac{6(1+\upsilon)}{(7+6\upsilon)} \tag{A.3}$$

For a thin-walled shaft:

$$\kappa = \frac{2(1+\upsilon)}{(4+3\upsilon)} \tag{A.2}$$

Where (υ) is Poisson's Ratio.

The transverse shear parameter (Φ),

$$\Phi = \frac{12EI}{\kappa AGl^2} \tag{A.4}$$

Where,

A = Shaft cross section area

E = Young's modulus

G = Shear modulus

l = length of element

I = Area moment of inertia

A.1.1 Shaft consistent Mass matrix

The shaft consistent mass matrix uses the following relationship.

Equation A.4 through A.10 developed for shaft mass-matrix.

$$r_g = \sqrt{\frac{I}{A}} \tag{A.4}$$

$$a = \frac{\rho A l}{(1+\Phi)^2}\left(\frac{13}{35} + \frac{7}{10}\Phi + \frac{2}{3}\Phi^2 + \frac{6}{5}\left(\frac{r_g}{l}\right)^2\right) \tag{A.5}$$

$$b = \frac{\rho A l}{(1+\Phi)^2}\left(\frac{9}{70} + \frac{3}{10}\Phi + \frac{1}{6}\Phi^2 - \frac{6}{5}\left(\frac{r_g}{l}\right)^2\right) \tag{A.6}$$

$$c = \frac{\rho A l^2}{(1+\Phi)^2}\left(\frac{11}{210} + \frac{11}{120}\Phi + \frac{1}{24}\Phi^2 + \left(\frac{1}{10} - \frac{1}{2}\Phi\right)\left(\frac{r_g}{l}\right)^2\right) \tag{A.7}$$

$$d = \frac{\rho A l^2}{(1+\Phi)^2}\left(\frac{13}{420} + \frac{3}{40}\Phi + \frac{1}{24}\Phi^2 - \left(\frac{1}{10} - \frac{1}{2}\Phi\right)\left(\frac{r_g}{l}\right)^2\right) \tag{A.8}$$

$$e = \frac{\rho A l^3}{(1+\Phi)^2}\left(\frac{1}{105} + \frac{1}{60}\Phi + \frac{1}{120}\Phi^2 + \left(\frac{2}{15} + \frac{1}{6}\Phi + \frac{1}{3}\Phi^2\right)\left(\frac{r_g}{l}\right)^2\right) \tag{A.9}$$

$$f = \frac{\rho A l^3}{(1+\Phi)^2}\left(\frac{1}{140} + \frac{1}{60}\Phi + \frac{1}{120}\Phi^2 + \left(\frac{1}{30} + \frac{1}{6}\Phi - \frac{1}{6}\Phi^2\right)\left(\frac{r_g}{l}\right)^2\right) \tag{A.10}$$

$$[M_h]_s^{(e)} = \begin{bmatrix} a & 0 & 0 & 0 & c & 0 & b & 0 & 0 & 0 & -d & 0 \\ 0 & a & 0 & -c & 0 & 0 & 0 & b & 0 & d & 0 & 0 \\ 0 & 0 & \frac{1}{3}\rho Al & 0 & 0 & 0 & 0 & 0 & \frac{1}{6}\rho Al & 0 & 0 & 0 \\ 0 & -c & 0 & e & 0 & 0 & 0 & -d & 0 & f & 0 & 0 \\ c & 0 & 0 & 0 & e & 0 & d & 0 & 0 & 0 & f & 0 \\ 0 & 0 & 0 & 0 & 0 & \frac{J\rho Al}{3A} & 0 & 0 & 0 & 0 & 0 & \frac{J\rho Al}{6A} \\ b & 0 & 0 & 0 & d & 0 & a & 0 & 0 & 0 & -c & 0 \\ 0 & b & 0 & -d & 0 & 0 & 0 & a & 0 & c & 0 & 0 \\ 0 & 0 & \frac{1}{6}\rho Al & 0 & 0 & 0 & 0 & 0 & \frac{1}{3}\rho Al & 0 & 0 & 0 \\ 0 & d & 0 & f & 0 & 0 & 0 & c & 0 & e & 0 & 0 \\ -d & 0 & 0 & 0 & f & 0 & -c & 0 & 0 & 0 & e & 0 \\ 0 & 0 & 0 & 0 & 0 & \frac{J\rho Al}{6A} & 0 & 0 & 0 & 0 & 0 & \frac{J\rho Al}{3A} \end{bmatrix} \quad \text{(A.11)}$$

$$[M_{bi}]_s^{(e)} = \begin{bmatrix} a & 0 & 0 & 0 & 0 & -c & b & 0 & 0 & 0 & 0 & d \\ 0 & \frac{1}{3}\rho Al & 0 & 0 & 0 & 0 & 0 & \frac{1}{6}\rho Al & 0 & 0 & 0 & 0 \\ 0 & 0 & a & c & 0 & 0 & 0 & 0 & b & -d & 0 & 0 \\ 0 & 0 & c & e & 0 & 0 & 0 & 0 & d & f & 0 & 0 \\ 0 & 0 & 0 & 0 & \frac{J\rho Al}{3A} & 0 & 0 & 0 & 0 & 0 & \frac{J\rho Al}{6A} & 0 \\ -c & 0 & 0 & 0 & 0 & e & -d & 0 & 0 & 0 & 0 & f \\ b & 0 & 0 & 0 & 0 & -d & a & 0 & 0 & 0 & 0 & c \\ 0 & \frac{1}{6}\rho Al & 0 & 0 & 0 & 0 & 0 & \frac{1}{3}\rho Al & 0 & 0 & 0 & 0 \\ 0 & 0 & b & d & 0 & 0 & 0 & 0 & a & -c & 0 & 0 \\ 0 & 0 & -d & f & 0 & 0 & 0 & 0 & -c & e & 0 & 0 \\ 0 & 0 & 0 & 0 & \frac{J\rho Al}{6A} & 0 & 0 & 0 & 0 & 0 & \frac{J\rho Al}{3A} & 0 \\ d & 0 & 0 & 0 & 0 & f & c & 0 & 0 & 0 & 0 & e \end{bmatrix} \quad \text{(A.12)}$$

$$[M_{bj}]_s^{(e)} = \begin{bmatrix} \frac{1}{3}\rho Al & 0 & 0 & 0 & 0 & 0 & \frac{1}{6}\rho Al & 0 & 0 & 0 & 0 & 0 \\ 0 & a & 0 & 0 & 0 & c & 0 & b & 0 & 0 & 0 & -d \\ 0 & 0 & a & 0 & -c & 0 & 0 & 0 & b & 0 & d & 0 \\ 0 & 0 & 0 & \frac{J\rho Al}{3A} & 0 & 0 & 0 & 0 & 0 & \frac{J\rho Al}{6A} & 0 & 0 \\ 0 & 0 & -c & 0 & e & 0 & 0 & 0 & -d & 0 & f & 0 \\ 0 & c & 0 & 0 & 0 & e & 0 & d & 0 & 0 & 0 & f \\ \frac{1}{6}\rho Al & 0 & 0 & 0 & 0 & 0 & \frac{1}{3}\rho Al & 0 & 0 & 0 & 0 & 0 \\ 0 & b & 0 & 0 & 0 & d & 0 & a & 0 & 0 & 0 & -c \\ 0 & 0 & b & 0 & -d & 0 & 0 & 0 & a & 0 & c & 0 \\ 0 & 0 & 0 & \frac{J\rho Al}{6A} & 0 & 0 & 0 & 0 & 0 & \frac{J\rho Al}{3A} & 0 & 0 \\ 0 & 0 & d & 0 & f & 0 & 0 & 0 & c & 0 & e & 0 \\ 0 & -d & 0 & 0 & 0 & f & 0 & -c & 0 & 0 & 0 & e \end{bmatrix} \quad (A.14)$$

Where,

ρ = Shaft density

J = Polar area moment of inertia

A.1.2 Shaft Stiffness Matrix

Equation A.15 through A.18 developed for shaft stiffness matrix.

$$a = \frac{12EI}{l^3(1+\Phi)} \quad (A.15)$$

$$b = \frac{6EI}{l^2(1+\Phi)} \quad (A.16)$$

$$c = \frac{(4+\Phi)EI}{l(1+\Phi)} \quad (A.17)$$

$$d = \frac{(2-\Phi)EI}{l(1+\Phi)} \quad (A.18)$$

$$[K_h]_s^{(e)} = \begin{bmatrix} a & 0 & 0 & 0 & b & 0 & -a & 0 & 0 & 0 & b & 0 \\ 0 & a & 0 & -b & 0 & 0 & 0 & -a & 0 & -b & 0 & 0 \\ 0 & 0 & \frac{AE}{l} & 0 & 0 & 0 & 0 & 0 & -\frac{AE}{l} & 0 & 0 & 0 \\ 0 & -b & 0 & c & 0 & 0 & 0 & b & 0 & d & 0 & 0 \\ b & 0 & 0 & 0 & c & 0 & -b & 0 & 0 & 0 & d & 0 \\ 0 & 0 & 0 & 0 & 0 & \frac{GJ}{l} & 0 & 0 & 0 & 0 & 0 & -\frac{GJ}{l} \\ -a & 0 & 0 & 0 & -b & 0 & a & 0 & 0 & 0 & -b & 0 \\ 0 & -a & 0 & b & 0 & 0 & 0 & a & 0 & b & 0 & 0 \\ 0 & 0 & -\frac{AE}{l} & 0 & 0 & 0 & 0 & 0 & \frac{AE}{l} & 0 & 0 & 0 \\ 0 & -b & 0 & d & 0 & 0 & 0 & b & 0 & c & 0 & 0 \\ b & 0 & 0 & 0 & d & 0 & -b & 0 & 0 & 0 & c & 0 \\ 0 & 0 & 0 & 0 & 0 & -\frac{GJ}{l} & 0 & 0 & 0 & 0 & 0 & \frac{GJ}{l} \end{bmatrix} \quad \text{(A.19)}$$

$$[K_{bi}]_s^{(e)} = \begin{bmatrix} a & 0 & 0 & 0 & 0 & -b & -a & 0 & 0 & 0 & 0 & -b \\ 0 & \frac{AE}{l} & 0 & 0 & 0 & 0 & 0 & -\frac{AE}{l} & 0 & 0 & 0 & 0 \\ 0 & 0 & a & b & 0 & 0 & 0 & 0 & -a & b & 0 & 0 \\ 0 & 0 & b & c & 0 & 0 & 0 & 0 & -b & d & 0 & 0 \\ 0 & 0 & 0 & 0 & \frac{GJ}{l} & 0 & 0 & 0 & 0 & 0 & -\frac{GJ}{l} & 0 \\ -b & 0 & 0 & 0 & 0 & c & b & 0 & 0 & 0 & 0 & d \\ -a & 0 & 0 & 0 & 0 & b & a & 0 & 0 & 0 & 0 & b \\ 0 & -\frac{AE}{l} & 0 & 0 & 0 & 0 & 0 & \frac{AE}{l} & 0 & 0 & 0 & 0 \\ 0 & 0 & -a & -b & 0 & 0 & 0 & 0 & a & -b & 0 & 0 \\ 0 & 0 & b & d & 0 & 0 & 0 & 0 & -b & c & 0 & 0 \\ 0 & 0 & 0 & 0 & -\frac{GJ}{l} & 0 & 0 & 0 & 0 & 0 & \frac{GJ}{l} & 0 \\ -b & 0 & 0 & 0 & 0 & d & b & 0 & 0 & 0 & 0 & c \end{bmatrix} \quad \text{(A.20)}$$

$$[K_{bj}]_s^{(e)} = \begin{bmatrix} \frac{AE}{l} & 0 & 0 & 0 & 0 & 0 & -\frac{AE}{l} & 0 & 0 & 0 & 0 & 0 \\ 0 & a & 0 & 0 & 0 & b & 0 & -a & 0 & 0 & 0 & b \\ 0 & 0 & a & 0 & -b & 0 & 0 & 0 & -a & 0 & -b & 0 \\ 0 & 0 & 0 & \frac{GJ}{l} & 0 & 0 & 0 & 0 & 0 & -\frac{GJ}{l} & 0 & 0 \\ 0 & 0 & -b & 0 & c & 0 & 0 & 0 & b & 0 & d & 0 \\ 0 & b & 0 & 0 & 0 & c & 0 & -b & 0 & 0 & 0 & d \\ -\frac{AE}{l} & 0 & 0 & 0 & 0 & 0 & \frac{AE}{l} & 0 & 0 & 0 & 0 & 0 \\ 0 & -a & 0 & 0 & 0 & -b & 0 & a & 0 & 0 & 0 & -b \\ 0 & 0 & -a & 0 & b & 0 & 0 & 0 & a & 0 & b & 0 \\ 0 & 0 & 0 & -\frac{GJ}{l} & 0 & 0 & 0 & 0 & 0 & \frac{GJ}{l} & 0 & 0 \\ 0 & 0 & -b & 0 & d & 0 & 0 & 0 & b & 0 & c & 0 \\ 0 & b & 0 & 0 & 0 & d & 0 & -b & 0 & 0 & 0 & c \end{bmatrix} \quad \text{(A.21)}$$

A.1.3 Shaft Gyroscopic Matrix

Equation A.22 through A.25 developed for a gyroscopic matrix of the shaft.

$$a = \frac{\rho A l}{(1+\Phi)^2}\frac{6}{5}\left(\frac{r_g}{l}\right)^2 \quad \text{(A.22)}$$

$$b = -\frac{\rho A l}{(1+\Phi)^2}\left(\frac{1}{10}-\frac{1}{2}\Phi\right)\frac{{r_g}^2}{l} \quad \text{(A.23)}$$

$$c = \frac{\rho A l}{(1+\Phi)^2}\left(\frac{2}{15}+\frac{1}{6}\Phi+\frac{1}{3}\Phi^2\right){r_g}^2 \quad \text{(A.24)}$$

$$d = -\frac{\rho A l}{(1+\Phi)^2}\left(\frac{1}{30}+\frac{1}{6}\Phi-\frac{1}{6}\Phi^2\right){r_g}^2 \quad \text{(A.25)}$$

$$\Omega[G_h]_s^{(e)} = 2\Omega \begin{bmatrix} 0 & a & 0 & b & 0 & 0 & 0 & -a & 0 & b & 0 & 0 \\ -a & 0 & 0 & 0 & b & 0 & a & 0 & 0 & 0 & b & 0 \\ 0 & 0 & 0 & 0 & 0 & 0 & 0 & 0 & 0 & 0 & 0 & 0 \\ -b & 0 & 0 & 0 & c & 0 & b & 0 & 0 & 0 & d & 0 \\ 0 & -b & 0 & -c & 0 & 0 & 0 & b & 0 & -d & 0 & 0 \\ 0 & 0 & 0 & 0 & 0 & 0 & 0 & 0 & 0 & 0 & 0 & 0 \\ 0 & -a & 0 & -b & 0 & 0 & 0 & a & 0 & -b & 0 & 0 \\ a & 0 & 0 & 0 & -b & 0 & -a & 0 & 0 & 0 & -b & 0 \\ 0 & 0 & 0 & 0 & 0 & 0 & 0 & 0 & 0 & 0 & 0 & 0 \\ -b & 0 & 0 & 0 & d & 0 & b & 0 & 0 & 0 & c & 0 \\ 0 & -b & 0 & -d & 0 & 0 & 0 & b & 0 & -c & 0 & 0 \\ 0 & 0 & 0 & 0 & 0 & 0 & 0 & 0 & 0 & 0 & 0 & 0 \end{bmatrix} \quad \text{(A.26)}$$

$$\Omega[G_{bi}]_s^{(e)} = 2\Omega \begin{bmatrix} 0 & 0 & -a & b & 0 & 0 & 0 & 0 & a & b & 0 & 0 \\ 0 & 0 & 0 & 0 & 0 & 0 & 0 & 0 & 0 & 0 & 0 & 0 \\ a & 0 & 0 & 0 & 0 & b & -a & 0 & 0 & 0 & 0 & b \\ -b & 0 & 0 & 0 & 0 & -c & b & 0 & 0 & 0 & 0 & -d \\ 0 & 0 & 0 & 0 & 0 & 0 & 0 & 0 & 0 & 0 & 0 & 0 \\ 0 & 0 & -b & c & 0 & 0 & 0 & 0 & b & d & 0 & 0 \\ 0 & 0 & a & -b & 0 & 0 & 0 & 0 & -a & -b & 0 & 0 \\ 0 & 0 & 0 & 0 & 0 & 0 & 0 & 0 & 0 & 0 & 0 & 0 \\ -a & 0 & 0 & 0 & 0 & -b & a & 0 & 0 & 0 & 0 & -b \\ -b & 0 & 0 & 0 & 0 & -d & b & 0 & 0 & 0 & 0 & -c \\ 0 & 0 & 0 & 0 & 0 & 0 & 0 & 0 & 0 & 0 & 0 & 0 \\ 0 & 0 & -b & d & 0 & 0 & 0 & 0 & b & c & 0 & 0 \end{bmatrix} \quad \text{(A.27)}$$

$$\Omega[G_{bj}]_s^{(e)} = 2\Omega \begin{bmatrix} 0 & 0 & 0 & 0 & 0 & 0 & 0 & 0 & 0 & 0 & 0 & 0 \\ 0 & 0 & a & 0 & b & 0 & 0 & 0 & -a & 0 & b & 0 \\ 0 & -a & 0 & 0 & 0 & b & 0 & a & 0 & 0 & 0 & b \\ 0 & 0 & 0 & 0 & 0 & 0 & 0 & 0 & 0 & 0 & 0 & 0 \\ 0 & -b & 0 & 0 & 0 & c & 0 & b & 0 & 0 & 0 & d \\ 0 & 0 & -b & 0 & -c & 0 & 0 & 0 & b & 0 & -d & 0 \\ 0 & 0 & 0 & 0 & 0 & 0 & 0 & 0 & 0 & 0 & 0 & 0 \\ 0 & 0 & -a & 0 & -b & 0 & 0 & 0 & a & 0 & -b & 0 \\ 0 & a & 0 & 0 & 0 & -b & 0 & -a & 0 & 0 & 0 & -b \\ 0 & 0 & 0 & 0 & 0 & 0 & 0 & 0 & 0 & 0 & 0 & 0 \\ 0 & -b & 0 & 0 & 0 & d & 0 & b & 0 & 0 & 0 & c \\ 0 & 0 & -b & 0 & -d & 0 & 0 & 0 & b & 0 & -c & 0 \end{bmatrix} \quad \text{(A.28)}$$

A.2 6-DOF Matrices

The bearings support the spinning shaft and are assumed to be rigid. As such, they contribute no mass to the system, but they do store and dissipates energy from the shaft. Stiffness and damping matrices are shown in equation A.29 and A.30. Both matrices are symmetric. The off-diagonal terms in either matrix may or may not equal zero, depending upon the assumption made and types of bearing used.

$$[K]_b = \begin{bmatrix} k_{xx} & & & & & sym \\ & k_{yy} & & & & \\ & & k_{zz} & & & \\ \vdots & & & K_{\theta x \theta x} & & \\ & & & & K_{\theta y \theta y} & \\ k_{x\theta x} & & \dots & & & K_{\theta z \theta z} \end{bmatrix} \tag{A.29}$$

Similarly,

$$[C]_b = \begin{bmatrix} c_{xx} & & & & & sym \\ & c_{yy} & & & & \\ & & c_{zz} & & & \\ \vdots & & & C_{\theta x \theta x} & & \\ & & & & C_{\theta y \theta y} & \\ C_{x\theta x} & & \dots & & & C_{\theta z \theta z} \end{bmatrix} \tag{A.30}$$

Appendix B : 12-DOF Mesh Stiffness Matric for Helical Gear

12 –DOF mesh stiffness matrix derived from the chapter 5 is presented in this appendix. For ease of writing matrix, the following shorthand are used.

$$c\varphi = cos\varphi$$

$$s\varphi = sin\varphi$$

$$c\phi_x = cos\phi_x = cos\beta\ cos\alpha_n$$

$$c\phi_y = cos\phi_y = sin\alpha_n \tag{B.1}$$

$$c\phi_z = cos\phi_z = sin\beta\ cos\alpha_n$$

$$s\varphi^2 = (sin\varphi)^2$$

$$c\varphi^2 = (cos\varphi)^2$$

Gear mesh stiffness matrix cam ne written as,

$$\begin{Bmatrix} F_i \\ F_j \end{Bmatrix} = [K]_{mesh} \begin{Bmatrix} q_i \\ q_j \end{Bmatrix} = K_m \begin{bmatrix} [K_{ii}] & [K_{ij}] \\ [K_{ji}] & [K_{jj}] \end{bmatrix} \begin{Bmatrix} q_i \\ q_j \end{Bmatrix} \tag{B.2}$$

The four sub-matrices of equation B.2 shown in equation B.3 through B.6

$$[K_{ii}] = \begin{bmatrix} (s\varphi c\phi_x + c\varphi c\phi_y)^2 & (s\varphi c\phi_x + c\varphi c\phi_y)(s\varphi c\phi_y - c\varphi c\phi_x) & c\phi_z(s\varphi c\phi_x + c\varphi c\phi_y) & s\varphi c\phi_z r_i(s\varphi c\phi_x + c\varphi c\phi_y) & -c\varphi c\phi_z r_i(s\varphi c\phi_x + c\varphi c\phi_y) & -c\phi_x r_i(c\varphi^2 + s\varphi^2)(s\varphi c\phi_x + c\varphi c\phi_y) \\ (s\varphi c\phi_x + c\varphi c\phi_y)(s\varphi c\varphi_y - c\varphi c\varphi_x) & (s\varphi c\phi_y - c\varphi c\phi_x)^2 & c\phi_z(s\varphi c\phi_y - c\varphi c\phi_x) & s\varphi c\phi_z r_i(s\varphi c\phi_y - c\varphi c\phi_x) & -c\varphi c\phi_z r_i(s\varphi c\phi_y - c\varphi c\phi_x) & -c\phi_x r_i(c\varphi^2 + s\varphi^2)(s\varphi c\phi_y - c\varphi c\phi_x) \\ c\phi_z(s\varphi c\phi_x + c\varphi c\phi_y) & c\phi_z(s\varphi c\phi_y - c\varphi c\phi_x) & c{\phi_z}^2 & s\varphi c{\phi_z}^2 r_i & -c\varphi c{\phi_z}^2 r_i & -c\phi_x c\phi_z r_i(c\varphi^2 + s\varphi^2) \\ s\varphi c\phi_z r_i(s\varphi c\phi_x + c\varphi c\phi_y) & s\varphi c\phi_z r_i(s\varphi c\phi_y - c\varphi c\phi_x) & s\varphi c{\phi_z}^2 r_i & s\varphi^2 c{\phi_z}^2 {r_i}^2 & -c\varphi s\varphi c{\phi_z}^2 {r_i}^2 & -c\phi_x s\varphi c\phi_z {r_i}^2(c\varphi^2 + s\varphi^2) \\ -c\varphi c\phi_z r_i(s\varphi c\phi_x + c\varphi c\phi_y) & -c\varphi c\phi_z r_i(s\varphi c\phi_y - c\varphi c\phi_x) & -c\varphi c{\phi_z}^2 r_i & -c\varphi s\varphi c{\phi_z}^2 {r_i}^2 & c\varphi^2 c{\phi_z}^2 {r_i}^2 & c\phi_x c\varphi c\phi_z {r_i}^2(c\varphi^2 + s\varphi^2) \\ -c\phi_x r_i(c\varphi^2 + s\varphi^2)(s\varphi c\phi_x + c\varphi c\phi_y) & -c\phi_x r_i(c\varphi^2 + s\varphi^2)(s\varphi c\phi_y - c\varphi c\phi_x) & -c\phi_x c\phi_z r_i(c\varphi^2 + s\varphi^2) & -c\phi_x s\varphi c\phi_z {r_i}^2(c\varphi^2 + s\varphi^2) & c\phi_x c\varphi c\phi_z {r_i}^2(c\varphi^2 + s\varphi^2) & c{\phi_x}^2 {r_i}^2(c\varphi^2 + s\varphi^2)^2 \end{bmatrix} \tag{B.3}$$

$$[K_{ji}] = \begin{bmatrix} -(s\varphi c\phi_x + c\varphi c\phi_y)^2 & -(s\varphi c\phi_x + c\varphi c\phi_y)(s\varphi c\phi_y - c\varphi c\phi_x) & -c\phi_z(s\varphi c\phi_x + c\varphi c\phi_y) & -s\varphi c\phi_z r_i(s\varphi c\phi_x + c\varphi c\phi_y) & c\varphi c\phi_z r_i(s\varphi c\phi_x + c\varphi c\phi_y) & c\phi_x r_i(c\varphi^2 + s\varphi^2)(s\varphi c\phi_x + c\varphi c\phi_y) \\ -(s\varphi c\phi_x + c\varphi c\phi_y)(s\varphi c\varphi_y - c\varphi c\varphi_x) & -(s\varphi c\phi_y - c\varphi c\phi_x)^2 & -c\phi_z(s\varphi c\phi_y - c\varphi c\phi_x) & -s\varphi c\phi_z r_i(s\varphi c\phi_y - c\varphi c\phi_x) & c\varphi c\phi_z r_i(s\varphi c\phi_y - c\varphi c\phi_x) & c\phi_x r_i(c\varphi^2 + s\varphi^2)(s\varphi c\phi_y - c\varphi c\phi_x) \\ -c\phi_z(s\varphi c\phi_x + c\varphi c\phi_y) & -c\phi_z(s\varphi c\phi_y - c\varphi c\phi_x) & -c{\varphi_z}^2 & -s\varphi c{\phi_z}^2 r_i & c\varphi c{\phi_z}^2 r_i & c\phi_x c\phi_z r_i(c\varphi^2 + s\varphi^2) \\ -s\varphi c\phi_z r_j(s\varphi c\phi_x + c\varphi c\phi_y) & -s\varphi c\phi_z r_j(s\varphi c\phi_y - c\varphi c\phi_x) & -s\varphi c{\phi_z}^2 r_j & -s\varphi^2 c{\phi_z}^2 r_i r_j & c\varphi s\varphi c{\phi_z}^2 r_i r_j & c\phi_x s\varphi c\phi_z r_i r_j(c\varphi^2 + s\varphi^2) \\ c\varphi c\phi_z r_j(s\varphi c\phi_x + c\varphi c\phi_y) & c\varphi c\phi_z r_j(s\varphi c\phi_y - c\varphi c\phi_x) & c\varphi c{\phi_z}^2 r_j & c\varphi s\varphi c{\phi_z}^2 r_i r_j & -c\varphi^2 c{\phi_z}^2 r_i r_j & -c\phi_x c\varphi c\phi_z r_i r_j(c\varphi^2 + s\varphi^2) \\ c\phi_x r_j(c\varphi^2 + s\varphi^2)(s\varphi c\phi_x + c\varphi c\phi_y) & c\phi_x r_j(c\varphi^2 + s\varphi^2)(s\varphi c\phi_y - c\varphi c\phi_x) & c\phi_x c\phi_z r_j(c\varphi^2 + s\varphi^2) & c\phi_x s\varphi c\varphi_z r_i r_j(c\varphi^2 + s\varphi^2) & -c\phi_x c\varphi c\varphi_z r_i r_j(c\varphi^2 + s\varphi^2) & -c\phi_x{}^2 r_i r_j(c\varphi^2 + s\varphi^2)^2 \end{bmatrix} \tag{B.4}$$

$$[K_{jj}] = \begin{bmatrix} (s\varphi c\phi_x + c\varphi c\phi_y)^2 & (s\varphi c\phi_x + c\varphi c\phi_y)(s\varphi c\phi_y - c\varphi c\phi_x) & c\phi_z(s\varphi c\phi_x + c\varphi c\phi_y) & s\varphi c\phi_z r_j(s\varphi c\phi_x + c\varphi c\phi_y) & -c\varphi c\phi_z r_j(s\varphi c\phi_x + c\varphi c\phi_y) & -c\phi_x r_j(c\varphi^2 + s\varphi^2)(s\varphi c\phi_x + c\varphi c\phi_y) \\ (s\varphi c\phi_x + c\varphi c\phi_y)(s\varphi c\varphi_y - c\varphi c\varphi_x) & (s\varphi c\phi_y - c\varphi c\phi_x)^2 & c\phi_z(s\varphi c\phi_y - c\varphi c\phi_x) & s\varphi c\phi_z r_j(s\varphi c\phi_y - c\varphi c\phi_x) & -c\varphi c\phi_z r_j(s\varphi c\phi_y - c\varphi c\phi_x) & -c\phi_x r_j(c\varphi^2 + s\varphi^2)(s\varphi c\phi_y - c\varphi c\phi_x) \\ c\phi_z(s\varphi c\phi_x + c\varphi c\phi_y) & c\phi_z(s\varphi c\phi_y - c\varphi c\phi_x) & c{\phi_z}^2 & s\varphi c{\phi_z}^2 r_j & -c\varphi c{\phi_z}^2 r_j & -c\phi_x c\phi_z r_j(c\varphi^2 + s\varphi^2) \\ s\varphi c\phi_z r_j(s\varphi c\phi_x + c\varphi c\phi_y) & s\varphi c\phi_z r_j(s\varphi c\phi_y - c\varphi c\phi_x) & s\varphi c{\phi_z}^2 r_j & s\varphi^2 c{\phi_z}^2 {r_j}^2 & -c\varphi s\varphi c{\phi_z}^2 {r_j}^2 & -c\phi_x s\varphi c\phi_z {r_j}^2(c\varphi^2 + s\varphi^2) \\ -c\varphi c\phi_z r_j(s\varphi c\phi_x + c\varphi c\phi_y) & -c\varphi c\phi_z r_j(s\varphi c\phi_y - c\varphi c\phi_x) & -c\varphi c{\phi_z}^2 r_j & -c\varphi s\varphi c{\phi_z}^2 {r_i}^2 & c\varphi^2 c{\phi_z}^2 {r_j}^2 & c\phi_x c\varphi c\phi_z {r_j}^2(c\varphi^2 + s\varphi^2) \\ -c\phi_x r_j(c\varphi^2 + s\varphi^2)(s\varphi c\phi_x + c\varphi c\phi_y) & -c\phi_x r_j(c\varphi^2 + s\varphi^2)(s\varphi c\phi_y - c\varphi c\phi_x) & -c\phi_x c\phi_z r_j(c\varphi^2 + s\varphi^2) & -c\phi_x s\varphi c\phi_z {r_j}^2(c\varphi^2 + s\varphi^2) & c\phi_x c\varphi c\phi_z {r_j}^2(c\varphi^2 + s\varphi^2) & c{\phi_x}^2 {r_j}^2(c\varphi^2 + s\varphi^2)^2 \end{bmatrix} \tag{B.5}$$

$$[K_{ij}] = [K_{ji}]^T \tag{B.6}$$

Appendix C: 12-DOF Mesh Stiffness Matric for Bevel Gear

12 –DOF mesh stiffness matrix derived from the chapter 6 is presented in this appendix. For ease of writing matrix, the following shorthand are used.

$$
\begin{aligned}
c\phi_x &= cos\phi_x = sin\,\alpha_n\, cos\,\gamma_i \\
c\phi_y &= cos\phi_y = sin\,\alpha_n\, sin\,\gamma_i \\
c\phi_z &= cos\phi_z = cos\,\alpha_n \\
s\theta_1 &= sin\theta_1 \\
s\theta_2 &= sin\theta_2 \\
c\theta_1 &= cos\theta_1 \\
c\theta_2 &= cos\theta_2 \\
{s\theta_1}^2 &= (sin\theta_1)^2 \\
{s\theta_2}^2 &= (sin\theta_2)^2 \\
{c\theta_1}^2 &= (cos\theta_1)^2 \\
{c\theta_2}^2 &= (cos\theta_2)^2
\end{aligned}
\tag{C.1}
$$

Gear mesh stiffness matrix cam ne written as,

$$
\begin{Bmatrix} F_i \\ F_j \end{Bmatrix} = [K]_{mesh} \begin{Bmatrix} q_i \\ q_j \end{Bmatrix} = K_m \begin{bmatrix} [K_{ii}] & [K_{ij}] \\ [K_{ji}] & [K_{jj}] \end{bmatrix} \begin{Bmatrix} q_i \\ q_j \end{Bmatrix} \tag{C.2}
$$

The four sub-matrices of equation C.2 shown in equation C.3 through C.6

$$[K]_{ii} = \begin{bmatrix} \left(c\phi_x c\theta_1 + c\phi_y s\theta_2 s\theta_1 - c\phi_z c\theta_2 s\theta_1\right)^2 & \left(c\phi_x c\theta_1 + c\phi_y s\theta_2 s\theta_1 - c\phi_z c\theta_2 s\theta_1\right) * \left(c\phi_y c\theta_2 + c\phi_z s\theta_2\right) & \left(c\phi_x c\theta_1 + c\phi_y s\theta_2 s\theta_1 - c\phi_z c\theta_2 s\theta_1\right) * \left(c\phi_x s\theta_1 - c\phi_y c\theta_1 s\theta_2 + c\phi_z c\theta_2 c\theta_1\right) \\ \left(c\phi_x c\theta_1 + c\phi_y s\theta_2 s\theta_1 - c\phi_z c\theta_2 s\theta_1\right) * \left(c\phi_y c\theta_2 + c\phi_z s\theta_2\right) & \left(c\phi_y c\theta_2 + c\phi_z s\theta_2\right)^2 & \left(c\phi_y c\theta_2 + c\phi_z s\theta_2\right) * \left(c\phi_x s\theta_1 - c\phi_y c\theta_1 s\theta_2 + c\phi_z c\theta_2 c\theta_1\right) \\ \left(c\phi_x c\theta_1 + c\phi_y s\theta_2 s\theta_1 - c\phi_z c\theta_2 s\theta_1\right) * \left(c\phi_x s\theta_1 - c\phi_y c\theta_1 s\theta_2 + c\phi_z c\theta_2 c\theta_1\right) & \left(c\phi_y c\theta_2 + c\phi_z s\theta_2\right) * \left(c\phi_x s\theta_1 - c\phi_y c\theta_1 s\theta_2 + c\phi_z c\theta_2 c\theta_1\right) & \left(c\phi_x s\theta_1 - c\phi_y c\theta_1 s\theta_2 + c\phi_z c\theta_2 c\theta_1\right)^2 \\ -r_i\, s\theta_1\left(c\phi_x c\theta_1 + c\phi_y s\theta_2 s\theta_1 - c\phi_z c\theta_2 s\theta_1\right) * \left(c\phi_y c\theta_2 + c\phi_z s\theta_2\right) & -r_i\, s\theta_1\left(c\phi_y c\theta_2 + c\phi_z s\theta_2\right)^2 & -r_i\, s\theta_1\left(c\phi_y c\theta_2 + c\phi_z s\theta_2\right) * \left(c\phi_x s\theta_1 - c\phi_y c\theta_1 s\theta_2 + c\phi_z c\theta_2 c\theta_1\right) \\ r_i\left(c\phi_x c\theta_1 + c\phi_y s\theta_2 s\theta_1 - c\phi_z c\theta_2 s\theta_1\right) * \left(s\theta_2 c\phi_y - c\phi_z c\theta_2\right) & r_i\left(s\theta_2 c\phi_y - c\phi_z c\theta_2\right) * \left(c\phi_y c\theta_2 + c\phi_z s\theta_2\right) & r_i\left(s\theta_2 c\phi_y - c\phi_z c\theta_2\right) * \left(c\phi_x s\theta_1 - c\phi_y c\theta_1 s\theta_2 + c\phi_z c\theta_2 c\theta_1\right) \\ r_i\, c\theta_1\left(c\phi_x c\theta_1 + c\phi_y s\theta_2 s\theta_1 - c\phi_z c\theta_2 s\theta_1\right) * \left(c\phi_y c\theta_2 + c\phi_z s\theta_2\right) & r_i\, c\theta_1\left(c\phi_y c\theta_2 + c\phi_z s\theta_2\right)^2 & r_i\, c\theta_1\left(c\phi_y c\theta_2 + c\phi_z s\theta_2\right) * \left(c\phi_x s\theta_1 - c\phi_y c\theta_1 s\theta_2 + c\phi_z c\theta_2 c\theta_1\right) \end{bmatrix}$$

$$\begin{bmatrix} -r_i\, s\theta_1\left(c\phi_x c\theta_1 + c\phi_y s\theta_2 s\theta_1 - c\phi_z c\theta_2 s\theta_1\right) * \left(c\phi_y c\theta_2 + c\phi_z s\theta_2\right) & r_i\left(c\phi_x c\theta_1 + c\phi_y s\theta_2 s\theta_1 - c\phi_z c\theta_2 s\theta_1\right) * \left(s\theta_2 c\phi_y - c\phi_z c\theta_2\right) & r_i\, c\theta_1\left(c\phi_x c\theta_1 + c\phi_y s\theta_2 s\theta_1 - c\phi_z c\theta_2 s\theta_1\right) * \left(c\phi_y c\theta_2 + c\phi_z s\theta_2\right) \\ -r_i\, s\theta_1\left(c\phi_y c\theta_2 + c\phi_z s\theta_2\right)^2 & r_i\left(s\theta_2 c\phi_y - c\phi_z c\theta_2\right) * \left(c\phi_y c\theta_2 + c\phi_z s\theta_2\right) & r_i\, c\theta_1\left(c\phi_y c\theta_2 + c\phi_z s\theta_2\right)^2 \\ -r_i\, s\theta_1\left(c\phi_y c\theta_2 + c\phi_z s\theta_2\right) * \left(c\phi_x s\theta_1 - c\phi_y c\theta_1 s\theta_2 + c\phi_z c\theta_2 c\theta_1\right) & r_i\left(s\theta_2 c\phi_y - c\phi_z c\theta_2\right) * \left(c\phi_x s\theta_1 - c\phi_y c\theta_1 s\theta_2 + c\phi_z c\theta_2 c\theta_1\right) & r_i\, c\theta_1\left(c\phi_y c\theta_2 + c\phi_z s\theta_2\right) * \left(c\phi_x s\theta_1 - c\phi_y c\theta_1 s\theta_2 + c\phi_z c\theta_2 c\theta_1\right) \\ {r_i}^2 {s\theta_1}^2\left(c\phi_y c\theta_2 + c\phi_z s\theta_2\right)^2 & -{r_i}^2 s\theta_1\left(c\phi_y c\theta_2 + c\phi_z s\theta_2\right) * \left(s\theta_2 c\phi_y - c\phi_z c\theta_2\right) & -{r_i}^2 s\theta_1 c\theta_1\left(c\phi_y c\theta_2 + c\phi_z s\theta_2\right)^2 \\ -{r_i}^2 s\theta_1\left(c\phi_y c\theta_2 + c\phi_z s\theta_2\right) * \left(s\theta_2 c\phi_y - c\phi_z c\theta_2\right) & {r_i}^2\left(s\theta_2 c\phi_y - c\phi_z c\theta_2\right)^2 & {r_i}^2 c\theta_1\left(s\theta_2 c\phi_y - c\phi_z c\theta_2\right) * \left(c\phi_y c\theta_2 + c\phi_z s\theta_2\right) \\ -{r_i}^2 s\theta_1 c\theta_1\left(c\phi_y c\theta_2 + c\phi_z s\theta_2\right)^2 & {r_i}^2 c\theta_1\left(s\theta_2 c\phi_y - c\phi_z c\theta_2\right) * \left(c\phi_y c\theta_2 + c\phi_z s\theta_2\right) & {r_i}^2 {c\theta_1}^2\left(c\phi_y c\theta_2 + c\phi_z s\theta_2\right)^2 \end{bmatrix}$$

(C.3)

$$[K]_{ij} = \begin{bmatrix} -\left(c\phi_x c\theta_1 + c\phi_y s\theta_2 s\theta_1 - c\phi_z c\theta_2 s\theta_1\right)^2 & -\left(c\phi_x c\theta_1 + c\phi_y s\theta_2 s\theta_1 - c\phi_z c\theta_2 s\theta_1\right) * \left(c\phi_y c\theta_2 + c\phi_z s\theta_2\right) & -\left(c\phi_x c\theta_1 + c\phi_y s\theta_2 s\theta_1 - c\phi_z c\theta_2 s\theta_1\right) * \left(c\phi_x s\theta_1 - c\phi_y c\theta_1 s\theta_2 + c\phi_z c\theta_2 c\theta_1\right) \\ -\left(c\phi_x c\theta_1 + c\phi_y s\theta_2 s\theta_1 - c\phi_z c\theta_2 s\theta_1\right) * \left(c\phi_y c\theta_2 + c\phi_z s\theta_2\right) & -\left(c\phi_y c\theta_2 + c\phi_z s\theta_2\right)^2 & -\left(c\phi_y c\theta_2 + c\phi_z s\theta_2\right) * \left(c\phi_x s\theta_1 - c\phi_y c\theta_1 s\theta_2 + c\phi_z c\theta_2 c\theta_1\right) \\ -\left(c\phi_x c\theta_1 + c\phi_y s\theta_2 s\theta_1 - c\phi_z c\theta_2 s\theta_1\right) * \left(c\phi_x s\theta_1 - c\phi_y c\theta_1 s\theta_2 + c\phi_z c\theta_2 c\theta_1\right) & -\left(c\phi_y c\theta_2 + c\phi_z s\theta_2\right) * \left(c\phi_x s\theta_1 - c\phi_y c\theta_1 s\theta_2 + c\phi_z c\theta_2 c\theta_1\right) & -\left(c\phi_x s\theta_1 - c\phi_y c\theta_1 s\theta_2 + c\phi_z c\theta_2 c\theta_1\right)^2 \\ r_i\, s\theta_1\left(c\phi_x c\theta_1 + c\phi_y s\theta_2 s\theta_1 - c\phi_z c\theta_2 s\theta_1\right) * \left(c\phi_y c\theta_2 + c\phi_z s\theta_2\right) & r_i\, s\theta_1\left(c\phi_y c\theta_2 + c\phi_z s\theta_2\right)^2 & r_i\, s\theta_1\left(c\phi_y c\theta_2 + c\phi_z s\theta_2\right) * \left(c\phi_x s\theta_1 - c\phi_y c\theta_1 s\theta_2 + c\phi_z c\theta_2 c\theta_1\right) \\ -r_i\left(c\phi_x c\theta_1 + c\phi_y s\theta_2 s\theta_1 - c\phi_z c\theta_2 s\theta_1\right) * \left(s\theta_2 c\phi_y - c\phi_z c\theta_2\right) & -r_i\left(s\theta_2 c\phi_y - c\phi_z c\theta_2\right) * \left(c\phi_y c\theta_2 + c\phi_z s\theta_2\right) & -r_i\left(s\theta_2 c\phi_y - c\phi_z c\theta_2\right) * \left(c\phi_x s\theta_1 - c\phi_y c\theta_1 s\theta_2 + c\phi_z c\theta_2 c\theta_1\right) \\ -r_i\, c\theta_1\left(c\phi_x c\theta_1 + c\phi_y s\theta_2 s\theta_1 - c\phi_z c\theta_2 s\theta_1\right) * \left(c\phi_y c\theta_2 + c\phi_z s\theta_2\right) & -r_i\, c\theta_1\left(c\phi_y c\theta_2 + c\phi_z s\theta_2\right)^2 & -r_i\, c\theta_1\left(c\phi_y c\theta_2 + c\phi_z s\theta_2\right) * \left(c\phi_x s\theta_1 - c\phi_y c\theta_1 s\theta_2 + c\phi_z c\theta_2 c\theta_1\right) \end{bmatrix}$$

$$\begin{bmatrix} -r_j\left(c\phi_z c\theta_1 + c\phi_x c\theta_2 s\theta_1\right) * \left(c\phi_x c\theta_1 + c\phi_y s\theta_2 s\theta_1 - c\phi_z c\theta_2 s\theta_1\right) & r_j c\phi_x s\theta_2\left(c\phi_x c\theta_1 + c\phi_y s\theta_2 s\theta_1 - c\phi_z c\theta_2 s\theta_1\right) & -r_j\left(c\phi_z s\theta_1 - c\phi_x c\theta_2 c\theta_1\right) * \left(c\phi_x c\theta_1 + c\phi_y s\theta_2 s\theta_1 - c\phi_z c\theta_2 s\theta_1\right) \\ -r_j\left(c\phi_z c\theta_1 + c\phi_x c\theta_2 s\theta_1\right) * \left(c\phi_y c\theta_2 + c\phi_z s\theta_2\right) & r_j c\phi_x s\theta_2\left(c\phi_y c\theta_2 + c\phi_z s\theta_2\right) & -r_j\left(c\phi_z s\theta_1 - c\phi_x c\theta_2 c\theta_1\right) * \left(c\phi_y c\theta_2 + c\phi_z s\theta_2\right) \\ -r_j\left(c\phi_z c\theta_1 + c\phi_x c\theta_2 s\theta_1\right) * \left(c\phi_x s\theta_1 - c\phi_y c\theta_1 s\theta_2 + c\phi_z c\theta_2 c\theta_1\right) & r_j c\phi_x s\theta_2\left(c\phi_x s\theta_1 - c\phi_y c\theta_1 s\theta_2 + c\phi_z c\theta_2 c\theta_1\right) & -r_j\left(c\phi_z s\theta_1 - c\phi_x c\theta_2 c\theta_1\right) * \left(c\phi_x s\theta_1 - c\phi_y c\theta_1 s\theta_2 + c\phi_z c\theta_2 c\theta_1\right) \\ r_i r_j s\theta_1\left(c\phi_z c\theta_1 + c\phi_x c\theta_2 s\theta_1\right) * \left(c\phi_y c\theta_2 + c\phi_z s\theta_2\right) & -r_i r_j c\phi_x s\theta_2 s\theta_1\left(c\phi_y c\theta_2 + c\phi_z s\theta_2\right) & r_i r_j s\theta_1\left(c\phi_z s\theta_1 - c\phi_x c\theta_2 c\theta_1\right) * \left(c\phi_y c\theta_2 + c\phi_z s\theta_2\right) \\ -r_i r_j\left(c\phi_z c\theta_1 + c\phi_x c\theta_2 s\theta_1\right) * \left(s\theta_2 c\phi_y - c\phi_z c\theta_2\right) & r_i r_j c\phi_x s\theta_2\left(s\theta_2 c\phi_y - c\phi_z c\theta_2\right) & -r_i r_j\left(c\phi_z s\theta_1 - c\phi_x c\theta_2 c\theta_1\right) * \left(s\theta_2 c\phi_y - c\phi_z c\theta_2\right) \\ -r_i r_j c\theta_1\left(c\phi_z c\theta_1 + c\phi_x c\theta_2 s\theta_1\right) * \left(c\phi_y c\theta_2 + c\phi_z s\theta_2\right) & r_i r_j c\phi_x s\theta_2 c\theta_1\left(c\phi_y c\theta_2 + c\phi_z s\theta_2\right) & -r_i r_j c\theta_1\left(c\phi_z s\theta_1 - c\phi_x c\theta_2 c\theta_1\right) * \left(c\phi_y c\theta_2 + c\phi_z s\theta_2\right) \end{bmatrix}$$

(C.4)

$$[K]_{ji}$$

$$= \begin{bmatrix} -(c\phi_x c\theta_1 + c\phi_y s\theta_2 s\theta_1 - c\phi_z c\theta_2 s\theta_1)^2 & -(c\phi_x c\theta_1 + c\phi_y s\theta_2 s\theta_1 - c\phi_z c\theta_2 s\theta_1) * (c\phi_y c\theta_2 + c\phi_z s\theta_2) & -(c\phi_x c\theta_1 + c\phi_y s\theta_2 s\theta_1 - c\phi_z c\theta_2 s\theta_1) * (c\phi_x s\theta_1 - c\phi_y c\theta_1 s\theta_2 + c\phi_z c\theta_2 c\theta_1) \\ -(c\phi_x c\theta_1 + c\phi_y s\theta_2 s\theta_1 - c\phi_z c\theta_2 s\theta_1) * (c\phi_y c\theta_2 + c\phi_z s\theta_2) & -(c\phi_y c\theta_2 + c\phi_z s\theta_2)^2 & -(c\phi_y c\theta_2 + c\phi_z s\theta_2) * (c\phi_x s\theta_1 - c\phi_y c\theta_1 s\theta_2 + c\phi_z c\theta_2 c\theta_1) \\ -(c\phi_x c\theta_1 + c\phi_y s\theta_2 s\theta_1 - c\phi_z c\theta_2 s\theta_1) * (c\phi_x s\theta_1 - c\phi_y c\theta_1 s\theta_2 + c\phi_z c\theta_2 c\theta_1) & -(c\phi_y c\theta_2 + c\phi_z s\theta_2) * (c\phi_x s\theta_1 - c\phi_y c\theta_1 s\theta_2 + c\phi_z c\theta_2 c\theta_1) & -(c\phi_x s\theta_1 - c\phi_y c\theta_1 s\theta_2 + c\phi_z c\theta_2 c\theta_1)^2 \\ -r_j(c\phi_z c\theta_1 + c\phi_x c\theta_2 s\theta_1) * (c\phi_x c\theta_1 + c\phi_y s\theta_2 s\theta_1 - c\phi_z c\theta_2 s\theta_1) & -r_j(c\phi_z c\theta_1 + c\phi_x c\theta_2 s\theta_1) * (c\phi_y c\theta_2 + c\phi_z s\theta_2) & -r_j(c\phi_z c\theta_1 + c\phi_x c\theta_2 s\theta_1) * (c\phi_x s\theta_1 - c\phi_y c\theta_1 s\theta_2 + c\phi_z c\theta_2 c\theta_1) \\ r_j c\phi_x s\theta_2 (c\phi_x c\theta_1 + c\phi_y s\theta_2 s\theta_1 - c\phi_z c\theta_2 s\theta_1) & r_j c\phi_x s\theta_2 (c\phi_y c\theta_2 + c\phi_z s\theta_2) & r_j c\phi_x s\theta_2 (c\phi_x s\theta_1 - c\phi_y c\theta_1 s\theta_2 + c\phi_z c\theta_2 c\theta_1) \\ -r_j(c\phi_z s\theta_1 - c\phi_x c\theta_2 c\theta_1) * (c\phi_x c\theta_1 + c\phi_y s\theta_2 s\theta_1 - c\phi_z c\theta_2 s\theta_1) & -r_j(c\phi_z s\theta_1 - c\phi_x c\theta_2 c\theta_1) * (c\phi_y c\theta_2 + c\phi_z s\theta_2) & -r_j(c\phi_z s\theta_1 - c\phi_x c\theta_2 c\theta_1) * (c\phi_x s\theta_1 - c\phi_y c\theta_1 s\theta_2 + c\phi_z c\theta_2 c\theta_1) \end{bmatrix}$$

$$\begin{bmatrix} r_i\, s\theta_1(c\phi_x c\theta_1 + c\phi_y s\theta_2 s\theta_1 - c\phi_z c\theta_2 s\theta_1) * (c\phi_y c\theta_2 + c\phi_z s\theta_2) & -r_i(c\phi_x c\theta_1 + c\phi_y s\theta_2 s\theta_1 - c\phi_z c\theta_2 s\theta_1) * (s\theta_2 c\phi_y - c\phi_z c\theta_2) & -r_i\, c\theta_1(c\phi_x c\theta_1 + c\phi_y s\theta_2 s\theta_1 - c\phi_z c\theta_2 s\theta_1) * (c\phi_y c\theta_2 + c\phi_z s\theta_2) \\ r_i\, s\theta_1(c\phi_y c\theta_2 + c\phi_z s\theta_2)^2 & -r_i(s\theta_2 c\phi_y - c\phi_z c\theta_2) * (c\phi_y c\theta_2 + c\phi_z s\theta_2) & -r_i\, c\theta_1(c\phi_y c\theta_2 + c\phi_z s\theta_2)^2 \\ r_i\, s\theta_1(c\phi_y c\theta_2 + c\phi_z s\theta_2) * (c\phi_x s\theta_1 - c\phi_y c\theta_1 s\theta_2 + c\phi_z c\theta_2 c\theta_1) & -r_i(s\theta_2 c\phi_y - c\phi_z c\theta_2) * (c\phi_x s\theta_1 - c\phi_y c\theta_1 s\theta_2 + c\phi_z c\theta_2 c\theta_1) & -r_i\, c\theta_1(c\phi_y c\theta_2 + c\phi_z s\theta_2) * (c\phi_x s\theta_1 - c\phi_y c\theta_1 s\theta_2 + c\phi_z c\theta_2 c\theta_1) \\ r_i r_j s\theta_1(c\phi_z c\theta_1 + c\phi_x c\theta_2 s\theta_1) * (c\phi_y c\theta_2 + c\phi_z s\theta_2) & -r_i r_j(c\phi_z c\theta_1 + c\phi_x c\theta_2 s\theta_1) * (s\theta_2 c\phi_y - c\phi_z c\theta_2) & -r_i r_j c\theta_1(c\phi_z c\theta_1 + c\phi_x c\theta_2 s\theta_1) * (c\phi_y c\theta_2 + c\phi_z s\theta_2) \\ -r_i r_j c\phi_x s\theta_2 s\theta_1 (c\phi_y c\theta_2 + c\phi_z s\theta_2) & r_i r_j c\phi_x s\theta_2 (s\theta_2 c\phi_y - c\phi_z c\theta_2) & r_i r_j c\phi_x s\theta_2 c\theta_1 (c\phi_y c\theta_2 + c\phi_z s\theta_2) \\ r_i r_j s\theta_1(c\phi_z s\theta_1 - c\phi_x c\theta_2 c\theta_1) * (c\phi_y c\theta_2 + c\phi_z s\theta_2) & -r_i r_j(c\phi_z s\theta_1 - c\phi_x c\theta_2 c\theta_1) * (s\theta_2 c\phi_y - c\phi_z c\theta_2) & -r_i r_j c\theta_1(c\phi_z s\theta_1 - c\phi_x c\theta_2 c\theta_1) * (c\phi_y c\theta_2 + c\phi_z s\theta_2) \end{bmatrix}$$

(C.5)

$$[K]_{jj}$$

$$= \begin{bmatrix} (c\phi_x c\theta_1 + c\phi_y s\theta_2 s\theta_1 - c\phi_z c\theta_2 s\theta_1)^2 & (c\phi_x c\theta_1 + c\phi_y s\theta_2 s\theta_1 - c\phi_z c\theta_2 s\theta_1) * (c\phi_y c\theta_2 + c\phi_z s\theta_2) & (c\phi_x c\theta_1 + c\phi_y s\theta_2 s\theta_1 - c\phi_z c\theta_2 s\theta_1) * (c\phi_x s\theta_1 - c\phi_y c\theta_1 s\theta_2 + c\phi_z c\theta_2 c\theta_1) \\ (c\phi_x c\theta_1 + c\phi_y s\theta_2 s\theta_1 - c\phi_z c\theta_2 s\theta_1) * (c\phi_y c\theta_2 + c\phi_z s\theta_2) & (c\phi_y c\theta_2 + c\phi_z s\theta_2)^2 & (c\phi_y c\theta_2 + c\phi_z s\theta_2) * (c\phi_x s\theta_1 - c\phi_y c\theta_1 s\theta_2 + c\phi_z c\theta_2 c\theta_1) \\ (c\phi_x c\theta_1 + c\phi_y s\theta_2 s\theta_1 - c\phi_z c\theta_2 s\theta_1) * (c\phi_x s\theta_1 - c\phi_y c\theta_1 s\theta_2 + c\phi_z c\theta_2 c\theta_1) & (c\phi_y c\theta_2 + c\phi_z s\theta_2) * (c\phi_x s\theta_1 - c\phi_y c\theta_1 s\theta_2 + c\phi_z c\theta_2 c\theta_1) & (c\phi_x s\theta_1 - c\phi_y c\theta_1 s\theta_2 + c\phi_z c\theta_2 c\theta_1)^2 \\ r_j(c\phi_z c\theta_1 + c\phi_x c\theta_2 s\theta_1) * (c\phi_x c\theta_1 + c\phi_y s\theta_2 s\theta_1 - c\phi_z c\theta_2 s\theta_1) & r_j(c\phi_z c\theta_1 + c\phi_x c\theta_2 s\theta_1) * (c\phi_y c\theta_2 + c\phi_z s\theta_2) & r_j(c\phi_z c\theta_1 + c\phi_x c\theta_2 s\theta_1) * (c\phi_x s\theta_1 - c\phi_y c\theta_1 s\theta_2 + c\phi_z c\theta_2 c\theta_1) \\ -r_j c\phi_x s\theta_2 (c\phi_x c\theta_1 + c\phi_y s\theta_2 s\theta_1 - c\phi_z c\theta_2 s\theta_1) & -r_j c\phi_x s\theta_2 (c\phi_y c\theta_2 + c\phi_z s\theta_2) & -r_j c\phi_x s\theta_2 (c\phi_x s\theta_1 - c\phi_y c\theta_1 s\theta_2 + c\phi_z c\theta_2 c\theta_1) \\ r_j(c\phi_z s\theta_1 - c\phi_x c\theta_2 c\theta_1) * (c\phi_x c\theta_1 + c\phi_y s\theta_2 s\theta_1 - c\phi_z c\theta_2 s\theta_1) & r_j(c\phi_z s\theta_1 - c\phi_x c\theta_2 c\theta_1) * (c\phi_y c\theta_2 + c\phi_z s\theta_2) & r_j(c\phi_z s\theta_1 - c\phi_x c\theta_2 c\theta_1) * (c\phi_x s\theta_1 - c\phi_y c\theta_1 s\theta_2 + c\phi_z c\theta_2 c\theta_1) \end{bmatrix}$$

$$\begin{bmatrix} r_j(c\phi_z c\theta_1 + c\phi_x c\theta_2 s\theta_1) * (c\phi_x c\theta_1 + c\phi_y s\theta_2 s\theta_1 - c\phi_z c\theta_2 s\theta_1) & -r_j c\phi_x s\theta_2 (c\phi_x c\theta_1 + c\phi_y s\theta_2 s\theta_1 - c\phi_z c\theta_2 s\theta_1) & r_j(c\phi_z s\theta_1 - c\phi_x c\theta_2 c\theta_1) * (c\phi_x c\theta_1 + c\phi_y s\theta_2 s\theta_1 - c\phi_z c\theta_2 s\theta_1) \\ r_j(c\phi_z c\theta_1 + c\phi_x c\theta_2 s\theta_1) * (c\phi_y c\theta_2 + c\phi_z s\theta_2) & -r_j c\phi_x s\theta_2 (c\phi_y c\theta_2 + c\phi_z s\theta_2) & r_j(c\phi_z s\theta_1 - c\phi_x c\theta_2 c\theta_1) * (c\phi_y c\theta_2 + c\phi_z s\theta_2) \\ r_j(c\phi_z c\theta_1 + c\phi_x c\theta_2 s\theta_1) * (c\phi_x s\theta_1 - c\phi_y c\theta_1 s\theta_2 + c\phi_z c\theta_2 c\theta_1) & -r_j c\phi_x s\theta_2 (c\phi_x s\theta_1 - c\phi_y c\theta_1 s\theta_2 + c\phi_z c\theta_2 c\theta_1) & r_j(c\phi_z s\theta_1 - c\phi_x c\theta_2 c\theta_1) * (c\phi_x s\theta_1 - c\phi_y c\theta_1 s\theta_2 + c\phi_z c\theta_2 c\theta_1) \\ r_j^2(c\phi_z c\theta_1 + c\phi_x c\theta_2 s\theta_1)^2 & -r_j^2 c\phi_x s\theta_2 (c\phi_z c\theta_1 + c\phi_x c\theta_2 s\theta_1) & r_j^2(c\phi_z c\theta_1 + c\phi_x c\theta_2 s\theta_1) * (c\phi_z s\theta_1 - c\phi_x c\theta_2 c\theta_1) \\ -r_j^2 c\phi_x s\theta_2 (c\phi_z c\theta_1 + c\phi_x c\theta_2 s\theta_1) & r_j^2 c\phi_x{}^2 s\theta_2{}^2 & -r_j^2 c\phi_x s\theta_2 (c\phi_z s\theta_1 - c\phi_x c\theta_2 c\theta_1) \\ r_j^2(c\phi_z c\theta_1 + c\phi_x c\theta_2 s\theta_1) * (c\phi_z s\theta_1 - c\phi_x c\theta_2 c\theta_1) & -r_j^2 c\phi_x s\theta_2 (c\phi_z s\theta_1 - c\phi_x c\theta_2 c\theta_1) & r_j^2(c\phi_z s\theta_1 - c\phi_x c\theta_2 c\theta_1)^2 \end{bmatrix}$$

(C.6)